SCUOLA DI DOTTORATO
UNIVERSITÀ DEGLI STUDI DI MILANO-BICOCCA

Dipartimento di / Department of Scienza dei Materiali

Dottorato di Ricerca in / PhD program
Scienza e nanotecnologia dei materiali

Ciclo / Cycle XXXI

Curriculum in (se presente / if it is) Ricerca Nanoscienze -79R-3

Nanoparticles-based delivery of biologic drugs: improvements and challenges

Cognome / Surname **Salvioni**

Nome / Name **Lucia**

Matricola / Registration number 810442

Tutore / Tutor: **Dr. Miriam Colombo**

Coordinatore / Coordinator: **Prof. Marco Bernasconi**

ANNO ACCADEMICO / ACADEMIC YEAR 2017-2018

A Lucia e Lori

Table of content

Project 2: Development of lipidic NPs as gene delivery vectors in triple negative breast cancer

List of abbreviations

BC breast cancer

BD biological drugs

BSA bovine serum albumin

CD chemical drugs

CS chitosan

DDS drug delivery systems

DLS dynamic light scattering

DNA deoxyribonucleic acid

DOTAP 1,2-dioleoyl-3- trimethylammonium-propane chloride salt

DS dextran sulfate

DSPE-PEG-mal 1,2-distearoryl-sn- glycero-3-phosphoethanolamine-N-[maleimide(polyethyleneglycol- 2000)] ammonium salt

DSPE-PEG-OCH_3 1,2-distearoryl-sn- glycero-3-phosphoethanolamine-N-[methoxy(polyethyleneglycol- 2000)] ammonium salt

EPR enhanced permeability and retention

FACS fluorescence-based flow cytometry

FDA food and drug administration

FI fluorescence intensity

GFP green fluorescent protein

MPS mononuclear phagocyte system

NaGly sodium glycocholate

NPs nanoparticles

NT nanoparticle tracking

NVV non-viral vectors

PB phosphate buffer

PBS phosphate-buffered saline

PDI polydispersity index

PDI polydispersity index

pDNA plasmid DNA

PEG polyethylene glycol

PEI polyethylenimine

RIP ribosome-inactivating protein

RISC RNA-induced silencing complex

RNA ribonucleic acid

RP-HPLC Reverse phase High-performance liquid chromatography

rRNA ribosomal RNA

SAPO saporin

SC subcutaneous

SD standard deviation

SE standard error

TEM transmission electron microscopy

TJ tight junctions

TNBC triple negative breast cancer

UPAR urokinase plasminogen activator receptor

UWL unstirred water layer

VV viral vectors

Abstract

Biological drugs (BD) include a wide range of products such as proteins, peptides, genetic materials and cells [1].

Compared with the traditional small chemical drugs, BD generally show higher potency and selectivity of action and, so, have the potential to address many chronic diseases and various unmet medical needs [2].

Unfortunately, most of BD are characterized by short circulating half-life, low stability and rapid body clearance *via* glomerular filtration [3].

Among the several strategies proposed to overcome these drawbacks, nanoparticles (NPs) are emerging as valid drug delivery tools: indeed, they are able to improve the drug distribution, reduce its inactivation and elimination and provide the opportunity of non-invasive administration [5] [6] [7].

The aim of this thesis was the development of NPs-based BD delivery systems.

In particular, I was involved in two distinct projects: one concerned the hormonal substitution therapy, while the second a suicide gene delivery.

In the first project, an oral nanocarrier for insulin colon delivery was developed. The novelty of this approach was the evaluation of the synergistic effect of colon release and muco-adhesive NPs in presence of a permeation enhancer. Insulin-loaded polymeric NPs (NI) were synthesized according to previously published protocols with several improvements. Then, NI were incorporated into cores that were subsequently coated with three overlapping layers, aiming to release insulin into the large intestine. The system was evaluated *in vitro* for its physico-technological characteristics, NPs dispersion, disintegration and release performance, showing delayed release behavior.

Finally, the coated nanoformulation effect was tested in diabetic rats: a significant hypoglycaemic activity, due to the synergistic effect of NPs and colon delivery, was observed. Based on the *in vivo* efficacy, scalable process and safety profile, the proposed multitasking system appears a promising way to control diabetes.

In the second project, lipid NPs with a selective targeting for poorly differentiated triple negative breast cancer (TNBC) cells were developed as a novel gene delivery system. In particular, the suicide gene included was Saporin encoding plasmid DNA, whereas the specific targeting was achieved by the functionalization with a ligand of urokinase plasminogen activator receptor.

Firstly, targeted lipid-protamine-DNA (LPD-U11) NPs were synthetized, characterized and their antitumoral effect tested on TBNC cell line. Then, fluorescent LPD-U11 NPs were developed and their binding and uptake profiles were evaluated *in vitro*. An enhanced performance was observed comparing the optimized LPD-U11 NPs with the non-targeted formulation. *In vivo* biodistribution experiment of LPD-U11 NPs in tumor bearing mice showed a time-dependent tumor infiltration and accumulation. Finally, the antitumoral activity was tested *in vivo*: under the investigated conditions, the selected system was able to significantly reduce the tumor progression without compromising major organs functionality.

Bibliography

[1] FDA, “What Are "Biologics" Questions and Answers,” FDA, [Online]. Available: https://www.fda.gov/aboutfda/centersoffices/officeofmedicalproductsandtobacco/cber/ucm133077.htm. [Accessed 7 August 2018].

[2] A. Zelikin, “Materials and methods for delivery of biological drugs,” Nat. Chem., vol. 8, p. 997-1007, 2016.

[3] R. Ho, Biotechnology and Biopharmaceuticals: Transforming Proteins and Genes Into Drugs, John Wiley & Sons, Inc., 2013.

[4] W. De Jong, “Drug delivery and nanoparticles: Applications and hazards,” International Journal of Nanomedicine, vol. 3, no. 2, p. 133-149, 2008.

[5] B. Kumar, “Recent advances in nanoparticle-mediated drug delivery,” J. of Drug Del. Science and Tech., vol. 41, p. 260-268, 2017.

[6] A. Wilczewska, “Nanoparticles as drug delivery systems,” Pharm. reports, vol. 64, p. 1020-1037, 2012.

Introduction

1. Biological drugs

1.1 Introduction

For most people, biotechnology is synonymous with “advanced technology”, even if the idea to use technology or products derived from biological molecules and processes is not new: already during 1800s, the use of biomolecules as therapeutic agents was described.

The term biotechnology was coined intended to describe the interaction of biology with technology, whereas biological drugs (BD) include a wide range of products such as proteins, peptides, genetic materials and cells (*e.g.* blood, somatic cells, tissues), produced by biotechnology [1] [2]. Due to the purpose of this thesis, protein- and gene-based drugs will only be discussed, but all the general remarks reported still apply to cells BD.

Despite the relatively old onset, the synthesis of BD at a quality and quantity suitable for therapeutic use is a recent achievement. Indeed, the basic knowledge about the DNA and the genetic code, protein synthesis and cellular biology provided the foundation for exponential growth of biotechnology and, hence, BD development.

BD, also called biologicals, biopharmaceuticals or biotech drugs, are manufactured in living biological systems. The expression systems normally employed are microorganisms, plant or mammalian cells generated through recombinant DNA technology, whereas, for producing recombinant antibodies, an immunization of living animals is required.

In any case, the heterogeneous final product requires a series of purification steps to remove all the contaminants and obtain the drug [3]. Because of this complex production, BD show greater safety risks than traditional pharmaceuticals and this makes the regulatory requirements for marketing approval really strict [2]. In addition, their spread is further limited by the high cost generally associated with BD based therapies.

Despite these challenges, the capital invested in BD development is increasing exponentially, from 46 to 221 billion dollars in 2012 and 2017 respectively (Fig. 1.1.1) [4]. Nowadays, in US more than 3,000 clinical trials are ongoing and the largest growth is occurring in cancer, rare diseases, neurologic and autoimmune disorders areas (Fig. 1.1.2) [5].

This triumph relies on BD ability to treat certain diseases targeting better with fewer side effects than chemical drugs. The main differences with the traditional drugs will be further explored in the next section.

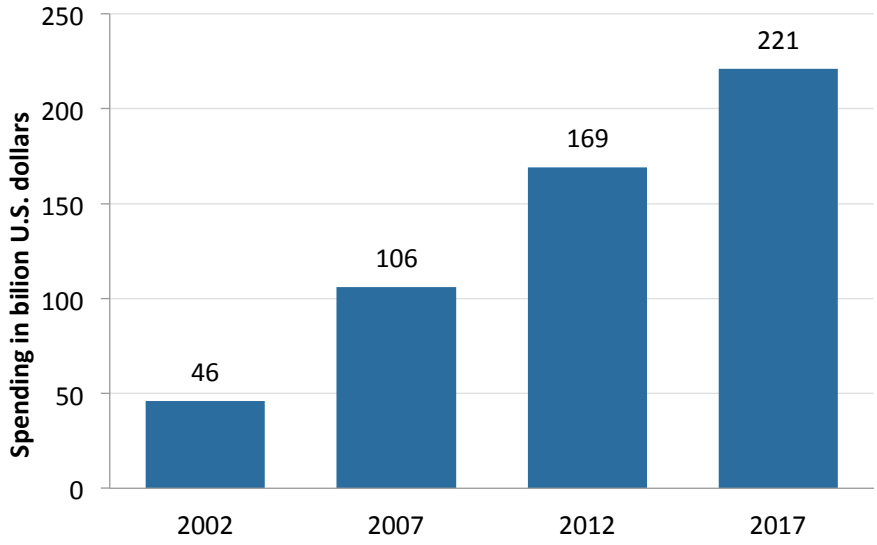

Fig. 1.1.1: Total global biologics spending from 2002 and 2017 (in billion U.S. dollars); adapted with permission from [4].

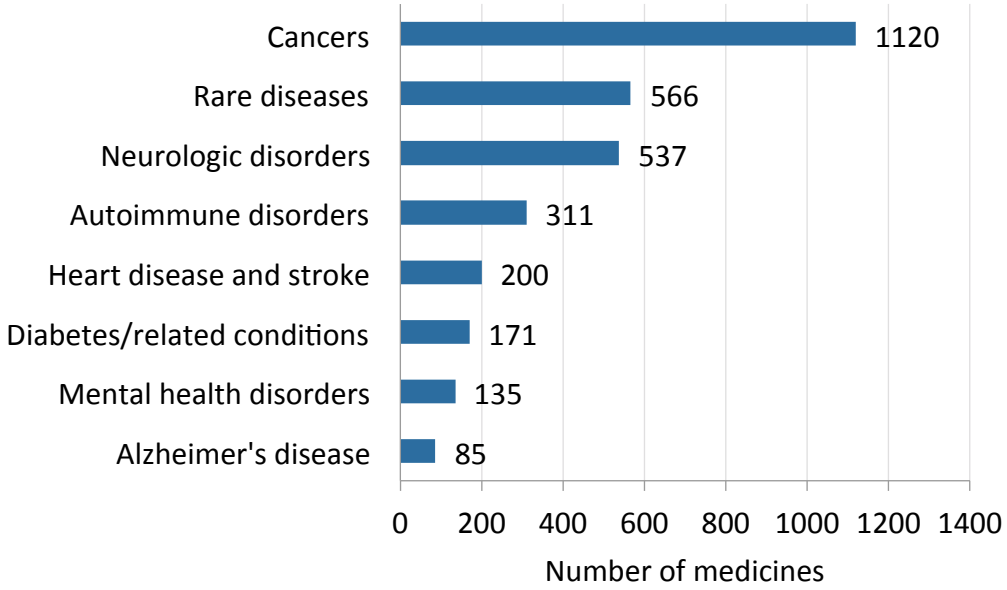

Fig. 1.1.2: Number of BD in development in US as May 2018 by therapeutic category; adapted with permission from [5].

1.2 Differences between chemical and biological drugs

Small, chemically manufactured molecules (chemical drug, CD) are the classic active substances and currently make up over 90% of the commercially available drugs [6].

CD typically exhibit a molecular weight of about 500 dalton (usually less than 1,000 dalton).

They are generally stable, easy and inexpensive to produce. Moreover, since they are synthetized by chemical reactions between different organic and/or inorganic compounds, the productive process is generally reproducible [6].

Because of their small size, any chemical modification can dramatically change their pharmacological activity and typically leads to novel drugs for new uses or indications (*e.g.* the addition of two or three methyl groups to specific

locations on the natural substance xanthine can produce the bronchodilator theophylline or the central nervous systems stimulants caffeine and theobromine [7]). In addition, CD generally lack target-binding specificity causing different side effects.

On the other hand, biopharmaceuticals are large molecules with a high molecular weight (order of magnitude = kDa). In contrast to the majority of CD, most biologics are complex mixtures that are not easily identified or characterized. As mentioned, their production is generally expensive (*e.g.* aseptic conditions are often required), with important reproducibility issues. Moreover, they are relatively unstable and sensitive to the external condition [8]. This physical-chemical instability may limit their versatility: indeed, in case of protein-based drugs, conformational changes seriously compromise their activity.

Besides these drawbacks, BD generally show high potency and selectivity of action and, so, have the potential to address many chronic diseases and various unmet medical needs [9]. Their development generally occurs after an accurate identification of key target for the disease treatment based on thorough understanding of the causes and pathological processes involved [10].

Lastly, small changes in biopharmaceuticals structure does not always lead to a new biotherapeutic product. For example, insulin, which is used to treat diabetes, contains two A and B polypeptide chains linked together by two disulfide bridges. Several variants of this biomolecule are approved for human use (Table 1.2.1): insulin extracted from beef, pork or insulin analogues, where the original structure was modified to produce more desirable

pharmacokinetic and disposition profiles. All the drugs reported, even the different composition, are used for the same treatment indication [11].

Table 1.2.1: Sequence variation between some insulin available for human use. Variations and modification made to the human insulin sequence are highlighted in bold and italic codes; reproduced with permission from [1].

	Insulin Amino Acid (sequence position)							
	A Chain			B Chain				
Name	8	10	21	3	28	29	30	31 & 32 insertion
Insulin-human	Thr	Ile	Asn	Asn	Pro	Lys	Thr	None
Insulin-beef	***Ala***	***Val***	Asn	Asn	Pro	Lys	***Ala***	None
Insulin-pork	Thr	Ile	Asn	Asn	Pro	Lys	***Ala***	None
Insulin-lispro	Thr	Ile	Asn	Asn	***Lys***	***Pro***	Thr	None
Insulin-aspart	Thr	Ile	Asn	Asn	***Asp***	Lys	Thr	None
Insulin-glargine	Thr	Ile	***Gly***	Asn	Pro	Lys	Thr	***Arg & Arg***
Insulin-glulisine	Thr	Ile	***Gly***	***Lys***	Pro	***Glu***	Thr	None

1.3 Properties and applications of biological drugs

1.3.1 Protein therapeutics

This class includes a wide range of drugs such as proteins, polypeptides and small peptides.

In accordance with their activity profiles, they are classified in hormones, enzymes, antibodies, vaccines, cytokines, interferons, hematopoietic growth and coagulation factors [12].

With the exception of vaccines, they may be used to replace deficient or defective endogenous proteins or as therapeutic agents: in replacement therapy it is necessary to maintain a stable level of the missing protein, whereas the therapeutic use requires timely delivery for blocking or boosting a specific pathway.

Hormones represent one of the largest class used in medical therapy. The main indications are metabolic diseases (*e.g.* diabetes mellitus and insipidus,

acute hypoglycemia), hormone-dependent cancers, growth disorders and fertility control [1].

On the other hand, monoclonal antibodies (mAb) are one of most broadly developed products: currently, mAb-based therapies account for 50 % of the top 100 drugs and are projected to maintain a dominant position in the pharmaceutical market over the coming years [13].

Therapeutic applications of these drugs are several. Besides the above-mentioned indications, they are extensively employed in autoimmune diseases treatment (*e.g.* Crohn's disease, ulcerative colitis, rheumatoid arthritis). Moreover, they have revolutionized cancer treatment limiting the side effect and stimulating the immune response.

Finally, the treatment of blood disorders is emerging as promise: indeed, according with a recent study, the protein therapeutics approved by U.S. Food and Drug Administration (FDA) between 2011 and 2016 are mainly indicated for oncology (26%) and hematology (29%) therapeutic areas [12].

1.3.1 Gene therapies

Gene therapy involves the intentional modulation of gene expression patterns through the delivery of exogenous genetic material.

The concept was originally designed for treating monogenic disorders that could be managed or potentially cured by the expression of an operational copy of the mutant or deleted gene [14]. Nowadays, this therapy is further explored for several multifactorial diseases such as cancer, muscular dystrophies, cardiovascular, blood, neurological and immune disorders [15] [14].

The treatment strategies may include the expression of a new or missing protein by transgene delivery, gene correction or protein expression silencing.

According to their mechanism of action, nucleic acids employed in gene therapy may be classified into two groups: transiently active payloads and genome editing systems [15].

The firsts can be further divided in expression-dependent and -independent systems.

The most common expression dependent systems are circular double-stranded DNAs, called plasmids (pDNA). pDNA were firstly observed in bacterial cells: normally separated from chromosomal DNA, they are able to independently replicate and express the carried gene.

Precisely this property leads to development of therapeutic pDNA: indeed, they are able to drive the expression of an inserted transgene. pDNA contains several basic components including the transgene expression system (*i.e.* promoter, gene of interest and terminator), regulatory signals, antibiotic resistance marker, origin of replication [15].

Among the expression independent systems, small double-stranded RNAs (*i.e.* siRNA, miRNA and shRNA) are extendedly investigated as interfering agents: indeed, through the activation of RNA-induced silencing complex (RISC), they are able to inhibit mRNA translation and, so, protein expression [16].

On the other side, genome editing systems are complex structures capable to introduce permanent genomic changes into host cells through gene correction, disruption or insertion [17].

1.4 Disposition of biological drugs

1.4.1 Absorption

Along with the high prescription costs and the production issues, the biopharmaceutical properties of BD strongly limit their use and development. Both protein- and gene-based drugs are poorly bioavailable, first because they generally exhibit high degradation rates: indeed, proteins are susceptible to protease degradation and denaturation in biological fluids, while endonucleases mediate nucleic acids breakdown [1] [15]. In addition, the large size and physicochemical properties of BD cause low permeability across biological membranes [18] [15]. This low bioavailability makes the parenteral route the most commonly method for BD administration and, in the recent years, numerous successful macromolecule-based products were developed [19]. The parenteral routes mainly used are reported below (Table 1.4.1.1 and Fig. 1.4.1.1).

Table 1.4.1.1: Comparison of various parenteral routes; reproduced with permission from [1].

Parenteral Routes	Bioavailability, Biologic Response, and Ease of Use
IV, intravenous	100% systemic availability; most rapid biological effect; potential for significant adverse effects; most invasive of parenteral routes; half-life governed by clearance
SC, subcutaneous	Less than complete systemic availability; half-life may be limited by absorption
IM, intramuscular	Systemic availability may be less than 100%; reduced peak concentrations compared to IV administration; potentially delayed and reduced biological effects; less invasive than IV route; half-life may depend on absorption

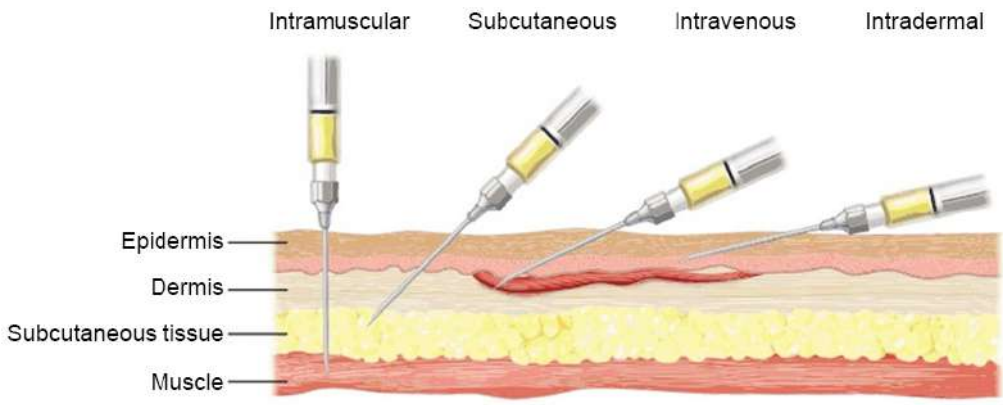

Fig. 1.4.1.1: Injection site representation; adapted with permission from [20].

The intravenous injection leads to a rapid therapeutic effect and the drug half-life is governed by clearance process, whereas the subcutaneous and intramuscular injections are generally preferred for chronic treatments and the onset of action is generally determined by the absorption process: lymphatic or blood absorption occurs depending on BD molecular size [10]. Regardless the injection type, an acceptable bioavailability is observed.

Despite the several advantages, the parenteral administration displays two major drawbacks:

1. Poor patient compliance: patients undergo frequent and painful injections, with a significant reduction in quality of life;
2. High costs: indeed, formulation process must be conducted in aseptic environment and specialized staff is often required for administration;

In addition, the high viscosity of BD-based products affects their syringeability and further reduces the patient acceptance [19].

Thus, it is not surprising that the research on non-invasive routes (*e.g.* nasal, transdermal, pulmonary and oral) is still appealing particularly for chronically used drugs.

1.4.2 Metabolism, distribution and elimination

Even overcoming the bioavailability limitation, the efficacy of BD is further affected by their metabolism, distribution and elimination.

The degradation of biomolecules is essential for the cell survival and the metabolism of BD normally occurs exploiting the same mechanisms: the protein degradation generally takes place intracellularly by the ubiquitin and lysosomal pathways, while tissue and serum nucleases cause the nucleic acid degradation in the extracellular space [10] [21].

Secondly, the distribution of BD might be an issue to consider: indeed, the drug must migrate from the blood circulation across the vascular wall to the site of action in order to exhibit its pharmacological activity. Two major steps can be distinguished namely the drug extravasation and its diffusion to extracellular matrix and both of them are strongly affected by the physico-chemical properties of the BD [10]. In particular, the extravasation is manly controlled by the vasculature porosity and thereby influenced by the molecular size of drug. Thus, a BD with a molecular weight greater than 150 kDa (approximately 5 nm) will have limited distribution and may be restricted to blood volume [1]. On the other hand, shape, charge and polarity of the macromolecule affect its diffusion capacity.

Lastly, the elimination contributes to determine the half-life of BD. In absence of significant receptor or cell interactions in the blood, the molecular size of BD mainly defines the manner and the rate of elimination. In general, relatively small BD (<40-50 kDa) are filtered by kidneys and excreted, without

reabsorption, into urine. When BD exceed a molecular weight of 200 kDa or drug aggregation occurred, phagocytosis plays an increasing role in elimination [1].

In view of the above, a proper delivery strategy might increase the potential of BD medicines by improving the drug distribution, reducing its inactivation and elimination and providing the opportunity for a non-invasive administration [15] [13] [9].

1.5 Immunological responses

Since the BD production is conducted in biological systems, the immunization issue may not be omitted.

Unlike small CD, exogenous macromolecules, even human-based recombinant protein, when given repeatedly, exhibit a high tendency to elicit an immune response in patients. Several factors influence this immunogenicity such as product purity and aggregation state, drug metabolism and conjugations, patient's immune status and administration conditions (dose, frequency and route) [1] [22].

This process influences the treatment efficacy: in fact, the binding with antibodies may neutralize the drug action or affect its distribution (*i.e.* the large size of BD-antibody complex limit tissue penetration) [22]. In addition, local and systemic allergic reactions may occur having a significant impact on safety profile of BD [1].

1.6 Drug delivery strategies

As reported in 1.4 and 1.5 sections, most of BD are characterized by short circulating half-life, low stability and rapid body clearance *via* glomerular filtration. Thus, several strategies have been proposed to overcome these drawbacks improving the drug efficacy.

It will be noted that most instances concern protein delivery and the reason is that the development of these therapeutics is more advanced than gene therapies.

The main strategies for BD delivery are enlisted below:

1. Chemical conjugations:

   In the context of chemical modifications, polymer conjugation is the most widely used approach to improve the drug efficacy.

   This modification is able to increase the overall hydrodynamic size of the BD reducing renal filtration [1]. Moreover, due to their hydrophilicity, the resulting bioconjugates are characterized by reduced immunogenicity and decreased antibody recognition [23].

   Commonly used polymers in drug delivery applications include poly(N-(2-hydroxypropyl) methacrylamide) (PHPMA), poly(oligoethylene glycol methyl ether methacrylate) (POEGMA), poly(D,L-lactic-co-glycolic acid) (PLGA), poly(glutamic acid) (PGA), poly(N-isopropyl acrylamide) (PNIPAM), poly(N,N'- diethyl acrylamide) (PDEAM), polystyrene and poly(ethylene glycol) (PEG). Due to its biocompatibility, PEG is identified as polymer of choice for bioconjugation and different

PEGylated drugs are already in the market and many in clinical trials [23].

Beside reducing the elimination rate, a chemical conjugation may increase the drug specificity or potency: for instance, in enzyme replacement therapy, the binding with mannose 6-phosphate improves the lysosome localization by promoting receptor mediated endocytosis [1].

2. Molecular approaches:

   The progress in recombinant technology and molecular design has allowed the development of molecular modifications.

   Compared with chemical modifications, they require major efforts and time, but less heterogeneous products are generally obtained.

   For protein drugs, many examples of recombinant biomolecules are reported and they generally designed for improving pharmacokinetics properties of BD.

   For example, a fusion protein containing the therapeutic moiety and a non-structured polypeptide based on Pro, Ala, and/or Ser (PAS) show a reduced renal filtration: indeed, as PEG, PAS forms a random coil that increase the hydrodynamic volume of the complex [9]. Another approach uses long-circulating protein fused with the therapeutic one: for instance, it has been proved that albumin or Fc conjugations are able to significantly extend the drug half-life [9].

   In some cases, even altering small portions of amino acids sequence may increase the protein drug efficacy. A result of this approach is the insulin analogues development. Indeed, standard insulin administrated by subcutaneous injection fails in mimicking the endogenous peptide

secretion. It was observed that small changes in insulin primary structure may improve its pharmacokinetics features controlling the peptide aggregation state and release. As result, rapidly and long acting insulin were developed significantly increasing the glycemic control [11].

3. The use of drug delivery systems (DDS):

   Whereas the chemical or biological modification of the drug leads to the creation of a new chemical entity, the development of a DDS involves lower-cost research and, hence, is a preferable approach for the pharmaceutical companies [24].

   A wide range of systems is reported increasing the drug delivery and availability.

   The nanoparticles, for instance, are emerging as versatile platforms: they are able to improve the biopharmaceutical properties of BD, protecting them from degradation and enhancing their permeability [25] [24]. The potential of this DDS will further explore in the section 2.

   Other examples reported are DDS for sustained release: these formulations are expected to reduce the frequency of administration providing greater safety, therapeutic efficacy and patient compliance. They are generally administered by parenteral route and they may be divided in solid implants, microparticles, solid crystals and hydrogels [24].

   In addition, many DDS are designed to improve the biodistribution of BD administered by non-invasive routes such as oral, pulmonary and intranasal [1] . As mentioned above (1.3 section), many BD are used to

treat chronic disorders, which requires long-term administration, and in these circumstances, the conventional parenteral route causes a poor patient compliance. Among all the non-invasive routes, the oral is the most investigated because of its convenience, ease of administration and improved patient acceptance [26]. The major challenge to oral DDS development is the poor bioavailability of BD: due to their chemical structure, they are susceptible to harsh conditions of the gastrointestinal tract and exhibit poor permeability.

Thus, different formulation strategies have been proposed to improve BD availability.

In protein-based therapy, the inclusion of protease-inhibiting excipient in the formulation limit the gastric and intestinal degradation, while the co-administration of permeation enhancers promotes transcellular (surfactants) or paracellular (polyamine and chitosan) absorption of the drug through the intestinal epithelium [27] [28] [24].

In order to prolong the residence time on the intestinal site, mucoadhesive systems have been developed: indeed, several polymers are able to bind the mucus layer by covalent (*e.g.*, disulfide bridging with cysteine residues of mucin) or non-covalent (*e.g.*, electrostatic forces, hydrophobic interactions, hydrogen bonding, van der Waals bonding) interactions [26] [29].

Another interesting approach proposed for protein delivery is the colonic release. Compared to the upper regions, the longer transit time and the concomitant lower levels of proteases and mucosal P-glycoproteins observed make the colon targeting really appealing for BD release and absorption. Thus, different DDS were developed

exploiting the singular environment of this region including microflora-, pH-, pressure- and time-dependent systems [30].

4. Physical approaches:

   In order to counteract the cell membrane barrier and improve the intracellular delivery of BD, many physical methods have been investigated especially in gene delivery.

   These approaches include electroporation, sonoporation, hydroporation and photoporation where electric forces, ultrasound waves, hydrodynamic pressure and single laser pulse respectively are used to transiently permeabilize the cell membrane [31].

2. Nanotechnology and nanomedicine

2.1 Introduction

Nanotechnology is defined as design, characterization, production and application of structures, devices and systems at the nanometer scale [32]. This scale typically refers to a size range included between 1-100 nanometers and nanomaterials show different or enhanced performance compared with the same at larger scale. This difference in physico-chemical properties, resulting from the relatively large surface area and the increased dominance of quantum effects, make them attractive for several purposes [32].

Among the potential application fields, the biomedical one is particularly relevant: indeed, biological systems may be considered as nanodevices, so their interaction with nanomaterials is generally promoted (Fig. 2.1.1). In nanomedicine, diseases diagnosis, drug delivery and molecular imaging are being the most extensively researched areas.

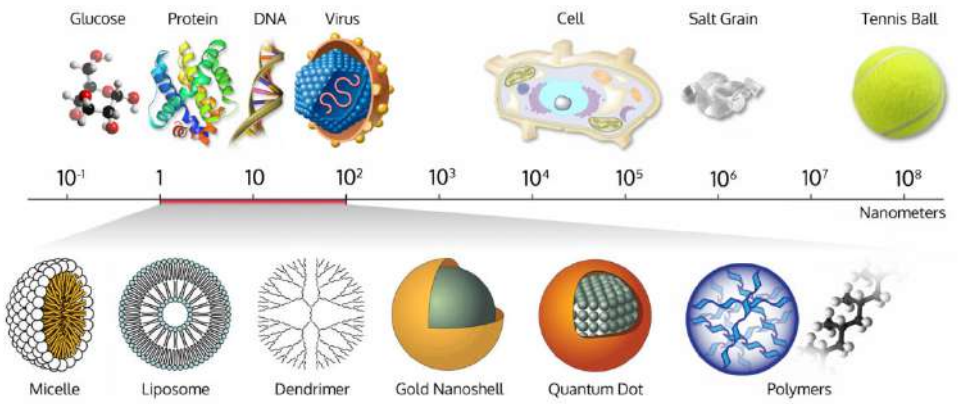

Fig 2.1.1: Size comparison of the most employed nanoparticles with same or larger scale materials; reproduced with permission from [33].

2.2 Nanoparticles for biomedical application

In nanomedicine, nanoparticles (NPs) are the most employed tools for biomedical applications. It has to be acknowledged that not all particles proposed comply with the generally accepted definition of a size lower than 100 nm. However, to some extent, this increase in size doesn't affect their biological properties [34]. In any case, the high surface area to mass ratio of NPs, combined with tunable characteristics and functionality, makes them really versatile and, thus, attractive in this field [35].

2.2.1 NPs requirements for *in vivo* administration

NPs suitable for medical purposes should be soluble in biological environment, biocompatible (able to integrate with a biological system without eliciting immune response or any negative effects) and nontoxic [36].

In drug delivery and imaging areas, acceptable biodistribution and pharmacokinetics properties are additionally required. Indeed, considering the framework of sequential barriers encountered by NPs upon the administration, many obstacles limit site-specific accumulation [37]. Therefore, properties of NPs should be optimized tailoring their specific application.

A summary of tunable properties of NPs is reported below (Fig. 2.2.1) [38].

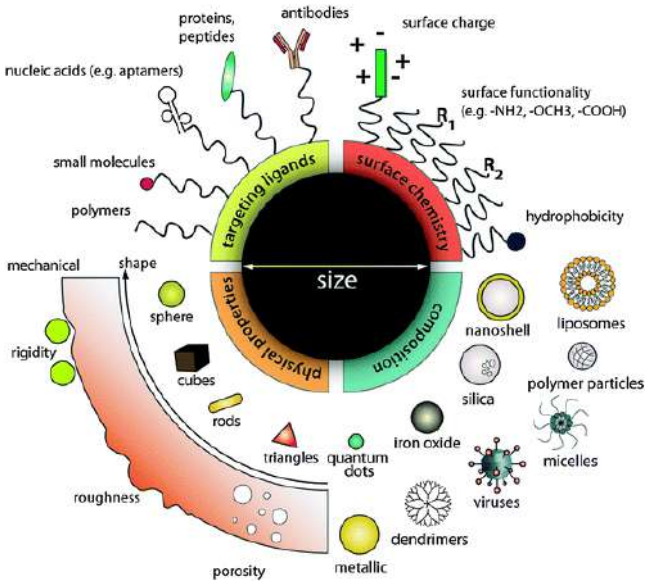

Fig. 2.2.1: Tunable properties of NPs; reproduced with permission from [38].

From a pharmacokinetic point of view, long circulating NPs are required and several properties such as size, shape and surface chemistry, affect the elimination process.

The biodistribution of the NPs in the major organs of clearance is shown in the Figure 2.2.2.

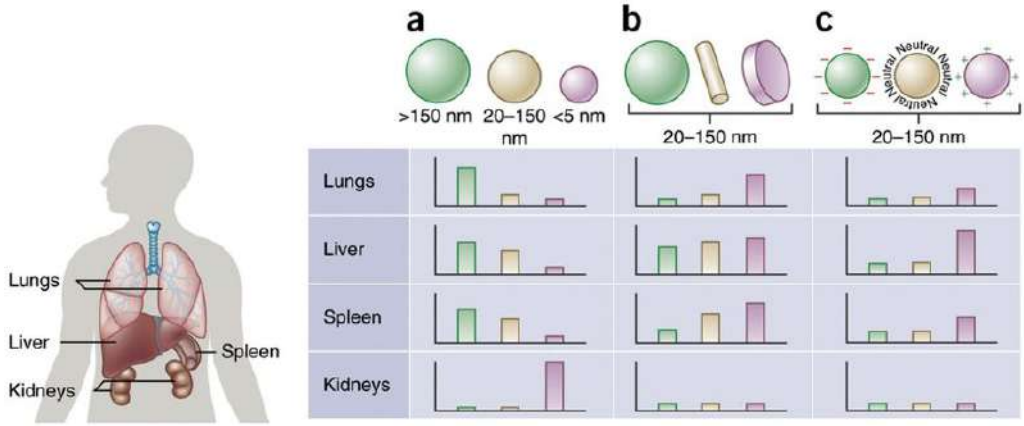

Fig 2.2.2: NPs biodistribution among the different clearance organs; reproduced with permission from [37].

NPs size (Fig. 2.2.2A) is an important design parameter that can be tailored to control the NPs biodistribution from the blood stream.

NPs with a diameter lower than 5 nm rapidly undergo renal clearance [39], while liver filtration principally involved objects included in the range between 50 and 100 nm [40]. Moreover, in case of NPs larger than 200 nm, a massive splenic accumulation is observed, due to the 200–500 nm size range of inter-endothelial cell fenestrations [41]. In addition, particles close to the micrometer readily accumulate in the lungs' capillaries.

According to what previously reported, it is generally accepted that ∼100 nm NPs prove long lasting in circulation [37].

Along with the filtration, the mononuclear phagocyte system (MPS) uptake plays an important role in NPs clearance. The MPS is composed of monocytes with high phagocytic activity, which include Kupffer cells in the liver and mononuclear cells accumulated in the spleen and lymph nodes, and generally provide to particulate greater than 500 nm [42].

Together with the size, the surface properties of the NPs are responsible of MPS uptake. For example, positively charged and highly protein-coated NPs are rapidly endocytosed by MPS, resulting in their removal from circulation and accumulation in organs, such as liver and spleen (Fig. 2.2.2C).

Moreover, the shape of NPs can have a profound effect on their *in vivo* intracellular delivery by affecting the series of extracellular transport events (*i.e.* circulation, extravasation, and tissue penetration) (Fig. 2.2.2B).

In order to extend NPs half-life, several approaches have been proposed (Fig 2.2.3): PEGylation or functionalization with highly hydrophilic polymers represent a classic strategy for phagocytosis avoiding. Indeed, grafting of PEG

to the NPs surface provides a hydrating layer that reduce the opsonization and, therefore, hide them from MPS [43]. Other strategies reported are the NPs coating with red blood cells- or leukocyte-derived membranes [45] [46] or the functionalization with self-peptides [44]. The latter approach is based on the use of portion of membrane proteins (*e.g.* CD47) that physiologically avoid the clearance of self cells.

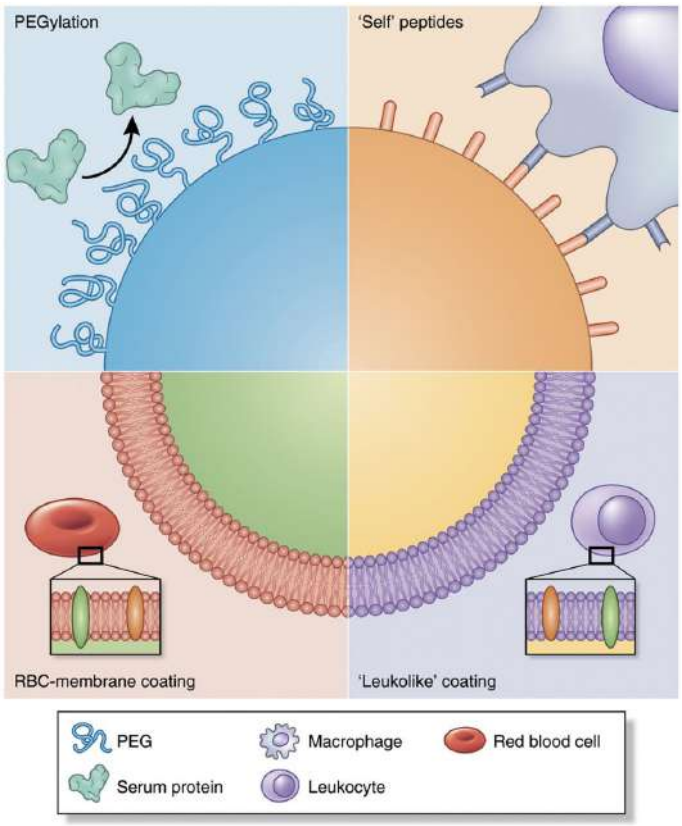

Fig 2.2.3: Strategies to achieve biomimetic NPs; reproduced with permission from [37].

Beside the pharmacokinetics properties optimization, the NPs distribution may be improved by targeting the site of action. Two main strategies called passive and active targeting respectively enhance the NPs effectiveness [47]. Passive

targeting exploits general features of the targeted tissues, whereas active targeting relies on specific recognition of ligands displayed on NPs surface by cell receptors. Several ligands have been proposed for active targeting purposes including aptamers, small molecules, peptides and proteins [38]. The NPs biofunctionalization with targeting agent can be obtained through electrostatic absorption, chemical conjugations or exploiting specific molecular interaction (*e.g.* streptavidin-biotin linkers).

A clear example of targeting implications and meaning is given by the use of NPs in cancer therapy and diagnosis (Fig 2.2.4).

A common characteristic shared by several tumors is the leaky blood vessels, consequence of a rapid and defective angiogenesis, and poor lymphatic drainage [47]. In this context, a nanocarrier can extravasate and be retained into the tumor tissue. The so-called enhanced permeability and retention (EPR) effect is responsible of a passive NPs accumulation in the tumor.

Once located in the desired site, the nanocarrier generally needs to be internalized by the tumor cells [48]. In these circumstances, the active targeting plays its role improving the surface binding and hence, receptor-mediated cellular uptake of the NP.

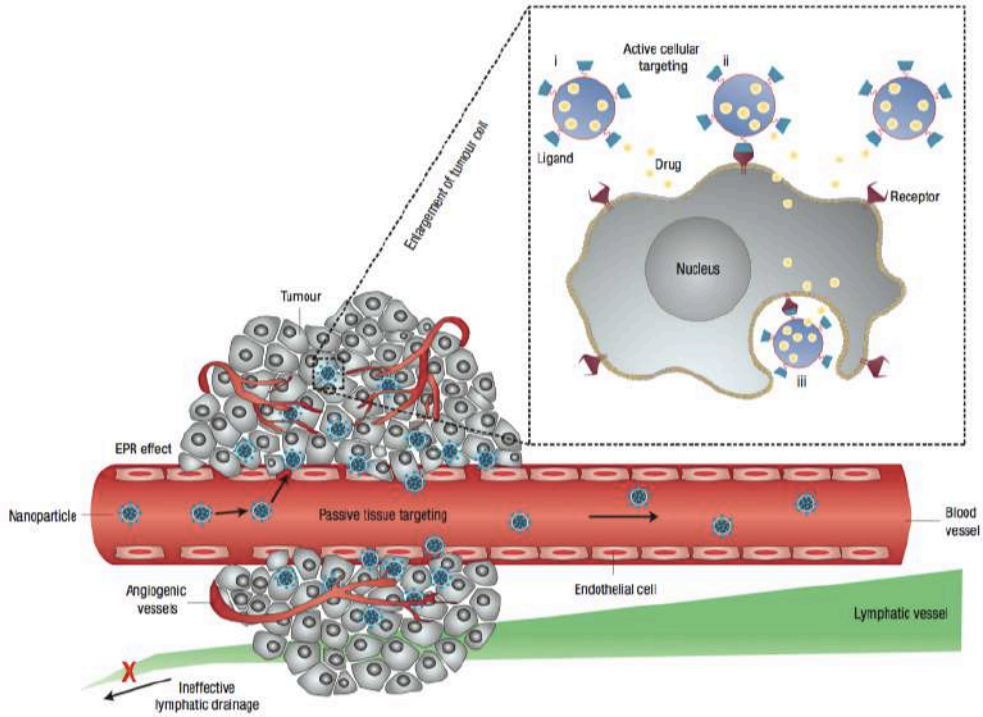

Fig 2.2.4: Schematic representation of passive and active targeting of NPs by tumor tissue; reproduced with permission from [47].

2.3 Nanoparticles as drug delivery systems

2.3.1 Properties

Among the nanomedicine applications, one of the most promising is the design of novel drug delivery systems (DDS). Indeed, the efficacy of some existing drugs is seriously limited by their poor solubility, short half-life, high toxicity and non-specific activity. Besides the enhanced performance, the development DDS involves low-cost research compared to the discovery of a new active molecule and the renewed formulation may increase the drug

lifespan or enhance the effective patent protection [49]. All the reasons mentioned above make the field attractive for most of pharmaceutical companies and, hence, the drug technology market worth is expected to be around 1,700 billion dollars by 2021 [50].

In this context, nanoparticles (NPs) are emerging as appealing drug carriers.

The active molecule can be encapsulated, entrapped or bound on the NPs surface leading to the formation of nanocapsules, nanospheres and nanoconjugates, respectively.

The improvements obtained by NPs-mediated delivery can be summarized as follow [25] [36] [34] [51] [47]:

1. Enhanced drug protection and permeability: Protein and gene-based drugs are massively inactivated through enzymatic degradation. Moreover, relatively large size of this biomolecules limits their permeability across biological barriers. In these circumstances, the nanocarrier use may improve both bioavailability and distribution properties of biologicals;
2. Extended drug half-life: NPs-mediated generally causes an improvement of drug pharmacokinetics profile by decreasing the binding with serum proteins, the renal and hepatic elimination;
3. Increased drugs solubility: NPs-mediated delivery increases the apparent drug solubility improving its distribution capabilities;
4. Improved drug therapeutic index: the low efficacy and side effects of some drugs are mainly associated to their limited selectivity. An improved drug accumulation and activity in the targeted tissue may be achieved by NPs use. The best example of this improvement may be observed by NPs-mediated administration of chemotherapeutics:

indeed, passive and active targeting of cancer tissue is able to improve their safety profile and decrease the required dose;

5. Controlling the drug release: the drug release may be controlled trough time, rate and site. In case of NPs, major efforts are focused on site targeting DDS where the key goal is to discharge the payloads specifically in the diseased tissue. The release could be triggered by internal (*e.g.* glutathione (GSH) or pH) or external (*e.g.* light) stimuli. Notably, the internal stimuli operate in a biologically control manner, whereas the external stimuli provide spatio-temporal control over the release.

2.3.2 Nanoparticles for biological drugs delivery

Biologic drugs (BD) play a valuable role in the treatment of numerous health conditions.

As stressed earlier (1.4 and 1.5 sections), a proper delivery strategy is required in order to overcome their poor bioavailability and increase the potential of BD based therapies.

Among all the technologies proposed, NPs have been largely investigated: indeed, they are potentially able to improve the drug distribution, reduce its inactivation and elimination and provide the opportunity of non-invasive administration.

In the next paragraphs, nanocarriers used for protein and gene delivery will be discussed.

2.3.2.1 Protein delivery systems

In order to select a proper nanocarrier for *in vivo* protein delivery, several issues need to be considered: first the manufacturing method must not compromise the chemical and physical stability of these drugs. Therefore, environmental factors such as pH, ionic strength, temperature, high pressure, non-aqueous solvents, metal ions, detergents, adsorption, and agitation and shearing shall be finely controlled [52].

In addition, nanocarriers suitable for *in vivo* administration shall be able to provide the cargo protection from denaturation and degradation.

Lastly, for many applications, controlled release, targeting ability or intracellular delivery are additionally required as a means to further reduce the therapeutic dose.

A wide range of nanomaterials have been investigated for this application, but here, for simplification purposes, I will only discuss polymer-, lipid- and protein- based NPs.

1. Polymeric NPs: due to their versatility, polymeric NPs are the most investigated tools. They may be composed by synthetic polymers, such as the FDA approved poly(lactic-co-glycolic acid) (PLGA) and polylactic acid (PLA), or natural polymers as chitosan, dextran, alginate and hyaluronic acid [53] [54]. The drug may be carried in several ways (*i.e.* encapsulation, entrapment, direct conjugation and physical absorption) in which protein-polymer interactions are mainly covalent or electrostatic [54]. The polymer selection is determined by the physico-chemical properties of the protein and the application of the final nanocarrier.

In this context, NPs administered by non-invasive routes (*e.g.* oral, pulmonary and intranasal) are extensively investigated as alternative to parenteral

formulations: indeed, most of protein therapeutics are used for chronic disorders and, so, long treatment times are required. As mentioned in 1.6 section, considerable efforts focus on the oral route because it is the most conventional and safest.

In the development of orally administered nanocarriers, cationic NPs are largely reported as protein delivery vectors [54]. The positively charged polymers are potentially able to enhance the protein bioavailability by two possible mechanisms: the muco-adhesion and the reversible increase in tight junction permeability.

The first action provides to extend the residence time of the drug by the interaction with negatively charged mucus protein (*i.e.* highly glycosylated mucins) [55], while the enhanced permeability may improve the paracellular absorption of the drug [27].

2. Lipidic NPs: these nanovectors are generally composed by biomimetic and biodegradable materials and they can be classified in liposomes and solid lipid NPs (SLN) [52].

Liposomes are a well-established and extensively investigated nanocarriers that consists of one or more phospholipid bilayers separated by aqueous compartments. Their compositions and surface features may be tailored for enhancing drug release properties [56]. Despite the intense researches, some disadvantages need to be overcome such as short shelf-life, poor *in vivo* stability, low encapsulation efficacy and reproducibility.

SLN are composed by a solid lipid phase (*e.g.* triglycerides, complex glyceride mixtures or waxes) stabilized with a surfactant [57]. The major limitation of protein-containing SLN is the hard control of drug release: indeed, due to their highly hydrophobic core, burst release is commonly obtained [52].

3. Protein NPs: they may be synthetized by desolvation (*e.g.* albumin and gelatin NPs) or composed by self-assembled macromolecules like in case of ferritin, virus like and vault cages [58]. Nowadays, they have extensively investigated as alternative nanocarriers due to their biodegradability, biofunctionality, high encapsulation efficiency and retention of drug bioactivity. Despite these advantages, several limitations generally associated with biomacromolecules remain including immunogenicity, poor stability and challenging regulatory approval (for additional information see 1.1, 1.2, 1.4 and 1.5 sections) [58].

2.3.2.2 Gene delivery systems

In gene therapy, the modulation of gene expression is obtained by the delivery of exogenous genetic material such as DNA (mainly pDNA), mRNA and RNA interfering molecules.

In order to be effective after *in vivo* administration, nucleic acids require to overcome various extracellular barrier and gain the cellular entry. Unlike several protein drugs, the cellular uptake is essential because the genetic modulation occurs in the cytosol (RNA) or in the nucleus (DNA) [15] (Fig. 2.3.2.2.1).

The poor permeability generally associated with large and negatively charged macromolecules makes the design of a functional gene delivery system so challenging. Indeed, besides increasing the drug accumulation in the targeted tissue, the ideal vector needs to provide its intracellular delivery [15].

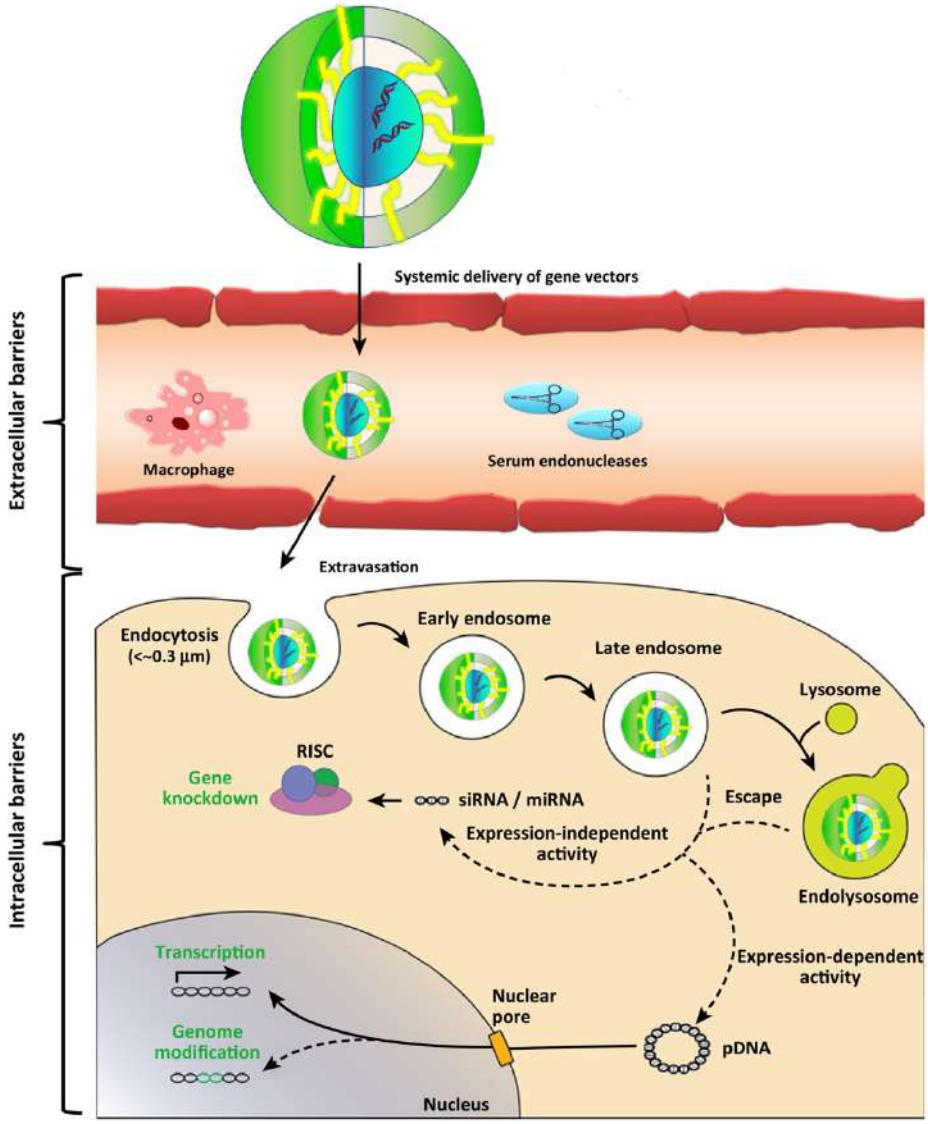

Fig. 2.3.2.2.1: Gene delivery mechanism; adapted with permission from [15].

The nanocarriers used for transfection purposes are conventionally classified in viral and non-viral vectors.

Currently, most of the clinical trials conducted for gene therapy purposes used viral vectors (VV) such as adeno-viruses, adeno-associated viruses (AAVs), lentiviruses, or retroviruses. They are obtained by substituting most of the viral

genome with the therapeutic nucleic acids of interest [59]. A brief overview of their properties is reported below (Table 2.3.2.2.1): in order to select the proper vector, several factors need to be considered including capacity, immunogenicity, tissue/cell specificity (tropism) or the type of expression (*e.g.* stable or transient) [59].

	Virus			
	Lentivirus	**AAV**	**Adenovirus**	**Retrovirus**
Expression	Stable	Transient	Transient	Stable
Genome	RNA	ssDNA	dsDNA	RNA
Packaging Capacity	<8 Kb	~4.5 Kb	>8 Kb	<8 Kb
Virus Size (nm)	80-130	18-26	105	80-130
Cells Infected	Dividing/ Non-dividing	Dividing/ Non-dividing	Dividing/ Non-dividing	Dividing
Target Cell Genome Integration	Yes	No	No	Yes
Immune Response	Low	Very Low	High	Moderate

Table 2.3.2.2.1: Viral vectors properties; adapted with permission from [60].

Despite their high transfection efficiency, VV have several drawbacks such as the limited DNA packaging capacity, the complex production procedure, the broad tropism and the serious safety risks (*i.e.* cytotoxicity, immunogenicity and tumorigenicity) [15]. Considering all the above, the investigation of alternative systems is still appealing.

The class of non-viral vectors (NVV) include several types of NPs that can be further divided in lipidic, polymeric, inorganic and biologically derived vectors.

The intense investigation associated to these “synthetic” vectors relies the flexibility in their design: indeed, whereas the VV structure and capacity are fixed, these NNV can be engineered for a specific application.

A brief overview of the main NNV is reported below:

1. Lipidic NPs: several lipids have been developed for gene transfer, but all of them share a similar structure: a hydrophilic cationic head connected by a linker to a hydrophobic moiety.

Due to their positive charges, these materials are able to electrostatically interact and condense with the nucleic acids forming the so called lipoplexes.

Among all, cationic liposomes have been shown as versatile and useful transfection tools [61]. These NPs are able to improve the cellular uptake by interaction with negatively charged cell membrane proteins and help cytoplasmic delivery of nucleic acids by the interruption of endosomal membrane [62]. The detailed mechanism of endosomal disruption is reported in Fig. 2.3.2.2.2.

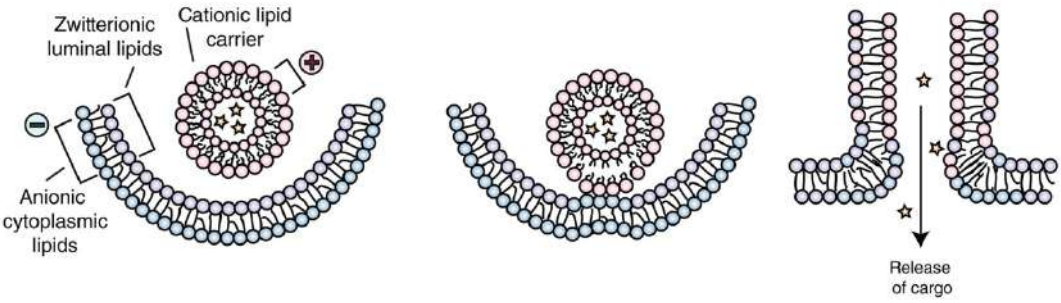

Fig. 2.3.2.2.2: Endosomal escape mediated by liposomes (reproduced with permission from [74]): cationic lipids interact with the endosomal membrane via ion-pairing, causing membrane fusion and payload release.

In contrast, the efficiency of this systems is strongly limited by high clearance from the bloodstream and inflammatory toxicity associated with large cationic

particles [64]. Moreover, the serum proteins interaction may induce liposomes destabilization and burst release of the payload.

Different strategies have been proposed for enhancing the drug delivery: PEG-grafting is a common approach for reducing the MPS uptake, while the NP biofunctionalization with specific ligands promotes the targeting of specific cells (see 2.2 section). In addition, cholesterol inclusion in liposomes formulation is reported to increase their physical stability and enhance the retention of the cargo [65].

Although the transfection capacity has been improved, further investigations are required to become a real alternative to the extremely efficient VV [15]. Besides the system efficacy, a further limitation for clinical development is short shelf-life generally associated with lipoplexes.

2. Polymeric NPs: the controlled condensation of cationic polymers with nucleic acids leads to polyplexes genesis. This nanosized complexes are more stable than lipoplexes and generally composed by polyethyleneimine, polylisine, chitosan, polymethacrylate or polyesters [61].

As cationic NPs they share all the pros and cons generally associated with the lipidic NPs.

In polyplexes, the intracellular delivery is mainly caused by the so-called proton sponge effect (Fig. 2.3.2.2.3): depending on their buffering capacity, cationic polymers are able to block the endosome acidification causing the osmotic swelling and membrane disruption [66].

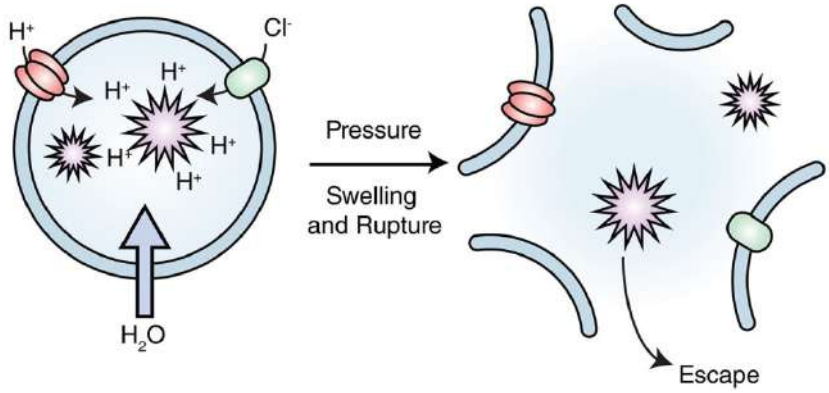

Fig. 2.3.2.2.3: Endosomal escape by proton sponge effect (reproduced with permission from [74]): polymers capable of buffering become protonated as protons are pumped into endosomes. Chloride ions are also transported to maintain the charge balance within the endosome. The increase in ion concentration causes osmotic swelling and ruptures the membrane.

3. Inorganic NPs: the most investigated systems are calcium phosphate and gold NPs.

The calcium phosphate is well-known biocompatible material generally employed for *ex vivo* transfections: indeed, an excess of bivalent cation is able to condense the DNA. Due to the low loading capacity and poor stability, calcium phosphate crystals have limited potential [61].

On the other hand, gold NPs are easy to prepare, inert and relatively stable. In addition, some properties such as the tunable size and surface properties and multifunctional capabilities makes this tool really attractive. In this case, the nucleic acids can be anchored onto NPs surface by covalent interaction [67].

4. Biologically derived vectors: unlike the other NVV, they are perceived as "fully compatible" materials and thus, able to mediate and enhance gene-delivery efficacy [15]. However, the complex synthesis and purification and

long lead times required for product reengineering significantly restrict their use.

Bibliography

[1] R. Ho, Biotechnology and Biopharmaceuticals: transforming proteins and genes into drugs, John Wiley & Sons, Inc., 2013.

[2] FDA, “What Are "Biologics" Questions and Answers,” FDA, [Online]. Available: https://www.fda.gov/aboutfda/centersoffices/officeofmedicalproductsandtobacco/cber/ucm133077.htm. [Accessed 7 August 2018].

[3] A. O'Connor, “Introduction to biotech drugs,” Regulatory Rapporteur, 2009.

[4] Statista, “Total global biologics spending from 2002 and 2017 (in billion U.S. dollars),” Statista, [Online]. Available: https://www.statista.com/statistics/280578/global-biologics-spending/. [Accessed 7 august 2018].

[5] Statista, “Number of biopharma medicines in development in the U.S. as of May 2018, by therapeutic category,” Statista, Available: https://www.statista.com/statistics/258152/biologic-medicines-in-development-by-therapeutic-category-2016/. [Accessed 07 August 2018].

[6] Bayer, “Small and Large molecules,” Bayer, [Online]. Available: http://pharma.bayer.com/en/innovation-partnering/technologies-and-trends/small-and-large-molecules/. [Accessed 6 August 2018].

[7] J. Monteiro, “Structure-Bioactivity Relationships of Methylxanthines: Trying to Make Sense of All the Promises and the Drawbacks,” Molecules, vol. 21, no. 8, 2016.

[8] GabiOnline, “Small molecule versus biological drugs,” GabiOnline, 29 June 2012. [Online]. Available: http://www.gabionline.net/Biosimilars/Research/Small-molecule-versus-biological-drugs. [Accessed 06 August 2018].

[9] A. Zelikin, “Materials and methods for delivery of biological drugs,” Nat. Chem., vol. 8, p. 997-1007, 2016.

[10] J. Lin, “Pharmacokinetics of Biotech Drugs: Peptides, Proteins and Monoclonal Antibodies,” Current Drug Metabolism, vol. 10, p. 661.691, 2009.

[11] I. Hirsch, “Insulin Analogues,” N Engl J Med, vol. 352, p. 174-183, 2005.

[12] H. Lagassé, “Recent advances in (therapeutic protein) drug development,” F1000Research 2017, vol. 6, p. 1-17, 2017.

[13] D. Hooven, “Opportunities and Challenges in Biologic Drug Delivery,” American Pharmaceutical Review, 22 December 2017. [Accessed 07 August 2018].

[14] J. Moss, “Gene therapy review,” Radiol Technol., vol. 86, no. 2, p. 155-180, 2014.

[15] A. Hill, “Overcoming Gene-Delivery Hurdles: Physiological Considerations for Nonviral Vectors,” Trends in Biotech., vol. 34, p. 91-105, 2016.

[16] NCBI, “RNA Interference (RNAi),” NCBI, [Online]. Available: https://www.ncbi.nlm.nih.gov/probe/docs/techrnai/. [Accessed 29 August 2018].

[17] D. Wang, “State-Of-The-Art Human Gene Therapy: Part II. Gene Therapy Strategies and Clinical Applications,” Discov. Med., vol. 18, no. 98, p. 151-161, 2014.

[18] A. Patel, “Recent Advances in Protein and Peptide Drug Delivery: A Special Emphasis on Polymeric Nanoparticles,” Protein Pept. Lett., vol. 21, p. 1102-1120, 2014.

[19] V. Agrahari, “Nanocarrier fabrication and macromolecule drug delivery: challenges and opportunities,” Ther. Deliv., vol. 7, p. 257-278, 2016.

[20] T. Ahmed, “Preparation, characterization, and potential application of chitosan, chitosan derivatives, and chitosan metal nanoparticles in pharmaceutical drug delivery,” Drug Des. Devel. Ther., vol. 10, p. 483-507, 2016.

[21] M. Barry, “Role of Endogenous Endonucleases and Tissue Site in Transfection and CpG-Mediated Immune Activation after Naked DNA Injection,” Human Gene Therapy, vol. 10, no. 15, p. 2461-2480, 2004.

[22] M. Deehan, “Managing unwanted immunogenicity of biologicals,” Autoimmunity Reviews, vol. 14, p. 569-574, 2015.

[23] C. Fee, “Protein PEGylation: An overview of chemistry and process considerations,” European pharmaceutical reviews, 22 February 2010. [Online]. Available: https://www.europeanpharmaceuticalreview.com/article/494/protein-pegylation-process/. [Accessed 10 August 2018].

[24] N. Škalko-Basnet, “Biologics: the role of delivery systems in improved therapy,” Biologics. 2014; 8: 107–114., vol. 8, p. 107-114, 2014.

[25] W. De Jong, “Drug delivery and nanoparticles: Applications and hazards,” International Journal of Nanomedicine, vol. 3, no. 2, p. 133-149, 2008.

[26] S. Chung, “Strategies for non-invasive delivery of biologics,” Journal of Drug Targeting, vol. 20, no. 6, p. 481-501, 2012.

[27] G. Ranaldi, “The effect of chitosan and other polycations on tight junction permeability in the human intestinal Caco-2 cell line,” Nutr. Biochem., vol. 13, p. 157-167, 2002.

[28] B. Aungst, “Absorption Enhancers: Applications and Advances,” The AAPS Journal, vol. 14, p. 10-18, 2012.

[29] A. Sosnik, “Mucoadhesive polymers in the design of nano-drug delivery systems for administration by non-parenteral routes: A review,” Progress in Polymer Science, vol. 39, p. 2030-2075, 2014.

[30] A. Gazzaniga, “Time-controlled oral delivery systems for colon targeting,” Exp. Opin. Drug Deliv., vol. 3, p. 583–597, 2006.

[31] S. Mehier-Humbert, “Physical methods for gene transfer: Improving the kinetics of gene delivery into cells,” Advanced Drug Delivery Reviews, vol. 57, p. 733–753, 2005.

[32] The Royal Society and Royal Academy of Engineering, “Nanoscience and nanotechnologies: opportunities and uncertainties,” The Royal Society and Royal Academy of Engineering, London, 2004.

[33] W. Lab, “Size-comparison bionanoparticles,” Wich Lab, [Online]. Available: http://www.wichlab.com/nanometer-scale-comparison-nanoparticle-size-comparison-nanotechnology-chart-ruler-2/. [Accessed 27 August 2018].

[34] B. Kumar, “Recent advances in nanoparticle-mediated drug delivery,” J. of Drug Del. Science and Tech., vol. 41, p. 260-268, 2017.

[35] J. Maximilien, “Nanoparticles in biomedical applications,” in Measuring biological impacts of nanomaterials, Springer, p. 177-210, 2015.

[36] A. Wilczewska, “Nanoparticles as drug delivery systems,” Pharm. reports, vol. 64, p. 1020-1037, 2012.

[37] E. Blanco, “Principles of nanoparticle design for overcoming biological barriers to drug delivery,” Nat. Biotech., vol. 33, p. 941-951, 2015.

[38] L. Chou, “Strategies for the intracellular delivery of nanoparticles,” Chem. Soc. Rev., vol. 40, p. 233-245, 2011.

[39] H. Choi, “Renal clearance of quantum dots,” Nat. Biotechnol., vol. 25, p. 1165–1170, 2007.

[40] F. Braet, “Contribution of high-resolution correlative imaging techniques in the study of the liver sieve in three-dimensions,” Microsc. Res. Tech., vol. 70, p. 230–242, 2007.

[41] L. Chen, “The role of the sinus wall in the passage of erythrocytes through the spleen,” Blood, vol. 41, p. 529–537, 1973.

[42] R. Ho, Biotechnology and Biopharmaceuticals: Transforming Proteins and Genes Into Drugs, John Wiley & Sons, Inc., 2013.

[43] C. Walkey, “Nanoparticle size and surface chemistry determine serum protein adsorption and macrophage uptake,” J. Am. Chem. Soc. 134, 2139–2147 (2012). vol. 134, p. 2139–2147, 2012.

[44] P. Rodriguez, “Minimal “Self” peptides that inhibit phagocytic clearance and enhance delivery of nanoparticles,” Science , vol. 339, p. 971–975, 2013.

[45] A. Parodi, “Synthetic nanoparticles functionalized with biomimetic leukocyte membranes possess cell-like functions,” Nat. Nanotechnol., vol. 8, p. 61–68, 2013.

[46] C. Hu, “Erythrocyte membrane-camouflaged polymeric nanoparticles as a biomimetic delivery platform,” Proc. Natl. Acad. Sci. USA, vol. 108, p. 10980–10985, 2011.

[47] D. Peer, “Nanocarriers as an emerging platform for cancer therapy,” Nat. Nanotech., vol. 2, p. 751-760, 2007.

[48] R. Misra, “Cancer nanotechnology: application of nanotechnology in cancer therapy,” Drug Discovery Today, vol. 15, p. 842-850, 2010.

[49] S. Sahoo, “Nanotech approaches to drug delivery and imaging,” Drug discovery today, vol. 8, p. 1112-1120, 2003.

[50] Marketsandmarkets, “Drug delivery technologies market forecasts,” Marketsandmarkets, January 2017. [Online]. Available: https://www.marketsandmarkets.com/Market-Reports/drug-delivery-technologies-market-1085.html. [Accessed 8 August 2018].

[51] C. Crucho, “Stimuli-Responsive Polymeric Nanoparticles for Nanomedicine,” ChemMedChem, vol. 10, p. 24-38, 2015.

[52] A. Almeida, “Solid lipid nanoparticles as a drug delivery system for peptides and proteins,” Advanced Drug Delivery Reviews, vol. 59, p. 478-490, 2007.

[53] M. Hamid Akash, “Natural and Synthetic Polymers as Drug Carriers for Delivery of Therapeutic Proteins,” Polymer Reviews, vol. 55, p. 371–406, 2015.

[54] H. Zhao, “Polymer-based nanoparticles for protein delivery: design, strategies and applications,” J. Mater. Chem. B, vol. 4, p. 4060-4071, 2016.

[55] L. Ensign, “Oral drug delivery with polymeric nanoparticles: the gastrointestinal mucus barriers,” Adv. Drug Deliv. Rev., vol. 64, p. 557-570, 2012.

[56] M. Focarete, Core-Shell Nanostructures for Drug Delivery and Theranostics, Woodhead Publishing, 2018.

[57] N. Naseri, “Solid Lipid Nanoparticles and Nanostructured Lipid Carriers: Structure, Preparation and Application,” Adv Pharm Bull., vol. 5, no. 3, p. 305–313, 2015.

[58] L. Herrera Estrada, “Protein nanoparticles for therapeutic protein delivery,” Biomater. Sci., vol. 3, p. 787-799, 2015.

[59] M. Giacca, “Virus-mediated gene delivery for human gene therapy,” J. of Controlled Release, vol. 161, p. 377-388, 2012.

[60] C.E. Thomas, “Progress and problems with the use of viral vectors for gene therapy,” Nat. Gen. Rev., vol. 4, p. 346-356, 2003.

[61] M. Ramamoorth, “Non Viral Vectors in Gene Therapy- An Overview,” J Clin Diagn Res. 2015 Jan; 9(1), vol. 9, no. 1, p. 1-6, 2015.

[62] Y. Zhao, “Lipid Nanoparticles for Gene Delivery,” Adv Genet., vol. 88, p. 13-36, 2014.

[63] S. Li, “Stealth nanoparticles: High density but sheddable PEG is a key for tumor targeting,” J. of Controlled Release, vol. 145, p. 178-181, 2010.

[64] R. Levine, “Preparation and Characterization of Liposome-Encapsulated Plasmid DNA for Gene Delivery,” Langmuir, vol. 29, p. 9208−9215, 2013.

[65] L. Tseng, “Liposomes incorporated with cholesterol for drug release triggered by magnetic field,” J. med. biol. eng., vol. 27, no. 1, p. 29-34, 2007.

[66] J. Behr, “The Proton Sponge: a Trick to Enter Cells the Viruses Did Not Exploit,” Chimia, vol. 51, p. 34-36, 1997.

[67] Y. Ding, “Gold Nanoparticles for Nucleic Acid Delivery,” Molecular therapy, vol. 22, no. 6, p. 1075-1083, 2014.

[68] W. Chen, “Microneedles as a Delivery System for Gene Therapy,” Front Pharmacol., p. vol. 26, no. 7, p.137., 2016.

[69] D.D. Young JL, “Electroporation-mediated gene delivery.,” Adv Genet., vol. 89, p. 49-88, 2015.

[70] E. McNeill, “Hydrodynamic Gene Delivery of CC Chemokine Binding Fc Fusion Proteins to Target Acute Vascular Inflammation *In Vivo*,” Sci Rep., vol. 5, no. 17404, 2015.

[71] Q.L. Zhou, “Ultrasound-mediated local drug and gene delivery using nanocarriers,” Biomed Res Int., vol. 2014, Article ID 963891, 13 pages, 2014.

[72] S.S. Titze de Almeida, “Delivery of miRNA-Targeted Oligonucleotides in the Rat Striatum by Magnetofection with Neuromag®,” Molecules, vol. 23, no. 7, 2018.

[73] D. Scherman, Advanced Textbook on Gene Transfer, Gene Therapy and Genetic Pharmacology, London: Imperial College Press, 2014.

[74] L.I. Selby, “Nanoescapology: progress toward understanding the endosomal escape of polymeric nanoparticles,” Wiley Interdiscip Rev Nanomed Nanobiotechnol., vol. 9, no. 5, 2017.

Aim

Biologic drugs (BD) include a wide range of products such as proteins, peptides, genetic materials and cells (*e.g.* blood, somatic cells, tissues), produced by biotechnology [1].

Compared with the traditional small chemical drugs, BD generally show higher potency and selectivity of action and, so, have the potential to address many chronic diseases and various unmet medical needs [2].

Unfortunately, most of BD are characterized by short circulating half-life, low stability, poor permeability and rapid body clearance *via* glomerular filtration [3]. Thus, several strategies have been proposed to overcome these drawbacks enhancing the drug efficacy [4] [2].

In this context, nanoparticles (NPs) emerge as valid drug delivery tools: indeed, they are potentially able to improve the drug distribution, reduce its inactivation and elimination and provide the opportunity of non-invasive administration [5] [6] [7].

In view of the above, the aim of this thesis was the development of NPs-based BD delivery systems.

In particular, I was involved in two distinct projects concerning the peptide and the gene delivery respectively.

1. Development of a nanocarrier for insulin oral administration

The current treatment of diabetes disease relies on insulin subcutaneous injection [8]. Because of parenteral administration drawbacks, alternative administration routes have been investigated [9]. Among all, the oral administration may lead to a better glucose regulation and enhanced patients' compliance [10]. However, the oral bioavailability of peptides is very low and

several efforts have been attempted to promote insulin bowel absorption. Despite all, the oral delivery of insulin remains an unmet need [9]. On this basis, the aim of work was to prepare, characterize and evaluate both *in vitro* and *in vivo* a novel nanoformulated multiple-unit colon delivery system, *i.e.* coated pellets, as a possible oral nanocarrier for insulin.

2. Development of lipidic NPs as gene delivery vectors in triple negative breast cancer

Triple negative breast cancer (TNBC) is one of the most aggressive and difficult cancer to treat and it accounts for 15-20% of breast cancers [8]. Actual therapies in use for TNBC treatment (including chemotherapy, radiotherapy and surgery) are characterized by restricted efficacy and serious side effects [9]. In this scenario, gene therapy has recently emerged as new therapeutic approach.

Numerous vectors have been developed to overcome the poor bioavailability and release specificity of nucleic acids. In this context, targeted lipidic NPs have been introduced as safe alternative to the commonly investigated viral vectors.

Given the above, the aim of the project was the development and the activity evaluation of lipid-protamine-DNA (LPD) NPs with a selective targeting for poorly differentiated TNBC cells.

The antitumoral activity of the nanocomplex was obtain by the inclusion of Saporin (SAPO) encoding plasmid DNA (pDNA), whereas the active targeting was achieved by the NPs functionalization with 11-amino-acid sequence called U11.

SAPO is a well-known ribosome-inactivating protein (RIP), that blocks protein synthesis inducing the cell death [13], while U11 was previously described as

ligand of urokinase plasminogen activator receptor (UPAR), normally overexpressed in TBCN [14]. The potential of this novel drug delivery system was studied both *in vitro* and *in vivo*.

Bibliography

[1] FDA, "What Are "Biologics" Questions and Answers," FDA , [Online]. Available: https://www.fda.gov/aboutfda/centersoffices/officeofmedicalproductsandtobacco/cber/ucm133077.htm. [Accessed 7 August 2018].

[2] A. Zelikin, "Materials and methods for delivery of biological drugs," Nat. Chem. , vol. 8, pp. 997-1007, 2016.

[3] R. Ho, Biotechnology and Biopharmaceuticals: Transforming Proteins and Genes Into Drugs, John Wiley & Sons, Inc., 2013.

[4] D. Hooven, "Opportunities and Challenges in Biologic Drug Delivery," American Pharmaceutical Review, 22 December 2017. [Online]. [Accessed 07 August 2018].

[5] W. De Jong, "Drug delivery and nanoparticles: Applications and hazards," International Journal of Nanomedicine , vol. 3, no. 2, pp. 133-149, 2008.

[6] B. Kumar, "Recent advances in nanoparticle-mediated drug delivery," J. of Drug Del. Science and Tech. , vol. 41, pp. 260-268, 2017.

[7] A. Wilczewska, "Nanoparticles as drug delivery systems," Pharm. reports, vol. 64, pp. 1020-1037, 2012.

[8] A. Maroni, "Oral colon delivery of insulin with the aid of functional adjuvants," Adv. Drug. Deliv. Rev., vol. 64, pp. 540-556, 2012.

[9] F. Sousa, "How to overcome the limitations of current insulin administration with new non-invasive delivery systems," Ther. Deliv., vol. 6, pp. 83-94, 2015.

[10] M. Patel, "Colon targeting: an emerging frontier for oral insulin delivery," Exp. Opin. Drug Deliv., vol. 10, pp. 731-739, 2013.

[11] G. Bianchini, "Triple-negative breast cancer: challenges and opportunities of a heterogeneous disease," Nat Rev Clin Oncol, vol. 13, no. 11, pp. 674-690, 2016.

[12] L. Newman, "The 2014 Society of Surgical Oncology Susan G. Komen for the Cure Symposium: triple-negative breast cancer.," Ann Surg Oncol, vol. 22, no. 3, p. 874, 2015.

[13] L. Polito, "Immunotoxins and Other Conjugates Containing Saporin-S6 for Cancer Therapy," Toxins, vol. 3, no. 6, pp. 697-720, 2011.

[14] Q. Huai, "Structure of human urokinase plasminogen activator in complex with its receptor," Science, vol. 311, pp. 656-659, 2006.

[15] A. Hill, "Overcoming Gene-Delivery Hurdles: Physiological Considerations for Nonviral Vectors," Trends in Biotech., vol. 34, pp. 91-105, 2016.

[16] H. Amer, "Gene therapy for cancer: present status and future perspective," Molecular and Cellular Therapies, vol. 2, no. 27, pp. 1-19, 2014.

Project 1:

Development of a nanocarrier

for insulin oral administration

1. Background

Diabetes mellitus is a group of metabolic diseases characterized by hyperglycemia resulting from defects in insulin secretion, action, or both. The current therapy for the treatment of diabetic patients relies on a correct diet, physical exercise, and oral hypoglycemic agents [1]. In the late stages of Type 2 diabetes or in Type 1 diabetes, when the β pancreatic cells failure is consistent, the replacement with exogenous insulin becomes mandatory for survival [1] [2]. Despite several insulin analogues were developed in order to finely control the glycemia and improve the treatment efficacy [3], nowadays all the commercially available insulin medications are administered by subcutaneous (SC) route which implies one or more daily injections, with a significant reduction in quality of life and, sometimes, poor patient adherence to therapy [4] [5].

Moreover, administration of insulin by SC injection induces portal hypoinsulinaemia and peripheral hyperinsulinaemia which is associated with neuropathy, retinoendopathy etc. [6] (Fig 1.1 panel A). In physiological conditions, half of insulin produced by the pancreas is used for liver metabolism via the portal circulation, resulting in fine regulation of blood glucose levels and adequate metabolism of carbohydrates and proteins [2]. Thus, several research studies have been focused on the development of novel formulations of the hormone through alternative administration routes [7]. Particularly, the oral route has been considered as potentially leading to a better glucose regulation exploiting the liver first-pass metabolism of insulin, preventing the risks of fluctuating blood glucose levels and possibly the

resulting morbidity due to chronic microvascular complications (Fig. 1.1 panel B) [8].

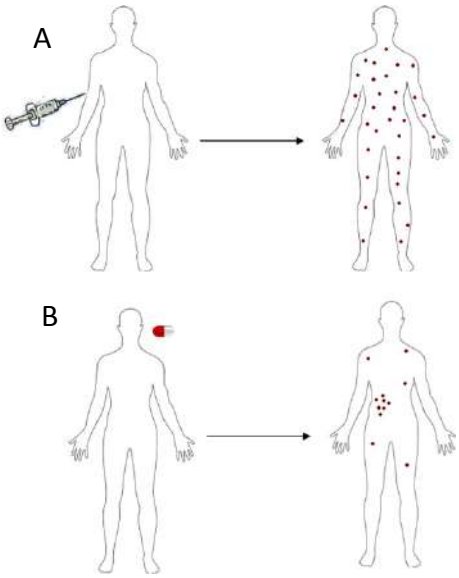

Fig 1.1: Biodistribution of insulin after parenteral (A) and oral (B) administration (reproduced with permission from [5]): after SC injection (A), insulin travels *via* the systemic circulation and only 20% of dose is estimated to accumulate in the liver. On the other hand, when administered by oral route (B), the peptide follows the normal physiological pathway where, via hepatic portal circulation, it first reaches liver and then the peripheral tissues.

Furthermore, in case of chronic treatments, this administration route is the most desirable in terms of patient acceptance [7].

Therefore, an oral formulation of insulin could revolutionize the management of insulin-dependent diabetic patients due to its potential clinical benefits. However, the oral bioavailability of insulin is very low and several efforts have been attempted to promote insulin bowel absorption, avoiding gastric or intestinal degradation by proteases.

Such attempts included formulations with protease inhibitors, absorption enhancers or mucoadhesive systems. Still, oral delivery of insulin remains an unmet medical need [4] [7].

As result of this, colonic delivery and release of insulin have gained increasing interest by researchers because of the longer transit time, prolonged drug localization on the gut mucosa, lower levels of proteases or mucosal P-glycoprotein and greater responsiveness to permeation enhancers compared to the more proximal regions of the gastrointestinal tract. Such features would point colon as interesting target organ for insulin oral delivery but, so far, an efficient drug delivery system for this purpose is still missing [4] [8] [9].

A few attempts to improve the oral delivery of insulin by means of nanoparticle-based vectors have been reported [10] [11] [12]. Several nanoparticles (NPs) types have been designed to protect biological drugs, including insulin, against chemical and enzymatic degradation and to enhance the intestinal absorption through paracellular and transcellular pathways [10] [11]. Structural characteristics of NPs, including size and surface charge, have been shown to influence the insulin absorption by the enterocytes. In general, small particles, provided with a positive charge are absorbed more efficiently through the intestinal epithelium [13]. This is due to the interaction of NPs bearing positive charges with mucin residues that are negatively charged at physiological pH. The consequent prolonged residence time and increased concentration gradient at the surface of the intestinal mucosa might therefore promote peptide/protein absorption [4] [11].

Ex-vivo and *in vivo* studies have also proven the potential of colloidal NPs in increasing insulin absorption throughout the colonic region, but the lack of an appropriate delivery system that ensures their safe transit through the upper

gastrointestinal tract strongly limits their usefulness [12]. Therefore, a solid dosage form, including pellets and tablets, which could host drug-loaded NPs and undergo a subsequent coating process, might represent a valuable strategy to enhance stability and provide release versatility of these colloidal systems administered via oral route [8] [9].

On this basis, as reported in a recently published paper (Paper 1 in list of personal publications) [39], the objective of this project was to prepare, characterize and test both *in vitro* and *in vivo* (*i.e.* diabetic rats), a novel nanoformulated, multiple-unit colon release system, *i.e.* coated pellets, as a possible oral nanocarrier for insulin.

The novelty of this approach was the evaluation of the synergistic effect of colon release and muco-adhesive NPs' use in presence of a permeation enhancer.

The proposed multi-approach strategy combines the well-known benefits of this multiple-unit formulation in terms of reproducible transit time through the gastrointestinal tract and the consequent absorption pattern with the advantages of colloidal NPs [14].

The schematic illustration of a delivery unit is reported below (Fig. 1.2): it consists of a solid core containing insulin NPs subsequently coated to achieve the colon release. For the latter purpose, a recently proposed three-layer release technology platform was used: in particular, a flexible film (Fig. 1.2 B) composed of a neutral polymethacrylate (Eudragit® NE) and a superdisintegrant EtOH-based sodium starch glycolate (Explotab®CLV), added as a pore former, is applied to a hydroxypropyl methylcellulose (HPMC - Methocel® E50) coating (Fig. 1.2 A) in order to improve the efficiency of the erodible layer in delaying the drug liberation [14] [15]. Finally, an outer

gastroresistant layer (Fig. 1.2 C) was also added to neutralize the variable residence time in the stomach of the coated dosage form and allow its activation only following the entry into the duodenum. This time-dependent drug delivery system relies on the relative consistency of small bowel transit time and the subsequent colon targeting which favour the intestinal absorption of insulin [16].

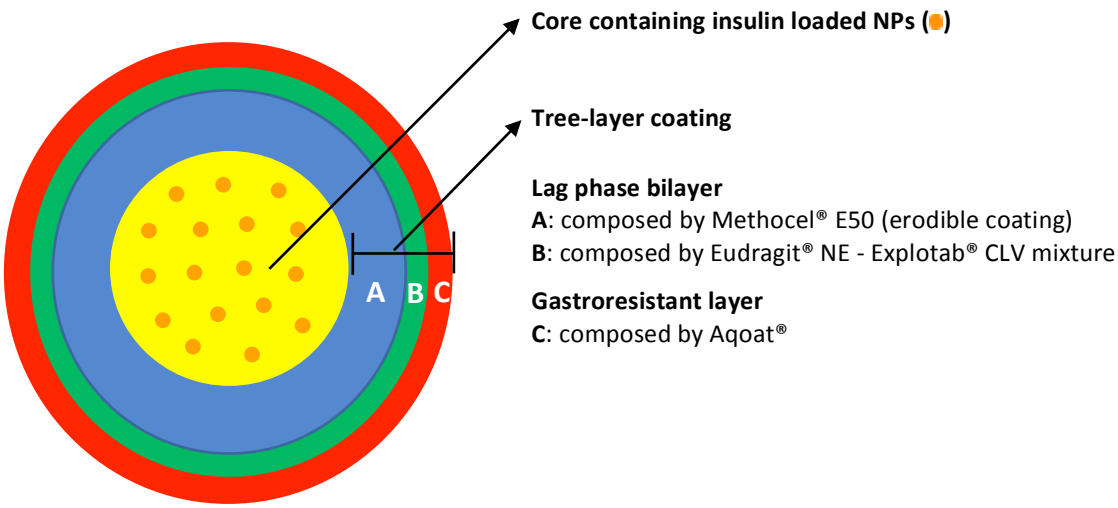

Fig 1.2: Schematic illustration of the developed delivery unit.

2. Results

2.1 NPs synthesis and characterization

For this study, polyethyleneimine (PEI) based polymeric insulin NPs were chosen and developed. As other cationic polymers, PEI is supposed to improve the drug release by oral route through different mechanisms: first though its mucoadhesive properties by the interaction with the negatively charged mucosal proteins [17] then increasing the intestinal paracellular permeation loosening the tight junctions (TJ) of epithelial cells [18].

Insulin-loaded polymeric NPs (NI) were firstly synthesized according to a previously published protocol [19]. Briefly, dextran sulfate (DS) and insulin solutions were mixed in basic tris buffer with an excess of PEI and the zinc added as stabilizer (Fig. 2.1.1). This procedure was selected because the mild preparation conditions (*i.e.* heat, vigorous stirring and organic solvent are not required) are not supposed to affect the peptide stability.

The driving force of NPs formation is the opposite charges of PEI and DS with the entrapment of insulin into the polymeric matrix. The weight ratio between the two polymers (PEI/DS=2.5) was optimized in order to control the particle size. The resulting NI were washed by dialysis against an aqueous solution of mannitol (5% w/V) and lyophilized [19].

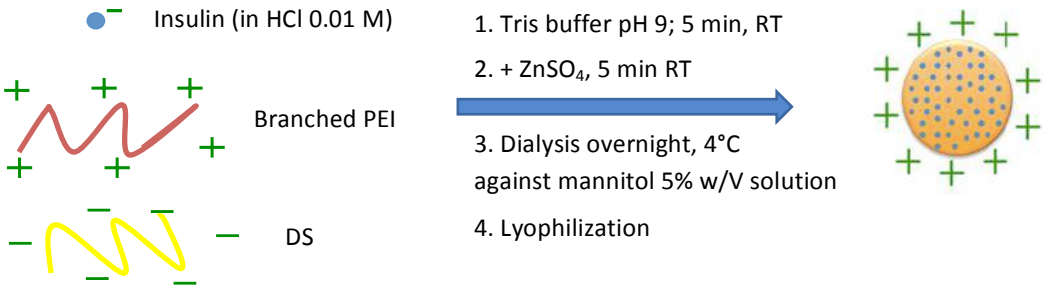

Fig. 2.1.1: Schematic representation of the published NPs synthesis method [19].

The NI obtained from this protocol have a hydrodynamic diameter of 150.8 nm with a polydispersity index (PDI) of 0.315 and a positive Z-potential (+33.8 mV) caused by charges abundance of PEI.

Since the project aim was NI inclusion in solid dosage form and the maximum dose deliverable for the next *in vivo* studies was 500 mg [20], some modifications of this protocol were needed.

First of all, the exclusion of lyophilization step was evaluated: indeed, due to its poor particle size distribution and electrostatic properties, the lyophilized powder in large amounts was not suitable for homogenous mixtures creation. In addition, the binding capacity of the water included in NI suspension could be exploited during dough formation preceding the pellets extrusion.

Afterwards, the recommended dialysis medium was replaced by milliQ water: mannitol, normally employed as bulking agent for lyophilization process, was no longer required for the formulation. Furthermore, it was assumed that NI stability wouldn't be affected by this medium replacement, due to their positive surface charges.

The NI obtained were characterized by Dynamic Light Scattering (DLS) and Z-potential analysis (Table 2.1.1): as expected, the positive Z-potential was maintained and the particle size distribution didn't show relevant differences.

Table 2.1.1: NI characterization comparing two dialysis methods.

Dialysis medium	Hydrodynamic diameter (DLS analysis, nm)	PDI	Z-potential (mV)
5% w/V mannitol	150.8	0.315	+33.8
milliQ water	141.9	0.343	+35.0

If on one hand the bulking agent exclusion didn't cause significant changes in NI properties, it drastically reduced the amount of the final product (Table 2.1.2). Indeed, the starting method led to the inclusion of large quantities of mannitol in the final formulation (*i.e.* 666% of the theoretical yield), whereas with the new dialysis medium around 70% of the theoretical amount was obtained. Hence, this synthesis modification significantly reduced the amount of excipients to include in the final formulation.

Table 2.1.2: Yield comparison; the numbers in parentheses indicate the standard deviation.

	weight (mg)	% of the theoretical yield
Theoretical reagents yield	11.1	100.0
NI obtained using water as dialysis medium (n=2)	7.7 (± 1.9)	69.5
NI obtained using 5% w/V mannitol as dialysis medium (n=5)	72.8 (± 10.5)	665.9

Afterwards, in order to further reduce the dosage of NI to be administered, the insulin loading was enhanced.

Insulin content was increased 2, 3 and 5-fold times from the starting protocol (*i.e.* 1X) obtaining respectively 2X, 3X and 5X formulations (Table 2.1.3): indeed, given the low insulin amount compared the total reagents, poor

contribution in NPs formation and no significant modification of NI properties were assumed.

Table 2.1.3: 1X, 2X, 3X and 5X formulation reagents amounts.

	Reagent amount (mg)				
Formulation	Insulin	PEI	DS	$ZnSO_4$	Total weight
1X	0.07	5	2	4.04	11.1
2X	0.14	5	1.93	4.04	11.1
3X	0.21	5	1.86	4.04	11.1
5X	0.35	5	1.72	4.04	11.1

The obtained NI were characterized by DLS and Z-potential analysis (Table 2.1.4). The positive Z-potential was maintained in all the cases, while slight changes in hydrodynamic diameter and polydispersity index were observed. These differences were considered acceptable due to the polydispersity of particle size distribution.

Table 2.1.4: Characterization of different NI formulations.

Formulation	Hydrodynamic diameter (DLS analysis, nm)	PDI	Z-potential (mV)
1X	141.9	0.343	+35.04
2X	161.4	0.206	+22.29
3X	196.9	0.319	+24.51
5X	174.2	0.219	+27.04

In order to select the best synthetic method, the insulin entrapment efficiency (EE) was determined by RP-HPLC after extraction in acidic solution. The results were expressed as percentage of the reacted amount (EE%).

In all the cases (Fig. 2.1.2), the EE% was between 70-80 with no significant difference among the formulations.

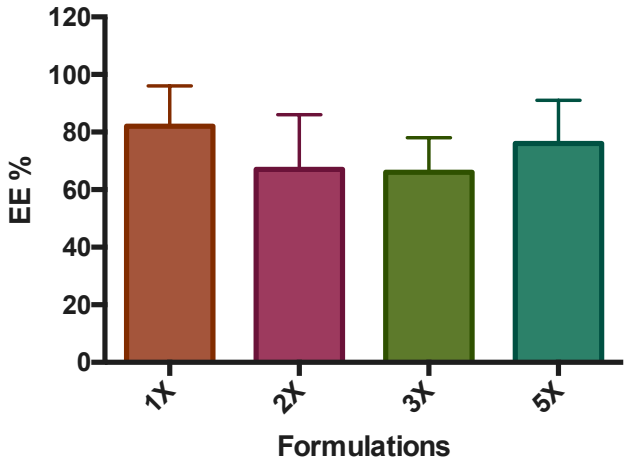

Fig. 2.1.2: Entrapment efficiency of 1X, 2X, 3X and 5X formulations evaluated by RP-HPLC (mean ± SD, n = 3).

In addition, the percentage of the main degradation product, A-21 desamido insulin (A21), was evaluated: indeed, the deamidation is a common post-translational modification occurring in biopharmaceutical proteins and it affects their structure and function [21].

As reported in the Table 2.1.5, A21 percentage (A21%) is below 4.5 in all cases indicating that no massive hydrolysis occurred during the synthesis.

Table 2.1.5: A21% of 1X, 2X, 3X and 5X formulation.

Formulation	A21%
1X	1.6
2X	4.4
3X	3.2
5X	1.9

Among all, 5X formulation showed the maximum insulin content and was therefore selected for further investigations.

In summary, compared to starting preparation, bulk stabilizer exclusion and the 5- fold increase of insulin loading, resulted in a 35-fold reduction of the material amount required to form the pellets.

The selected formulation (5X NI) were then subjected to release test (Fig. 2.1.3): a fast peptide dissolution at pH 6.8 (over 90% within 5 min) was observed. This behavior is consistent with that of the NPs previously reported [19], proving that the synthesis optimization didn't cause any relevant change in NI properties.

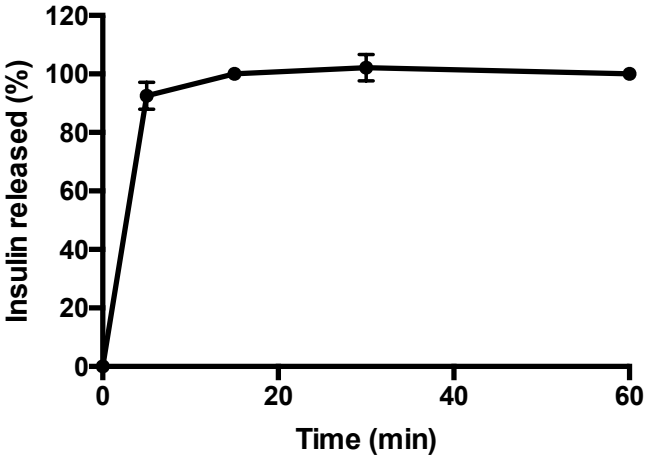

Fig. 2.1.3: Release study from 5X formulation evaluated by RP-HPLC; the test was conducted at 37°C in phosphate buffer (pH = 6.8) and the % of the released insulin calculated (mean ± SD, n = 3).

Finally, since the minimum amount of NI suitable for pellets formation is at grams scale, a scale-up of the process was required. Furthermore, besides

increasing the reagents amounts, a more concentrated colloidal suspension was needed: indeed, with the previously optimized method, grams of resulting NI were suspended in liters of solution making really challenging the next step (*i.e.* dough formation during the cores preparation).

First of all, the minimum volumes needed to ensure the reagents solubility were investigated and the peptide was identified as the less soluble reagent (10 mg/mL in HCl 0.01 M). Once determined the acidic solution volume, all the others were calculated in order to maintain their proportions and, so, the pH balance (Table 4.2.2.1 in materials and methods section).

Because of the low mass percentage of insulin (almost 3% w/w) and its huge cost, the development of the new method was made preparing placebo NPs (NC) batches; indeed, it was assumed that the peptide was more entrapped in the polymeric matrix than involved in the nanoparticulate formation.

During the optimization, it was noticed that the solution viscosity could affect the formation of homogeneous NPs. Thus, the reaction temperature was increased at 40°C, reducing the solution viscosity without compromising the insulin stability.

The NC obtained with the optimized method were characterized as described above (Table 2.1.6).

Despite the scale-up, the size distribution properties and the Z-potential were consistently maintained.

Table 2.1.6: Characterization of placebo NPs (NC) after scaling up the procedure (mean ± SD, n = 3).

Hydrodynamic diameter (DLS analysis, nm)	PDI	Z-potential (mV)
166.5 ± 6.5	0.275 ± 0.013	+ 27.8 ± 0.87

These encouraging bases led to the synthesis of insulin containing NPs then characterized by transmission electron microscopy (TEM), DLS, Z-potential and EE% analysis (Table 2.1.7 and Fig. 2.1.4).

As reported in Fig. 2.1.4, a uniform particles dispersion was obtained as indicated by the unimodal size distribution and the correlogram from DLS analysis. The detected hydrodynamic size of NI was 177.1 ± 12.3 nm (mean ± SD, n = 3) and the Z-potential was +28.9 ± 0.5 mV (mean ± SD, n = 3).

TEM images of the negatively stained NI showed spherical and nearly monodisperse ~ 30 nm NPs (Fig. 2.1.5). The difference observed between TEM and DLS analysis was probably due to the high solvation efficiency of the polymeric matrix.

The EE% determined was 62.3 ± 3.5% (mean ± SD, n = 3), while the A21% was 1.2 ± 0.1% (mean ± SD, n = 3). Although slightly lower than previously reported [19], EE% was in the range of interest to conduct the subsequent loading steps. In addition, the A21% levels below the limits reported in the bovine insulin monograph of the European Pharmacopeia 8th Edition (Pharm. Eur. 8th Ed.), namely 3%, confirmed that no major hydrolytic degradation occurred.

Table 2.1.7: Characterization of NI after scaling up the procedure (mean ± SD, n = 3).

Hydrodynamic diameter (DLS analysis, nm)	PDI	Z-potential (mV)	EE%	A21 (%)
177.1 ± 12.3	0.224 ± 0.023	28 ± 0.45	62.5 ± 3.5	1.2 ± 0.1

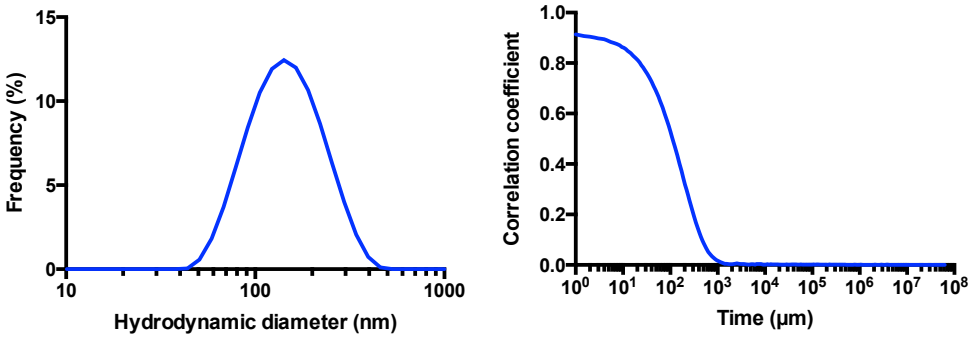

Fig. 2.1.4: Size intensity distribution and correlogram of NI measured by DLS analysis.

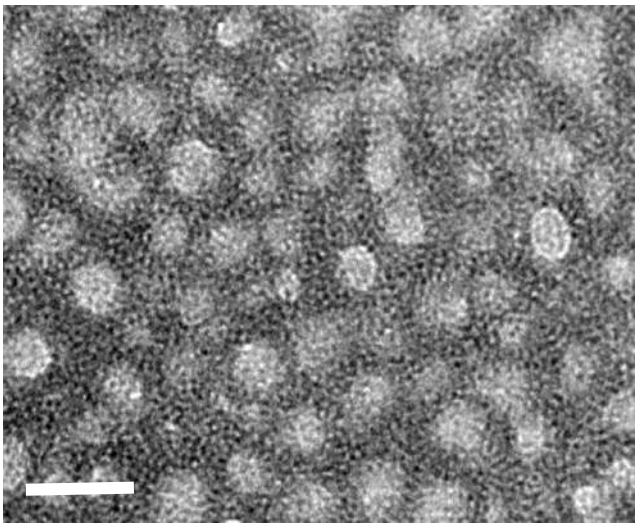

Fig. 2.1.5: TEM images of negatively stained NI (scale bar = 50 nm).

2.2 Solid formulation preparation

2.2.1 Cores preparation and characterization

The NI optimized in the previous phase were then included in a solid dosage formulation. For this purpose, the extrusion–spheronization process was selected as pelletization technique.

This process can be summarized in four steps [21]:

1. Preparation of the dough;
2. Shaping the wet mass into small cylinders (passing through 850 μm extruder);
3. Breaking up the extrudate and rounding of the particles into spheres (spheronization);
4. Drying of the obtained cores.

In order to achieve a prompt release of the NPs at the desired site, an appropriate core formulation should be designed.

A cellulose derivative, Avicel® CL611, a co-processed microcrystalline cellulose and sodium carboxymethyl cellulose, was identified as suitable spheronization agent due to the well-known advantages in terms of improved disintegration and dissolution performance over the traditional formulations based on microcrystalline cellulose [22] [23]. A 1:1 Avicel® CL611/NPs binary mixture (formulation 1) was acknowledged as starting formulation suitable to lead to a dough with appropriate plasticity.

A superdisintegrant agent (Explotab® CLV) and a soluble diluent (lactose) were added in an alternative formulation (formulation 2) in order to further improve the pursued fast-disintegration properties.

For optimizing the process conditions, preliminary trials were conducted with placebo NPs (NC): PNC1 and PNC2 cores relative compositions are reported below (Table 2.2.1.1).

Table 2.2.1.1: NC containing cores compositions.

	% w/w				
Formulations	Placebo NPs (NC)*	Avicel®CL611	NaGly	Lactose	Explotab®CLV
PNC1	50.0	50.0	-	-	-
PNC2	50.0	26.4	-	15.7	7.9

* The percentage refers to the solid NPs

In all the cases, the possible issue associated with the large amount of colloidal suspension needed to obtain the required insulin dose for the *in vivo* studies (*i.e.* 4:1 w/w water vs. total solid mass) was overcome by adding the liquid in small aliquots and allowing the subsequent evaporation that limited the moisture content of the extrudable mass.

Both the batches showed a mean particle size comprised within the desired 710–1400 µm range and a nearly spherical shape as shown by aspect ratio value (Table 2.2.1.2, Fig 2.2.1.1). The process yields (> 40%) were considered satisfying considering the low amounts of processed material.

Table 2.2.1.2: Physico-chemical properties and process yield of cores prepared by extrusion and spheronization.

Formulations	d_{geo} (µm)	σ_{geo} (µm)	Aspect Ratio	Yield (%)
PNC1	913	1.18	1.36 ± 0.18	59.9
PNC2	804	1.21	1.38 ± 0.2	40.1

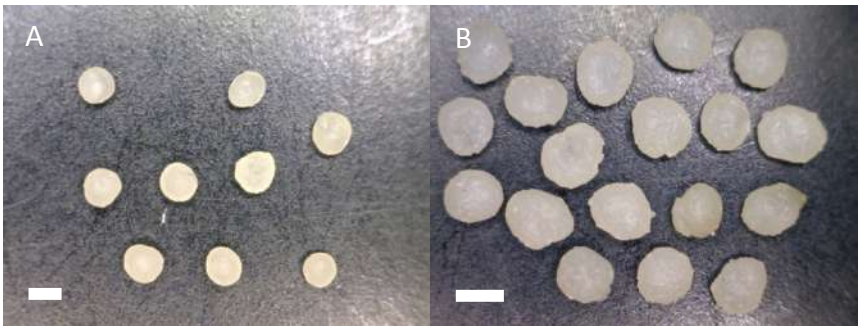

Fig. 2.2.1.1 Digital photographs of PN1 (A) and PN2 (B) cores; scale bar 1 mm.

These promising results led to the preparation of cores containing NI.

In this case, sodium glycocholate (NaGly), an absorption enhancer with protease inhibition properties, was additionally included in the formulation [24]. The latter functional agent was indeed demonstrated to promote the oral absorption of a pancreatic hormone in rats administered with a minitablet formulation at 1:10 protein/adjuvant ratio. In addition, NaGly, due to its high solubility in aqueous media, could help to prevent the undesired matrix formation when pellets interact with water, thus possibly aiding their disintegration.

PNI1 and PNI2 cores relative compositions are reported below (Table 2.2.1.3).

Table 2.2.1.3: NI containing cores compositions

	% w/w				
Formulations	Insulin NPs (NI)*	Avicel®CL611	NaGly	Lactose	Explotab®CLV
PNI1	43.2	43.2	13.6	-	-
PNI2	43.2	22.7	13.6	13.8	6.7

* The percentage refers to the solid NPs

In both the cases, the process appeared facilitated probably due to the concomitant decrease of NPs amount and increase in the total solid mass attributable to the presence of the NaGly powder.

The obtained cores were characterized as above, and the insulin content evaluated after cores dissolution by RP-HPLC (Table 2.2.1.4, Fig. 2.2.1.2).

No differences in size or shape were observed between placebo and insulin-loaded pellets, which was not surprising considering that the final core product structure was not significantly affected by the low amount of protein payload within the colloidal suspension. The yield values were in accordance with the previous data.

The protein content in the pellets was ≥ 90% of the theoretical amount and, despite the long wetting and evaporation phases, the % of A21 remained below the limits indicated in the monograph of bovine insulin reported of Pharm. Eur. 8th Ed., *i.e.* 3%. The overall results suggested that extrusion-spheronization might be a promising technology for loading a NPs suspension into pellets.

Table 2.2.1.3: Physico-chemical properties and process yield of cores prepared by extrusion and spheronization.

	d_{geo} (μm)	σ_{geo} (μm)	Aspect Ratio	Yield (%)	Insulin recovery (%)	A21 (%)
PNI1	809	1.21	1.21 ± 0.18	41.3	102.1 ± 1.6	1.8 ± 0.2
PNI2	1137	1.28	1.16 ± 0.10	61.9	88.8 ± 3.7	0.9 ± 0.3

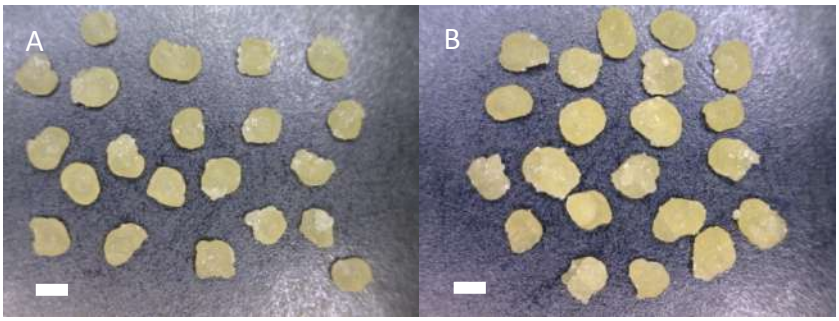

Fig. 2.2.1.1: Digital photographs of PNI1 (A) and PNI2 (B) cores; scale bar 1 mm.

2.2.2 *In vitro* studies on cores

Pellets containing the insulin-loaded NPs were subjected to studies aiming to assess the disintegration and insulin release performances from the two different formulations.

PNI2 formulation showed enhanced disintegration compared to PNI1, *i.e.* 26.4 ± 8.7 vs. 10.8 ± 3.6 (mean ± SD expressed as %). This behavior could be ascribed to the inclusion of Explotab®CLV and lactose in PNI2: these excipients, acting respectively as superdisintegrant and pore former, were actually able to improve cores properties compared to PNI1 where the only excipients was Avicel® CL611. However, comparing such performance with that of a reference formulation containing paracetamol as analytical tracer instead of insulin NPs and Avicel® CL611/lactose/Explotab® CLV in the same ratios as PNI2 formulation, a disintegration of 75.4 ± 9.5% (mean ± SD) was obtained. It can be inferred that the presence of NPs considerably contributed to the formation of a slow-eroding matrix.

To confirm the different formulations behavior, a dissolution test of PNI1 and PNI2 was performed.

As expected, the release capacity of the two formulations was different: indeed, PNI2 showed a faster insulin release compared to the started formulation (74% vs 16.7 at 1h) (Fig. 2.2.2.1).

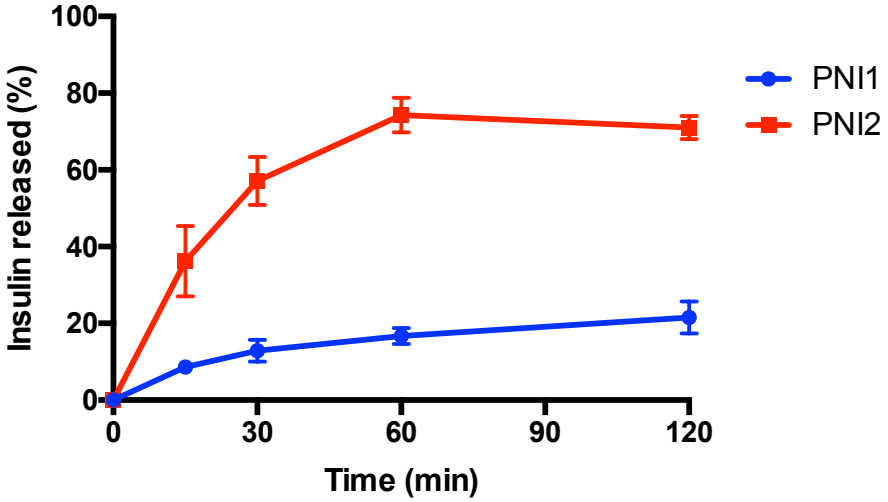

Fig. 2.2.2.1: insulin release of PNI1 and PNI2 cores evaluated by RP-HPLC; the test was conducted at 37°C in phosphate buffer (pH = 6.8) and the % of the released insulin calculated (mean ± SD, n = 3).

Afterwards, re-dispersion studies were performed on batch PNI2, which appeared the most promising one. These studies were set up in order to evaluate the presence of NI after exposure of the solid dosage form to aqueous fluids. Samples of this medium were collected, filtered in 0.45 µm membrane and analyzed by DLS. NPs with a mean diameter of 146.1 ± 1.0 nm (n=3) were detected. Comparing the size of NI before and after extrusion-spheronization process, the hydrodynamic diameter was slightly lower (-23.2%) than the initial value (177.1 ± 12.3 nm), although the size distribution appeared to be maintained as evaluated by the polydispersity index (0.296 ± 0.005). A diameter reduction (-17.8%) was observed also testing cores that

include NC (PNC2 formulation). To figure out the cause of this reduction, the same test was performed on 25 mg of a dried dough obtained by using the same components and operating conditions of the cores of PNI2 batch avoiding extrusion and spheronization steps. Even in this case, a decrease of mean diameter occurred (-28%), suggesting that it may depend on the mechanical stress during the dough formation (Fig. 2.2.2.2). However, the NPs were detected in the media suggesting that cores under investigation might convey and liberate the colloidal system upon exposure to aqueous environment.

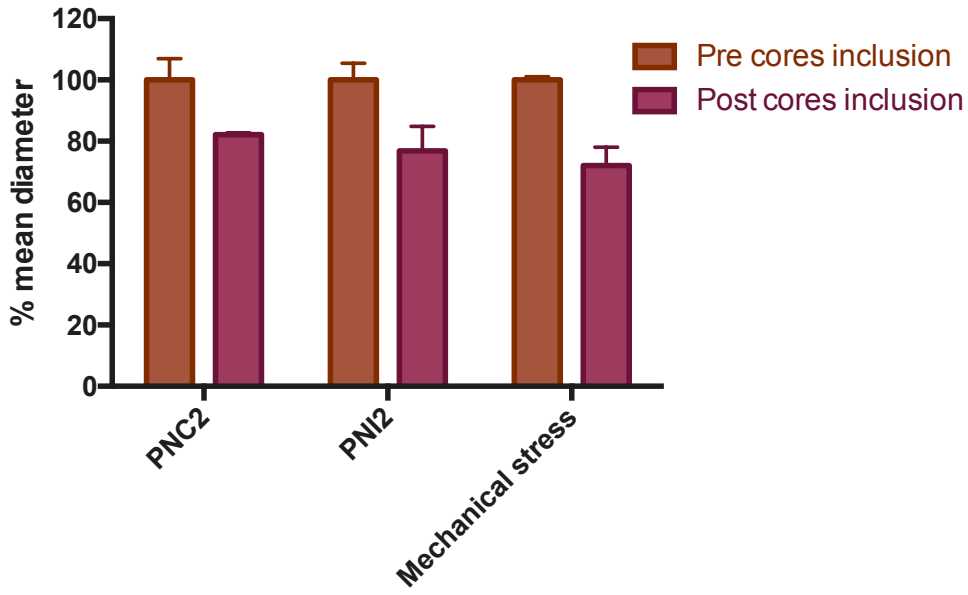

Fig. 2.2.2.2: NPs re-dispersion after the inclusion in solid formulation evaluated by DLS analysis; PNC2 and PNI2 refers to cores containing placebo and insulin loaded NPs respectively, while the in the sample reported as “Mechanical stress” NI suspension was added in small aliquots to the powder blend under continuous mixing mimicking the preparation of the dough; the results are expressed % of the started NPs diameter (mean ± SD, n = 3).

2.2.3 Preparation and characterization of coated pellets

PNI2 was selected as most promising formulation in terms of disintegration and dissolution properties.

The cores were therefore coated in turn with a Methocel® E50-, Eudragit® NE/Explotab® CLV- and Aqoat®- based formulations in order to prepare three-layer colonic system (CPNI) (Fig. 2.2.3.1 A).

In particular, the hydrophilic layer based on Methocel® E50 was demonstrated to delay the drug release by a swelling/erosion mechanism, while the Eudragit® NE/Explotab® CLV film was aimed at prolonging the duration of the lag phase as imparted by the underlying HPMC coating [25].

Finally, an outer enteric film composed by acetate succinate cellulose (Aqoat®) was added: this acid-insoluble polymer led to overcome the unpredictable gastric residence time of the system thus allowing its activation only at the duodenum and the consequent colonic release based on a time-dependent approach [16] [25].

In order to assess the colon release contribution to insulin absorption, a gastroresistant formulation (GPNI) was as well developed (Fig. 2.2.3.1B): this DDS was designed to release NI in the small bowel after passing the stomach.

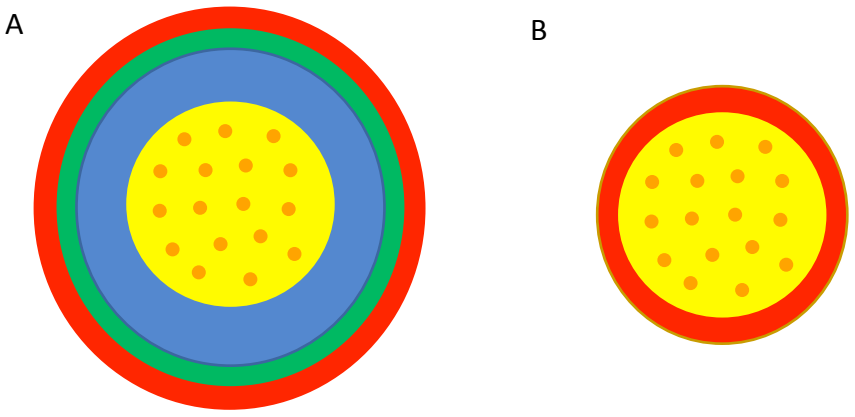

Fig. 2.2.3.1: Colonic three-layer (A) and gastroresistant (B) systems representation; the inner circle represents the NI containing cores while blue, green and red layers represent Methocel® E50-, Eudragit® NE/Explotab® CLV- and Aqoat®- coating respectively.

The adopted process operative conditions and the coating levels needed to achieve gastroresistance or colonic delivery were previously set up with an analogous formulation containing paracetamol as analytical tracer.

In particular, gastroresistance criteria were accomplished with an Aqoat® coating level of 12–13 mg/cm^2. When using colonic systems, an lag time of approximately 60 min in phosphate buffer (PB) at pH 6.8 corresponded to 85–90 mg/cm^2 of Methocel® E50, 3.0-4.0 mg/cm^2 of Eudragit® NE-Explotab® CLV 20% and 12–13 mg/ cm^2 of Aqoat® [25].

Particularly, a similar multiple-unit system with an lag phase of the latter duration showed an insulin peak in rats and a corresponding drop in blood glucose levels 6 h post-dose following oral administration.

Based on typical gastrointestinal transit times reported in the literature for rats, the delivery system, after this lag time, was expected to be able to arrive, mostly intact, to the ileo-colonic region [20].

In addition to PNI2 batches, cores based on formulation 2 loading free insulin (PI2) were prepared and coated as described above (GPI and CPI): they will be used as reference in the subsequent experiments.

As reported (Tab. 2.2.3.1), all coated batches showed a mean particle size in the 1.3-2.1 mm range and coating levels in line with what expected based on preliminary set up results. The shape was closer to roundness than the starting cores, as a result of the subsequent coating steps.

Table 2.2.3.1: Physico-technological characteristics of gastroresistant and three-layer colonic pellets. Layers 1, 2 and 3 refer to Methocel® E50, Eudragit® NE - Explotab® CLV (20%), Aquoat® coating respectively.

	d_m (µm)	SD (µm)	Aspect Ratio	Layer 1 mg/cm^2	Layer 2 mg/cm^2	Layer 3 mg/cm^2
GPNI	1355	114	1.14	-	-	13.1
CPNI	1865	102	1.07	89.9	4.0	13.0
GPI	1392	121	1.25	-	-	11.9
CPI	2070	149	1.24	85.1	3.1	12.5

All the formulations reported were subjected to release test: the coated pellets were first incubated with HCl 0.1 M (pH = 1) in order to test their gastroresistance and, after 2 h, exposed to a pH 6.8 PB (Fig. 2.2.3.2).

As expected from the previous results, all formulation met gastroresistance criteria (< 10% release after 2 h in 0.1 M HCl), albeit the release test was conducted under more vigorous stirring, performed by magnetic stirrer, compared to the compendial method.

When exposed to a pH 6.8 PB, all enteric systems GPNI and GPI showed a prompt release due to core disintegration following dissolution of the enteric coat. The CPI pellet formulation used as reference showed a short lag time (< 1 h), caused by the adopted release testing conditions, followed by prompt peptide release.

The three-layer colonic systems containing the NI (CPNI) showed a lag-phase preceding the onset of release and, compared with CPI system, the release rate was clearly reduced. This behavior was probably caused by the formation of a slow eroding matrix involving the NPs and the inner layer. Despite the deviation from the ideal performance (*i.e.* prompt release after a lag-phase),

the CPNI was considered acceptable for the next activity experiment given the generally long time of residence of the pharmaceutical form in the ileo-colon region.

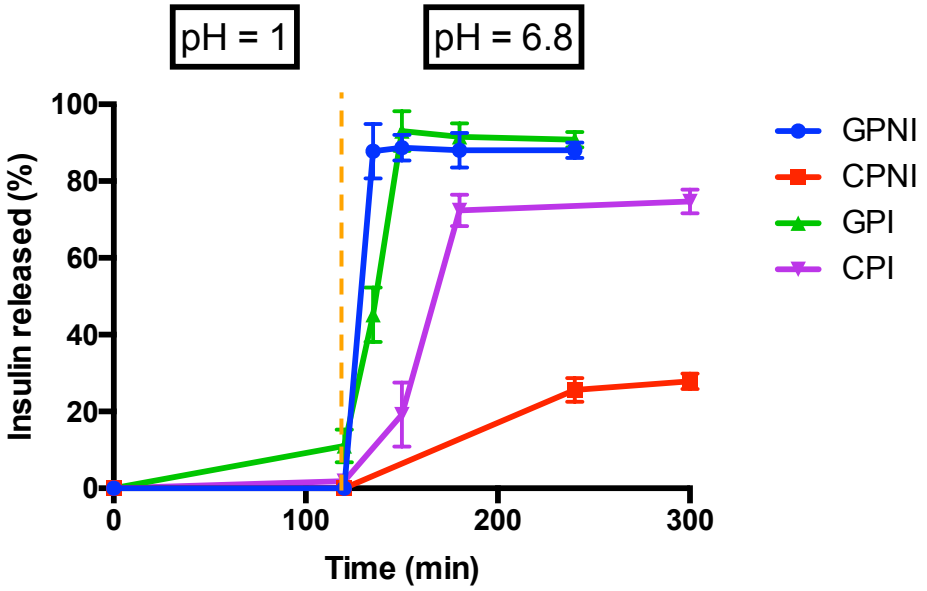

Fig 2.2.3.2: insulin release of coated pellets evaluated by RP-HPLC; the formulations were incubated at 37°C first in HCl solution (pH = 1) then in phosphate buffer (pH = 6.8); % of the released insulin were calculated (mean ± SD, n = 3). Formulation tested: CPI – colon insulin pellets; GPI – gastroresistant insulin pellets; GPNI – gastroresistant insulin NPs pellets; CPNI – colon insulin NPs pellets.

2.3 *In vivo* hypoglycaemic effect

The NI loaded into the pellets were tested *in vivo* in diabetic rats. The rat model was chosen since the relative gastrointestinal transit time is comparable to that of humans [26].

First, the animal model of diabetic rat was set up. Streptozotocin is well known for its diabetogenic properties: indeed, it is able to induce pancreatic beta cells destruction following by insulin lack [27]. So, diabetes was induced by two intraperitoneal injections (once a week) of streptozotocin.

After the first injection, around 40% of treated rats developed glycemic values over 350 mg/dL, indicative of diabetes onset [28]. All animals were treated again and, after further seven days, were obtained 75–80% of stably diabetic rats (glucose concentration ranging between 350 and 600 mg/dL).

The diabetic animals were then subjected to one of the following treatments: 1) oral administration of 1.33 mg/kg insulin (OI) or as NI, 2) subcutaneous injection of 0.07 mg/kg insulin (SCI), 3) insertion through gastrostomy of different amounts of pellets in capsules (GPI, GPNI, CPI, CPNI) to allow administration of 1.33 mg/kg. A group of non-treated rats was used as control (NT). The SCI was tested, since it is the gold standard treatment. Fig. 2.3.1 shows the % variation of glycaemia from 1 to 48 h post-treatment. The baseline for each experimental group was the mean value of blood glucose measured before the treatment, considered as 100%. In the first 8 h post-treatment, physiological oscillation of glucose blood levels was observed in NT rats, which however did not exceed 30% of the initial value. Orally administered insulin, either free or in NI, had no significant effect on blood glucose levels, while the SCI of insulin caused a rapid and marked reduction of

glycemia to 25 % of the initial values at 1 h post-treatment. However, blood glucose levels returned to the initial level when measured after 8 h. The treatment with GPI or GPNI did not show any significant effect on the glucose blood levels as compared to NT during the first 8 h. In contrast, the rats treated with CPNI were able to induce an immediate, significant decrease in blood sugar levels as compared to the NT, with a significant fall in glycaemia, as much as 50% of the initial value, at 6 h post-treatment, and a subsequent further decrease of up to 30% at 8 h. On the other hand, the treatment with CPI did not exert any significant hypoglycemic effect. At longer times (48 h), NT and SCI-, OI-, NI-, and GPI-administered rats had blood glucose equal the initial values, while in rats administered with CPNI the glucose concentration remained at 45% of the starting level and significantly different from those of all other experimental groups. At 48 h post-treatment, a slight decrease of glycaemia was observed upon administration of CPI, while in GPNI-treated rats glucose values became about 70% of initial values and significantly lower than those of controls.

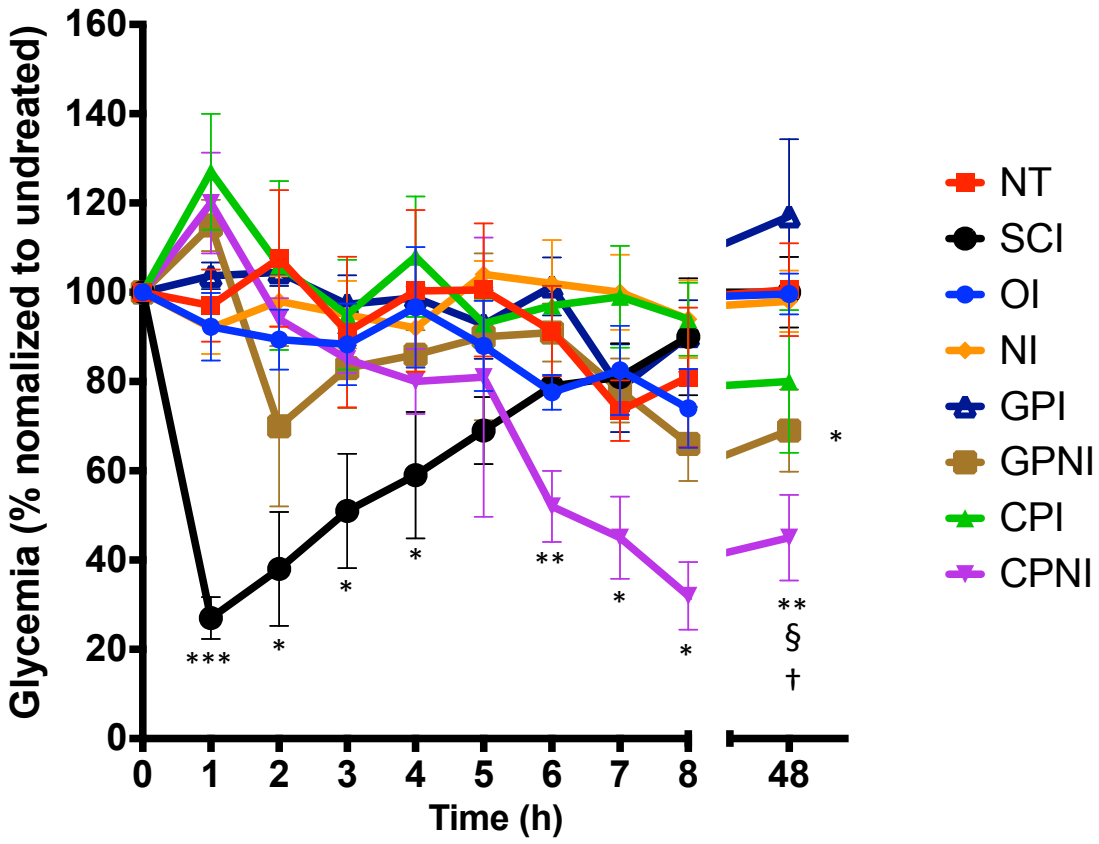

Fig. 2.3.1: Time course of *in vivo* activity of different insulin formulations expressed as percentage variation of rat blood glucose levels after treatment. Diabetic rats were exposed to oral (OI) (n=5) or subcutaneous (SCI) (n=3) administration of insulin, oral administration of insulin NPs (NI) (n=6), or insertion through gastrostomy of capsules containing gastroresistant pellet-formulated insulin (GPI) (n=3) or insulin-NPs (GPNI) (n=5), colon-release pellet-formulated insulin (CPI) (n=4) or insulin-NPs (CPNI) (n=4); NT: untreated rats (n=5). Mean ± SE are represented. ***$p < 0.005$, **$p < 0.01$, *$p < 0.05$ vs NT; **§** $p < 0.005$ vs OI, NI, GPI and SCI; **†** $p < 0.05$ vs GPNI and CPI.

3. Discussion

Current therapies of Type 1 and advanced Type 2 diabetes are based on parenteral administration of insulin, that, although efficient, are associated with severe side effects [1]. Therefore, several research studies are now focused on the development of insulin-containing oral formulation that may lead to a better glucose regulation, avoiding peripheral hypoglycaemia, and increase the patient compliance [8].

Although numerous delivery strategies have been proposed, the oral delivery of insulin is still an unmet medical need.

In light of the above, the purpose of this study was to develop an oral nanocarrier of insulin combining several approaches (i.e. colon-targeting and NPs-based delivery) reported for increasing its bioavailability.

Firstly, the optimization of NI synthesis method allows a considerable amount of peptide loaded into a concentrated nano-suspension: these factors are both favorable for the preparation of NI loaded pellets with a significant overall reduction of the dosage (~ 35-fold).

Afterwards, a multiple-unit solid dosage form was developed: this system was preferred over the classic single-unit formulation because of the increased loading capacity and the low inter- and intra-subject variability in gastrointestinal transit time [14].

In particular, the extrusion-spheronization of a formulation containing Avicel® CL611, lactose and Explotab® CLV wetted by nano-suspension led to cores with technological and biopharmaceutical characteristics suitable for the following coating steps.

Finally, *in vitro* performances of three layers coated pellets ensured a delayed release that possibly promote a colon targeting.

When tested in diabetic rats, orally administered insulin, either “free” or formulated in NPs (NI), were not effective in reducing blood glucose levels at 8 h after treatment. That was expected since insulin is rapidly degraded in the stomach. On the other hand, the subcutaneous injection of insulin, used in clinical practice, caused a rapid and significant hypoglycemic effect with a subsequent gradual return to the initial blood glucose levels at 8h.

Curiously, at 1 h post-treatment all rats treated with the different capsules (GPI, GPNI, CPNI, or CPI) showed a temporary increase in blood glucose concentrations, possibly due to the effect of surgery and anesthesia which is known to cause stress-related acute hyperglycaemia in fed rats [29].

The treatments with GPI or GPNI, enteric coated pellets which were supposed to release the peptide in small intestine (i.e. duodenum-jejunum tract), did not significantly reduce the blood glucose levels as compared to NT in the first 8 h ($p > 0.05$). This may be due to the degradation of insulin by the high proteolytic activity of pancreatic peptidases, but also to the effect of the insulin-degrading enzymes inside the cytosol of the small intestine enterocytes which can internalize the peptide by specific insulin receptors [30] [31].

In contrast, the rat treatment with CPNI induced a significant decrease in blood glucose levels as compared to the NT group. The reduction was significant at 6 h post-treatment with as much as 50% of the initial values, with a subsequent further decrease of up to 30% at 8 h. This result suggested that, unlike the gastroresistant pellet which released the insulin into active small intestine, the three-layer colon-release pellets passed this tract without being degraded and released the NI in the distal part of the small intestine or in the

colon. There are several reasons which make the colon as a desirable tract for insulin delivery and release: 1) the enzymatic activity, such as pancreatic endopeptidases, is remarkably lower and most of proteins, including insulin, would be available to intestinal absorption; 2) the microvilli are less developed in this tract as compared to the small intestine and their membrane-associated peptidases are limited making such microvilli more susceptible to permeation; 3) there is a prolonged localization of insulin on the colonic mucosa due to slow transit time, thinner unstirred water layer (UWL) adjacent to mucosa and slow turnover of colon mucosal film [7]. The lack of significant decrease in glycaemia of the rats treated with CPI indicates that the delivery of insulin as such to the colon by pellets was not sufficient to exert the hypoglycemic effect. A drug delivery system was required to properly address and release insulin to the colonic mucosa. Therefore, insulin nanoformulation plays a key role in reaching this goal. It has been demonstrated that PEI, as other cationic polymers (e.g. chitosan (CS)), is able to loosen tight junctions (TJ) resulting in increased permeability of intestinal epithelium cells, which leads to paracellular permeation of molecules [18]. Many studies have already demonstrated the ability of different kinds of CS NPs to increase the intestinal permeation of conjugated insulin through TJ opening [32]. In particular, Lin and colleagues suggested a mechanism for the paracellular transport of insulin to the blood circulation based on CS NPs, whose stability and release of loaded insulin greatly depended on the environmental pH. In this model, the neutral pH, typical of the jejunum and the ileum, favors the degradation of the nanocomplex resulting in the complete release of CS and insulin. CS interaction with the TJ proteins enhances the paracellular pathway, promoting the absorption of greater amounts of insulin [33]. An equivalent mechanism

could be suggested also for the NI released from pellets into the colon. Indeed, the pH values of this tract, from 6.5 in the ascending colon to 7 in the descending colon, could promote NPs instability and cause the release of insulin. Considering that the entire nanocomplex was not allowed to permeate across the TJ, even under the effect of paracellular enhancers, a few conclusions can be drown: 1) the released NI undergoes degradation in the colon lumen; 2) the released insulin, that is not subjected to significant proteolytic activity in this tract of the gut, and the PEI fragments both reach the mucosal surface; 3) PEI is supposed to interact with the TJ and opens the paracellular pathway, thus promoting a significant insulin absorption [34]. In addition, the presence of sodium glycocholate, that is known to promote insulin passage through the colonic mucosa by different mechanisms, including the rearrangement of the phospholipid bilayer and increase of the relevant fluidity, could have a synergistic effect on the overall protein absorption.

At 48 h, NT and SCI-, OI-, NI-, and GPI-administered rats had the blood glucose values return to initial levels while in rats administered with CPNI the blood glucose levels remained persistently and significantly reduced, as compared to the initial values. Such a long-lasting effect could be ascribed to the mucoadhesive properties of the nanocomplex, involving ionic interactions between the positively charged PEI and the negative charges of the mucosal surface. It may be hypothesized that, even if most of the NPs were degraded in the colon lumen, part of them still interacted with the membrane-bound mucins on the intestinal epithelium, releasing the insulin beyond UWL, in the proximity of the absorptive cells. The UWL, forming a diffusion barrier between the luminal contents and the epithelium, maintained an adequate concentration of insulin in proximity of the enterocytes, allowing a prolonged

insulin absorption over the whole period. On the contrary, most of the other administered formulations were previously eliminated. These results suggest a two-phase mechanism in rats administered with CPNI. During the first phase, a massive release of insulin took place within the initial hours from the treatment (i.e. 6–8 h) as an effect of the rapid release of the drug from the NPs into the colon lumen followed by the PEI-mediated opening of the paracellular route. During the second phase, a long-lasting absorption of the insulin released in proximity of the colon epithelium by the NPs was triggered by active interaction with the negatively charged mucus layer.

At 48 h post-treatment, a slight decrease of blood glucose levels, not significantly different from that observed in NT and orally treated rats, was observed upon administration of CPI, while in GPNI-treated rats, glucose values were still about 70% of the initial values and significantly lower than those of controls. It is likely that the hypoglycemic effect could be attributed to the release of insulin by those NPs which escaped luminal degradation and reached the mucosal surface. In this case, a certain amount of the protein, protected from the proteolytic activity due to the presence of the secretory mucin barrier [35], was still available for the intestinal absorption. This likely occured through the PEI-activated paracellular pathway.

The colonic delivery of nanoformulated insulin holds a significant potential in clinical practice. This study provides the proof of the concept that insulin may survive the hostile environments of gastric acidity or the peptidase rich small bowel thanks to its targeted and NPs-mediated oral delivery. Moreover, blood glucose remained nearly half of the initial levels at 48h post- administration of CPNI, thanks to slow and continuous release of insulin in the colon. This fact is particularly significant, since it may indicate that a prolonged control of

glycaemia may be reached with a possible reduction in the overall insulin requirements (i.e. number of daily injections) of the patient. This would result in improved quality of life and potential reduction in long-term complications related to unstable glycemic control.

Another goal reached by this novel insulin nanoformulation was the restoration of a physiological delivery of insulin into the portal vein, with a proper liver metabolism. This avoids fluctuating blood glucose levels and allows a more precise control of glycaemia. No fluctuation was observed in blood glucose levels of CPNI-treated rats, in favor of a progressive regular fall of the glycaemia [2] [8]. Furthermore, mimicking the physiological insulin circulation in the portal vein and the extraction by the liver, this formulation might obviate the drawbacks of insulin administered subcutaneously: systemic hyperinsulinemia with subsequent possible hypoglycemia, local lipoatrophy with consequent day-to-day variability of subcutaneous absorption, weight gain, atherogenesis and enhanced lipogenesis. The peripheral administration of insulin is also implicated in the worsening of insulin resistance which makes the adjustment of insulin dosing difficult in, for instance, diabetes Type 2 patients.

Therefore, the multitasking nanodevice described in this study for oral delivery of insulin is promising, although further research is needed to study, for example, the peptide bioavailability or better clarify the variations caused by oral insulin on various others metabolic and diabetes indicators, such as glucagon, insulin-like growth factor 1 (IGF-1), fructosamine and glycated hemoglobin.

4. Conclusion

The most adopted strategy for insulin substitution therapy is the multiple daily injections of long- and rapid-acting analogues of the hormone: the first ensure basal insulin replacement, whereas the second are administered at mealtimes [40].

Despite several efforts have been made to design a formulation suitable for insulin oral administration, there is still no product available on the market. Actually, several ongoing clinical trials propose to combine different strategies reported for increasing both the peptide stability and permeability [41] [42]. In this study as well, the colon release aimed to protect the drug in the hostile GI tract, while the cationic NPs, along with the sodium glycocholate, were supposed to enhance the overall insulin bioavailability by means of their mucoadhesive and permeabilization actions.

As it was showed *in vivo*, only the proposed formulation was able to induce a significant fall in glucose levels demonstrating the synergistic effect exerted by the colon-targeting and NPs use.

The slow and persistent decrease of the glycemia observed make this preparation a suitable candidate for the replacement of long-acting insulin injections.

5. Materials and methods

5.1 Materials

Bovine insulin (MW 5734 Da), polyethylene imine (MW 750 kDa), dextran sulfate (MW > 500 kDa), zinc sulfate, streptozotocin (STZ) and cellulose ester dialysis membrane tubing with a molecular weight cut-off (MWCO) of 1.000.000 Da (Spectra/Por Biotech CE) were purchased from Sigma-Aldrich (St Louis, MO, US). All chemicals were used as received without further purification. Lactose was obtained from Prodotti Gianni (Milan, Italy). Micro-crystalline cellulose co-processed with sodium carboxymethyl cellulose (Avicel® CL611) and hydroxypropyl methyl cellulose acetate succinate (Aqoat® LG, HPMCAS) were gifts from FMC Europe (Brussels, Belgium, distributed by IMCD Italia, Milan, Italy) and from Shin-Etsu (Tokyo, Japan, distributed by Seppic, Milan, Italy), respectively. Hydroxypropyl methylcellulose (Methocel® E50, HPMC) was kindly donated by Colorcon (Milano, Italy). Poly (ethylacrylate, methylmethacrylate) (2:1 monomer molar ratio) as 30% w/V aqueous dispersion (Eudragit® NE 30 D) of Evonik Röhm (Darmstadt, Germany) was a kind gift of Rofarma (Gaggiano, Italy). Polyethylene glycol (PEG 400) and size 4 hard-gelatin capsules were purchased from ACEF (Fiorenzuola D'Arda, Italy). Sodium glycocholate (NaGly) was obtained from and Tokyo Chemical Industry (Tokyo, Japan). Sodium starch glycolate (Explotab® CLV) was a gift from JRS Rettenmaier Italia (Castenedolo, Italy).

5.2 Synthesis of insulin-containing NPs (NI)

5.2.1 Synthesis of 1X, 2X, 3X, 5X of NI

1% w/V dextran sulfate (DS) solution, polyethylene imine (PEI) solution of 1 % w/V and 10 mM tris buffer (pH 9) were added under stirring (500 rpm) to a solution of insulin (0.07 mg/mL) in 0.01 M HCl. Reagents volumes for each formulation are reported below.

	Solution volumes (μL)			
Formulations	Insulin	PEI	DS	Tris Buffer
1X	100	500	200	400
2X	200	500	193	400
3X	300	500	186	400
5X	500	500	172	400

After 5 min, 30 μL of zinc sulfate solution (1 M) were added and the product was stirred an additional 5 min. Finally, the obtained NI were dialyzed against Milli-Q water with cellulose ester dialysis membrane tubing with a molecular weight cut-off (MWCO) of 1.000.000 Da.

5.2.2 Scale up of NI synthesis

22.1 mL of insulin solution (10 mg/mL in 0.01 M HCl), 10.8 mL of a 10% w/V DS solution and 18.0 mL of 10 mM tris buffer, pH 9, were added under stirring (500 rpm) to 12.6 mL of PEI solution (25% w/V). Afterwards, the mixture was heated at 40°C, maintained under stirring because of its high viscosity and 7.8 mL zinc sulfate solution (2 M) were added, dropwise. As a result of the

addition of the stabilizer, the formation of the NPs took place and the viscosity of the solution decreased. The product was additionally stirred for 15 min at 40°C. The obtained NI were finally dialyzed as previously described.

The reagents' amounts were calculated simply scaling up those of the 5X formulation, whereas the relative volumes were calculated in order to maximize the concentration of the colloidal suspension.
For the latter purpose, after the identification of insulin as less soluble reagent (10 mg/mL in HCl 0.01 M), HCl 0.01 M volume was established and all the others were calculated in order to maintain their proportions (Table 5.2.2.1).

Table 5.2.2.1: Relative medium volumes calculation; MilliQ water was the dispersant of PEI, DS and $ZnSO_4$ powders.

Medium	Volumes in the 5X formulation synthesis (mL)	Relative percentages (%)	Volumes in scaled up synthesis (mL)
HCl 0.01 M	0.5	31.3	22.1
MilliQ water	0.7	43.8	30.9
Tris buffer	0.4	25.0	17.7

5.3 Synthesis of placebo NPs (NC)

22.1 mL of HCl 0.01 M, 10.8 mL of a 10% w/V DS solution and 18.0 mL of 10 mM tris buffer, pH 9, were added under stirring (500 rpm) to 12.6 mL of polyethylene imine (PEI) solution (25% w/V) and then treated as described above.

5.4 NPs characterization

A. Dynamic light scattering (DLS) and Z-potential measurements

The mean diameter and surface charge of the NPs were assessed with a Zetasizer Nano ZS ZEN3600 from Malvern Instruments Ltd (Worcestershire, United Kingdom) operating at a light source wavelength of 633 nm and a fixed scattering angle of 173°. The sample concentration was chosen to keep attenuator values between 7 and 9. The measurements were performed in triplicate, after dilution of the NPs respectively with MilliQ water and aqueous solution of sodium chloride (1 mM).

B. Transmission electron microscopy (TEM) analysis

NPs were visualized using 120 keV TEM (Jeol 1010, Tokyo, Japan). 2 µL of the sample, along with 2% w/V uranyl acetate solution, were deposited onto a piece of ultrathin 200-mesh copper grid (Ted-pella, Redding, CA, US) and left to dry in air before examination by TEM.

C. Determination of the entrapment efficiency (EE%) of insulin into the NPs

The amount of insulin encapsulated into the NPs was determined suspending the NI, corresponding to 30 µg/mL theoretical insulin concentration, in 0.05 M HCl and centrifuging at 12000 rpm for 20 min (ScanSpeed 1730R, Labogene, Lynge, Denmark). After centrifugation, the amount of insulin in supernatant was measured by a reverse-phase, high-performance liquid chromatography (RP-HPLC) analysis with a method reported in Eur. Pharm. 8th Ed. for insulin

and its degradation product A21-desamido insulin (A21) quantitation [36]. Insulin quantitation was performed using a freshly prepared standard having identical insulin concentration and analyzed the same day of NPs. The EE% is expressed as ratio percentage between the insulin amount in the suspension and the theoretical value of the insulin added.

D. *In vitro* insulin release from NI

In vitro release was assessed following incubation of the nanoparticle suspension containing theoretically 0.35 mg of insulin in 10 mL of 0.095 M phosphate buffer pH 6.8 prepared as indicated in the Eur. Pharm. 8th Ed. at 37°C under stirring (MIX15eco, 2mag, München, Germany; 600 rpm). Bovine albumin (0.2% w/V) was added to the dissolution medium to avoid non-specific adsorption of insulin to glass surface. At pre-determined time intervals, 1 mL of medium was withdrawn, filtered by 0.2 m polyethersulfone (PES) membrane (VWR) and acidified with 40 µL of 1 M HCl before the analysis by RP-HPLC as previously described. Dissolution studies were performed in triplicate.

5.5 Preparation and coating of cores

Powders (9.2 g for PNI1 and 2; 7 g for PNC1 and 2; composition reported in Tab. 5.5.1) were mixed in a mortar for 5 min. Nanoparticle suspensions, either placebo or loaded with insulin, were then added in small aliquots to the powder blend under continuous mixing, in the same mortar, over a total period of 8 h; during that time the most of water could evaporate allowing the moisture content suitable to the next step. The room was maintained at 30°C

with 25% relative humidity. The resulting wetted mass was extruded through an 850 μm sieve. Spheronization was performed in a spheronizer (Nica™ S320, GEA, Düsseldorf, Germany) with a cross-hatched plate (400 rpm, 5 min). Pellets cores were finally dried in a static oven at 40°C for 24 h.

Table 5.5.1: compositions of cores under investigation.

Formulations	% w/w					
	NI	NC	Avicel®CL611	NaGly	Lactose	Explotab®CLV
PNC1	-	50.0	50.0	-	-	-
PNC2	-	50.0	26.4	-	15.7	7.9
PNI1	43.2	-	43.2	13.6	-	-
PNI2	43.2	-	22.7	13.6	13.8	6.7

As a reference for *in vivo* studies, a pellet formulation containing insulin was prepared by mixing its powder with Avicel® CL611, NaGly, lactose and Explotab® CLV (9.4 g) and adding deionized water (3.5 g). The E-S was then performed as for NPs loaded formulations.

In order to obtain three-layer colonic systems, pellets were coated in a fluid bed (GCPG 1.1, Glatt®, Binzen, Germany). The following formulations were in turn sprayed: i) a hydro-alcoholic solution (1:9w/w, water/ethanol) of Methocel® E50 (5% w/w) and PEG 400 (0.5% w/w) (10g/min spray rate), ii) an aqueous suspension of Eudragit® NE 30D-Explotab®CLV (20% vs. solid Eudragit®NE) (1.4 g/min) and iii) a hydro-alcoholic solution (23% w/w, water/ethanol) of Aqoat® (5.8% w/w) (8 g/min). In the case of the coatings with the hydro-alcoholic solutions of both Methocel® E50 and Aqoat® the rotor insert was employed while for Eudragit® NE-based suspension a Wurster process was applied. In the case of gastroresistant formulations, pellets were

directly coated with the hydro-alcoholic solution of Aqoat®, as previously described. The operating conditions for all coatings were: inlet air temperature, 40°C; product temperature, 33–35°C; airflow rate, 70 m^3/h; nozzle diameter, 1.2 mm; spray pressure, 2.0 bar; final drying time at 40°C, 5 min. A curing step in a static oven at 40°C was performed on intermediate systems coated with Eudragit®NE-Explotab® CLV and final enteric formulations for 24 h and 2 h, respectively. In all process steps, placebo mini-tablets (weight 10.5 mg, diameter 2.5 mm, height 2.3 mm) were added in the process chamber to reach the minimum capacity of the fluid bed.

5.6 Cores and pellets characterization

A. Particle size and shape analyses

Particle size distribution of the pellets was determined by a set of analytical sieves (500, 600, 710, 850, 1000, 1180, 1400, 1700, 2000 m) piled in a sieve shaker (Endecotts, Octagon 200, London, United Kingdom) operated for 5 min at an amplitude of 4. From the weight distribution, the geometric mean diameter (d_{geo}) and geometric standard deviation (σ_{geo}) were calculated.

Mean diameter (d_m) and aspect ratio were determined using an image analysis system. Digital photomicrographs (n = 30, DinoCapture, Hsinchu, Taiwan) were analyzed by ImageJ software that allow calculation of cores or pellets dimensional and shape descriptors. The aspect ratio (AR) was calculated as follows:

Aspect ratio (AR) = Major Axis/Minor Axis

AR indicates the particle's fitted ellipse.

Yield% was calculated as ratio between the mass of obtained cores (500–2000 µm range) and the weighed amount of excipients.

B. Disintegration test

Disintegration test was performed in a dissolution apparatus 2: 300 mg of pellets in the 850–1000 m range were poured in a vessel containing 1000 mL of pH 6.8 phosphate buffer (37.0 ± 0.5 °C), and stirred at 100 rpm for 30 min. Then, pellets retained by a 400 µm net were dried (40 ° C, 24 h) and weighted; finally, the percentage of mass loss was calculated (n=2).

C. Insulin assay and *in vitro* release

In order to assess insulin content, approximately 10 mg of cores of pellets, exactly weighed, were added to 0.05M HCl, stirred at 350 rpm for 10 min, sonicated for 10 min and centrifuged (12000 rpm, 20 min). The supernatant was analyzed by RP-HPLC analysis as described in section 5.4.3. *In vitro* release from uncoated cores and coated pellets was assessed following incubation in 10 mL of phosphate buffer (pH = 6.8) containing 0.2% bovine albumin at 37°C under stirring (n = 3). At pre-determined time-points, 1 mL of medium was withdrawn and replaced with fresh buffer solution, centrifuged and analyzed by RP-HPLC as previously described. In the case of three-layer and gastro-resistant formulations, coated pellets were tested in HCl 0.1 M for 2 h prior to the buffer stage.

D. Redispersion studies

25 mg of NI and NC containing cores were incubated in 5 mL of 0.1 M HCl at 37°C under stirring (600 rpm) for 5 h. After incubation, an aliquot (2mL) was filtered with 0.45 µm membrane and analyzed by DLS. The choice of the medium occurred by checking the non-influence of other excipients in analysis result and the stability of the NPs in this solution. The study was conducted in triplicate.

5.7 *In vivo* studies

5.7.1 Diabetic rat model

For the in vivo experiments, Sprague Dawley rats, purchased by Charles River Laboratories (Calco, Italy), were maintained in a fully-equipped facility in appropriate cages and provided with a proper environment. Diabetes was induced by two intraperitoneal injections of 50 mg/kg streptozotocin diluted in 0.1 M sodium citrate buffer pH 4.5 (one injection per week for two weeks). Seven days after the first administration, all rats were weighted and glycaemia was measured by puncturing the tail vein with an 18-gauge needle and collecting the blood droplet in the test strip of a blood glucose meter (Contour Link, Bayer, Milan, Italy). After the first injection, around 40% of treated rats developed glycemic values over 350 mg/dL, indicative of diabetes onset [28]. All animals were treated again and, after further seven days, we obtained 75–80% of stably diabetic rats (glucose concentration ranging between 350 and 600 mg/dL).

5.7.2 Administration of insulin formulations to diabetic rats

Three groups of diabetic rats have been in turn injected subcutaneously with a solution of free insulin (n = 3, 0.07 mg/kg in phosphate buffer pH 6.8), and orally by gavage with a peptide solution (n = 5, 1.33 mg/kg in 10^{-3} M HCl) as well as with a nanoparticle formulation (n = 6, NI, 1.33 mg/kg). All other rats have undergone a surgical gastrostomy, upon anesthetization by intraperitoneal injection of 500 mg/kg of Avertin, for the insertion into the stomach of one capsule containing pellets formulations loaded with insulin (1.33 mg/kg): GPNI (n = 5, 53 mg), GPI (n = 3, 55 mg) CPNI (n = 4, 168 mg), CPI (n = 4, 63 mg). After insertion of the capsule, the stomach was sutured with 4-0 resorbable running suture, and the abdomen closed by 2-0 silk interrupted stitches. The gastrostomy procedure was chosen due to the impossibility to obtain a suitable oral administration of the free pellets in aqueous solution: low stability and high electrostatic interaction with the gavage tube were observed. One group of 5 rats was left untreated. The blood glucose levels were monitored by collecting blood droplets as described above at 1, 2, 3, 4, 5, 6, 7, 8, and 48 h post-treatment. Rats were used in accordance with an experimental protocol subjected to the direct approval of the Italian Ministry of Health.

Bibliography

[1] T. Bailey, “Options for combination therapy in type 2 diabetes: comparison of the ADA/EASD position statement and AACE/ACE algorithm,” Am. J. Med., vol. 126, p. S10-20, 2013.

[2] S. Dal, “Portal or subcutaneous insulin infusion: efficacy and impact on liver inflammation,” Fundam. Clin. Pharmacol., vol. 29, p. 488-498, 2015.

[3] I. Hirsch, “Insulin Analogues,” N Engl J Med, vol. 352, p. 174-183, 2005.

[4] A. Maroni, “Oral colon delivery of insulin with the aid of functional adjuvants,” Adv. Drug. Deliv. Rev., vol. 64, p. 540-556, 2012.

[5] M. Rekha, “Oral delivery of therapeutic protein/peptide for diabetes-Future perspectives,” Int. J. Pharm., vol. 440, p. 48-62, 2013.

[6] V. Agarwal, “Current status of the oral delivery of insulin,” Pharm. Technol., vol. 10, p. 76-90, 2001.

[7] F. Sousa, “How to overcome the limitations of current insulin administration with new non-invasive delivery systems,” Ther. Deliv., vol. 6, p. 83-94, 2015.

[8] M. Patel, “Colon targeting: an emerging frontier for oral insulin delivery,” Exp. Opin. Drug Deliv., vol. 10, p. 731-739, 2013.

[9] A. Gazzaniga, “Time-controlled oral delivery systems for colon targeting,” Exp. Opin. Drug Deliv., vol. 3, p. 583–597, 2006.

[10] C. Damge, “Nanoparticle strategies for the oral delivery of insulin,” Exp. Opin. Drug Deliv., vol. 5, p. 45-68, 2008.

[11] L. Ensign, “Oral drug delivery with polymeric nanoparticles: the gastrointestinal mucus barriers,” Adv. Drug Deliv. Rev., vol. 64, p. 557-570, 2012.

[12] A. Bayat, “Nanoparticles of quaternized chitosan derivatives as a carrier for colon delivery of insulin: ex vivo and *in vivo* studies,” Int. J. Pharm., vol. 356, p. 259-266, 2008.

[13] R. Diab, “Engineered Nanoparticulate Drug Delivery Systems: The Next Frontier for Oral Administration?,” AAPS J. , vol. 14, no. 4, p. 688-702, 2012 Dec; 14(4).

[14] L. Palugan, “Coated pellets for oral colon delivery,” J. Drug Deliv. Sci. Technol., vol. 25, p. 1-15, 2015.

[15] M. Del Curto, “Erodible time-dependent colon delivery systems with improved efficiency in delaying the onset of drug release,” J. Pharm. Sci. 103 (2014) 3585–3593, vol. 103, p. 3585-3593, 2014.

[16] S. Davis, “The design and evaluation of controlled release systems for the gastrointestinal tract,” J. Control Release, vol. 2, p. 27–38, 1985.

[17] E. Herrero, “PolymerMbased oral peptide nanomedicines.,” Therapeutic Delivery, vol. 3, no. 5, p. 657-668, 2012.

[18] G. Ranaldi, “The effect of chitosan and other polycations on tight junction permeability in the human intestinal Caco-2 cell line,,” Nutr. Biochem., vol. 13, p. 157-167, 2002.

[19] W. Tiyaboonchai, "Insulin containing cointaining polyethylenimine-dextran sulfate nanoparticles," International Journal of Pharmaceutics, vol. 255, no. 1-2, p. 139-151, 2003.

[20] C. Tuleu, “Gastrointestinal transit of pellets in rats: effect of size and density,” International Journal of Pharmaceutics, vol. 180, no. 1, p. 123-131, 1999.

[21] D. Gervais, “Protein deamidation in biopharmaceutical manufacture: understanding, control and impact,” J Chem Technol Biotechnol, vol. 91, p. 569–575, 2016.

[22] S. Muley, “Extrusion–spheronization a promising pelletization technique: In-depth review,” Asian Journal of Pharmaceutical Science, vol. 11, no. 6, p. 684-699, 2016.

[23] F. Casati, “Co-processed microcrystalline cellulose and sodium carboxymethyl cellulose as spheronization aid for disintegrating pellets,” in 54° AFI symposium, Rimini (IT), 2014.

[24] G. Di Pretoro, “Extrusion-spheronisation of highly loaded 5-ASA multiparticulate dosage forms,” Int. J. Pharm., vol. 402, p. 153-164, 2010.

[25] H. Tozaki, “Chitosan capsule for colon-specific drug delivery: improvement of insulin absorption from the rat colon,” J. Pharmaceutical Science, vol. 86, p. 1016-1021, 1997.

[26] A. Maroni, “Preliminary *in vivo* evaluation of an oral multiple-unit formulation for colonic delivery of insulin,” in 41st Annual Meeting & Exposition of the Controlled Release Society, Chicago, 2014.

[27] J. De Sesso, “Anatomical and physiological parameters affecting gastrointestinal absorption in humans and rats,” Food Chem. Toxicol., vol. 39, p. 209-228, 2001.

[28] A. Like, “Streptozotocin-Induced Pancreatic Insulitis/ New Model of Diabetes Mellitus,” Science, vol. 193, no. 4251, p. 415-417, 1976.

[29] J. Lee, “Characterization of Streptozotocin-induced diabetic rats and pharmacodynamics of Insulin formulations,” Biosci. Biotechnol. Biochem., vol. 67, p. 2396-2401, 2003.

[30] J. Saha, “Acute hyperglycemia induced by ketamine/xylazine anesthesia in rats: mechanisms and implications for preclinical models, Exp. Biol. Med. 230 (2005) 777–784.,” Exp. Biol. Med., vol. 230, p. 777-784, 2005.

[31] J. Bai, “Transepithelial transport of Insulin: i. Insulin degradation by insulin-degrading enzyme in small intestinal epithelium,” Pharm. Res., vol. 12, p. 1171-1175, 1995.

[32] L. Chang, “Immunohistochemical localization of insulin-degrading enzyme along the rat intestine in the human colon adenocarcinoma cell line (Caco-2), and in human ileum,” J. Pharm. Sci., vol. 86, p. 116-119, 1997.

[33] G. Sharma, “Nanoparticle based insulin delivery system: the next generation efficient therapy for Type 1 diabetes,” J. Nanobiotechnol., vol. 13, p. 74-87, 2015.

[34] Y. Lin, “Novel nanoparticles for oral insulin delivery via the paracellular pathway,” Nanotechnology 18 (2007) 105102, vol. 18, no. 105102, 2007.

[35] A. Adson, “Passive diffusion of weak organic electrolytes across Caco-2 cell monolayers: uncoupling the contributions of hydrodynamic, transcellular, and paracellular barriers,” J. Pharm. Sci. 84 (1, vol. 84, p. 1197-1204, 1995.

[36] G. Strous, “Mucin-type glycoproteins,” Crit. Rev. Biochem. Mol. Biol., vol. 27, p. 57-92, 1992.

[37] A. Maroni, “Feasibility, stability and release performance of a time-dependent insulin delivery system intended for oral colon release,” Eur. J. Pharm. Biopharm, vol. 72, p. 246–251, 2009.

[38] A. Yamamoto, “Effects of various protease inhibitors on the intestinal absorption and degradation of insulin in rats,” Pharmaceutical Research, vol. 11, p. 1496-1500, 1994.

[39] L. Salvioni, “Oral delivery of insulin via polyethylene imine-based nanoparticles for colonic release allows glycaemic control in diabetic rats,” Pharmaceutical Research, vol. 110, p. 122-130, 2016.

[40] S. Mazzucchelli, “Diabetes management strategies: can nanoparticles be used to therapeutically deliver insulin?,” Ther Deliv, vol. 8, p. 49-51, 2017.

[41] E. Zijlstra, “Oral Insulin Reloaded: A Structured Approach,” J Diabetes Sci Technol, vol. 8, p. 458-465, 2014.

[42] M. Lopes, “Why most oral insulin formulations do not reach clinical trials,” Ther Deliv, vol. 6, p. 973-987, 2015.

Project 2:

Development of lipidic NPs

as gene delivery vectors

in triple negative breast cancer

1. Background

Breast cancer (BC) is the most common type of cancer found in women and, due to its heterogeneity, represents a significant challenge to public health [1]. Among the BC subtypes, triple-negative breast cancers (TNBC) lack the expression of estrogen receptor (ER), progesterone receptor (PR) and epidermal growth factor receptor type 2 (HER2) [2]. Whereas many BC are successfully treated by hormonal and anti-HER2 targeted therapy, TNBC patients typically have a relatively poor clinical outcome and frequent local and distant recurrences [3]. Nowadays, the recommended option for TNBC treatment is the cytotoxic chemotherapy, but new systemic therapies, that provide enhanced efficacy and minimize off- target toxicity, are urgently needed [4].

In this context, considerable research efforts have been focused to gene therapy: indeed, the introduction of genetic material may directly induce cancer cell death, revert the malignant phenotype or stimulate the immune system (immunotherapy) [5]. Several strategies have been reported for cancer cell killing namely suicide gene therapy, gene silencing, microRNA-based therapy [6]. Particularly, suicide gene therapy is based on cancer cells delivery of transgenes encoding for cytotoxic proteins such as toxins, pro-apoptotic macromolecules, pro-drug activating enzymes [7]. Although several clinical trials have been proposed for latter approach, the use of toxins is still appealing due to their direct action: indeed, all the issues connected with the pro-drug use are avoided since the transgene directly encode for cell-death inducers. In this regard, among the therapeutic proteins, Saporin (SAPO) has been extensively reported as cytotoxic agent for cancer treatment purposes

[8]. This plant toxin belongs to type-1 ribosome-inactivating proteins (RIP) family, a class of enzymes that remove an adenine residue on a sequence universally conserved among eukaryotic rRNA [9]. Hence, damaging the ribosomes irreversibly, SAPO is able to inhibit protein synthesis killing both quiescent and rapidly dividing cancer cells [10]. Despite this favourable cell cycle-independent action, SAPO efficacy is strongly limited because it is poorly bioavailable and, in contrast with type-2 RIP, it lacks the membrane binding domain necessary for the cellular internalization [11]. Several strategies are indicated for increasing drug activity such as drug conjugates or transgene delivery. The latest approach may represent attractive alternative to protein-substitution therapy since the transgene expression generally leads to stable levels of the drug; in principle, one single molecule introduced in the malignant cells is sufficient to induce the intracellular expression of toxin causing cell death [12]. In addition, the production and purification of plasmid DNA is fast, cheap and easily scalable.

In gene therapy, numerous non-viral systems have been developed to overcome the poor bioavailability and release specificity of nucleic acids. Due to their efficient DNA condensation capacity and easy functionalization with targeting ligands, cationic lipid nanoparticles (NPs) have been extensively reported as gene delivery vectors.

Exploiting one of these promising carriers, the aim of this project was to develop and test both *in vitro* and *in vivo* a nanovector of SAPO encoding pDNA with a selective targeting for poorly differentiated TNBC cells (MDA-MB-231 cell line).

Among the lipid nanocarriers reported, lipid-protamine-DNA (LPD) NPs were selected because the use of polycations (*i.e.* protamine) as condensing agent is

generally able to improve the lipofection efficacy by promoting a more efficient endosomal escape and nuclear translocation of DNA [13] [45] [46].

In addition, in order to improve the cancer cells uptake, a peptide called U11 (VSNKYFSNIHW) was chosen as targeting ligand for urokinase plasminogen activator receptor (UPAR). Indeed, UPAR was found overexpressed in TNBC and generally associated with cancer invasion and metastasis [14] [15], whereas U11 represents a prominent part of the recognition fragment in UPAR natural ligand [16]. A schematic representation of the vector is reported below (Fig. 1.1).

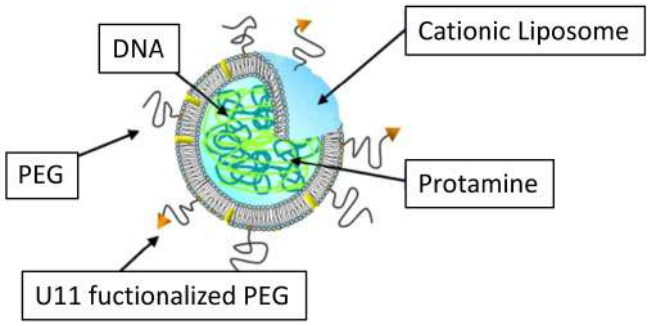

Fig. 1.1: Schematic illustration of the gene delivery system investigated.

2. Results

2.1 NPs synthesis

LPD NPs were synthetized according to a previously reported protocol [17]. Briefly (Fig. 2.1.1), an excess of DNA was condensed with protamine sulfate producing a negatively charged complex. Afterwards, the addition of cationic liposomes caused their collapse and bilayer fusion around the core [18].
Lastly, the final particle was obtained by the inclusion of PEGylated lipids. To achieve the UPAR targeting, a lipid functionalized with U11 was included in the last step of the reaction resulting in LPD-U11 NPs (details reported in 2.1.1 section).

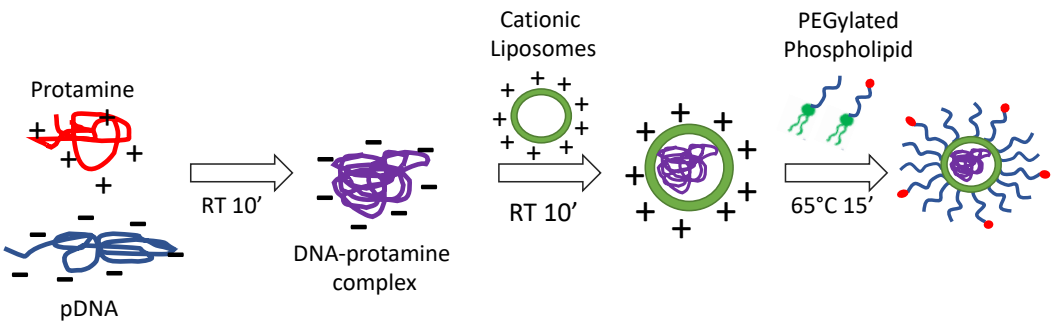

Fig. 2.1.1: Schematic representation of the synthesis method; the cationic liposomes were composed by the cationic dioleoyl-trimethylammonium propane (DOTAP) and cholesterol (1:1 mol), whereas the PEGylated phospholipid mixture by 1,2-distearoyl-sn- glycero-3-phosphoethanolamine-N-[methoxy(polyethylene glycol)-2000] (ammonium salt) (DSPE-PEG-OCH_3) and the functionalized DSPE-PEG-U11 (targeting agent). The lipid reagent structures are reported in Material and Method section.

The liposomes, composed by equal molar amounts of cholesterol and the cationic dioleoyl-trimethylammonium propane (DOTAP), were synthetized by extrusion and characterized by DLS and Z-potential analysis. The mean hydrodynamic diameter was included in a range between 100 and 120 nm and the Z-potential was ~ +50 mV.

2.1.1 DSPE-PEG-U11 conjugate synthesis

The conjugation of 1,2-distearoyl-sn- glycero-3-phosphoethanolamine-N-[maleimide(polyethylene glycol)-2000] (ammonium salt) (DSPE-PEG-mal) and U11 peptide was obtained though the maleimide-thiol condensation (Fig. 2.1.1.1): the lipid containing maleimide group reacted with thiol functionalization introduced in U11 by adding an extra N-terminal cysteine residue.

The reaction was conducted in a polar solvent (N,N dimethylformamide (DMF)) under base catalysis (triethylamine (Et_3N)) in order to improve its efficacy and kinetic properties [19].

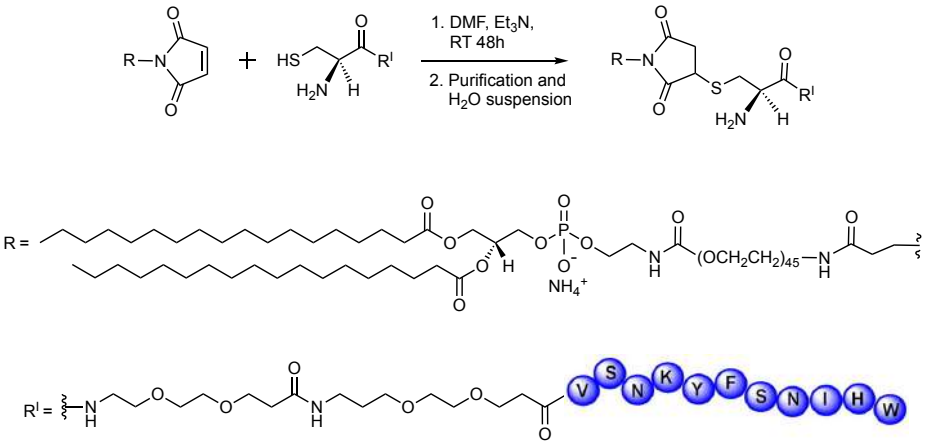

Fig. 2.1.1.1: Synthesis route of DSPE-PEG-U11 conjugate.

After product purification, the reaction efficiency was evaluated by direct spectrophotometric determination.

In particular, the absorbance of the conjugated peptide was assessed at 280 nm, where the presence of aromatic amino acids tryptophan (W) and tyrosine (Y) determined strong light absorption. Since absorbance of U11 is proportional to its concentration (Beer-Lambert law), a standard curve was used as reference for the product quantification (Fig. 2.1.1.2). The yield was 84.4 ± 11.0 (n=6), expressed as percentage of the starting reagent amount.

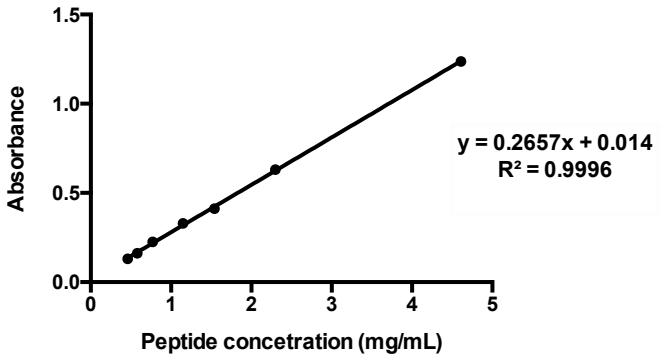

Fig. 2.1.1.2: Absorbance detected at 280 nm wavelength as a function of peptide concentration.

To assess the method reliability, the possible interference of the lipid portion in the quantification was estimated. For this purpose, DSPE-PEG-U11 and DSPE-PEG-mal spectra were recorded and compared with U11 profile. As reported (Fig. 2.1.1.3), the product spectra perfectly overlapped with the peptide one indicating the successful conjugation, whereas DSPE-PEG-mal exhibited a different profile caused by the light absorption of maleimide group. Since the functional group was no longer included in the final product,

the interference DSPE-PEG-mal at the selected wavelength (*i.e.* 280 nm) was considered irrelevant in the yield calculation.

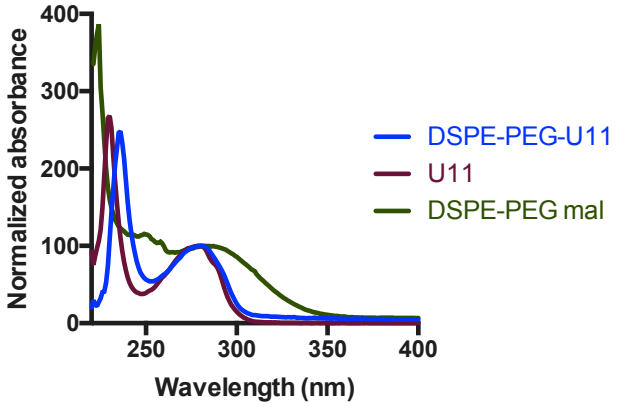

Fig. 2.1.1.3: UV-vis absorbance spectra (normalized to the maximum absorbance).

2.1.2 LPD-U11 NPs synthesis optimization

LPD-U11 NPs were firstly synthesized following the lipid percentages reported in literature [20]: in that formulation, the functionalized DSPE-PEG was 2.8 mol % of the total lipid content and the targeting agent was a small molecule.

Using this protocol, the obtained NPs (2.8 mol % formulation) tended to aggregate: as shown by DLS analysis (Fig. 2.1.2.1, Tab. 2.1.2.1), their mean hydrodynamic diameter and polydispersity index (PDI) significantly increased compared to non-targeted NPs (0 mol % formulation).

This aggregation was probably caused by the peptide presence: indeed, in a previous publication [21], U11 was shown to form β-sheets on the surface of liposomes when inserted at high densities. However, at lower concentrations (1 mol %), the same peptide–lipid conjugates appear to rearrange into more separated structures inside the liposome bilayer [21].

Thus, 1 mol % formulation was prepared and characterized. In this case, the distribution was unimodal and the mean diameter along with PDI slightly increased from 0 % formulation values (Fig. 2.1.2.1, Tab. 2.1.2.1).

This increment related with DSPE-PEG-U11 insertion was considered acceptable and this formulation chosen for the next investigations.

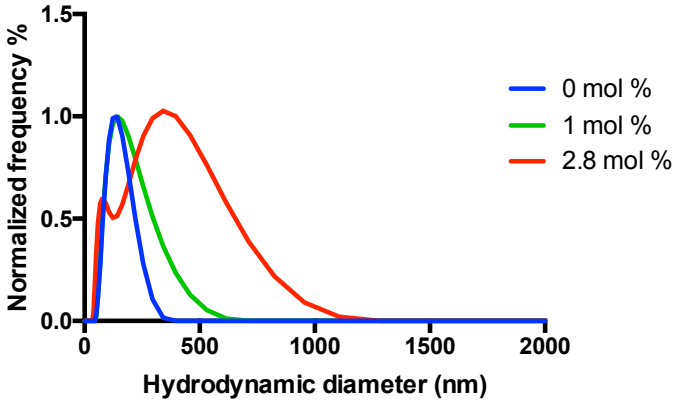

Fig. 2.1.2.1: Size distribution of LPD-U11 with different DSPE-PEG-U11 content (1 and 2.8 mol %) in comparison with non-targeted formulation (0 mol %) evaluated by DLS analysis.

Table 2.1.2.1: Characterization of LPD-U11 with different DSPE-PEG-U11 content (1 and 2.8 mol %) in comparison with non-targeted formulation (0 mol %) by DLS analysis. Mean ± SD (n = 3) are reported.

DSPE-PEG-U11 amount (mol %)	Hydrodynamic diameter (nm)	PDI
0	154.5 ± 11.4	0.231 ± 0.041
1	173.3 ± 5.15	0.281 ± 0.006
2.8	284.2 ± 48.6	0.274 ± 0.084

Afterwards, PEGylation process was optimized: the aim of this functionalization was to limit the extensive mononuclear phagocyte system (MPS) uptake associated with positively charged NPs.

In the starting formulation, the amount of PEGylated lipids was 5.6 mol % of the total lipid content, while 10, 12.5 and 15 mol % formulations were proposed for this study increasing DSPE-PEG-OCH_3 amount.

After the synthesis, all the batches were characterized by DLS and Z-potential analysis.

As reported (Tab. 2.1.2.2), the mean diameter and PDI increased with the degree of PEGylation, whereas a relevant Z-potential decrease was not observed.

On this basis, 5.6 mol % formulation was selected for further investigations.

Table 2.1.2.2: Characterization of different formulations by DLS and Z-potential analysis (mean ± SD n=3).

PEGylated lipids amount (mol %)	Hydrodynamic diameter (nm)	PDI	Z-potential (mV)
5.6	173.3 ± 5.15	0.281 ± 0.006	+35.0 ± 0.3
10	184.1 ± 9.25	0.321 ± 0.020	+31.2 ± 0.1
12.5	213.9 ± 27.7	0.369 ± 0.018	+28.9 ± 1.5
15	248.3 ± 32.6	0.381 ± 0.009	+30.4 ± 0.4

The formulation optimized by the previous studies was further characterized by TEM analysis (Fig. 2.1.2.2): the effective diameter was 104.5 ± 19.2 (n=60) and the difference with the DLS analysis (*i.e.* 173.3 ± 5.15) was caused by the high solvation efficiency of the lipid NPs.

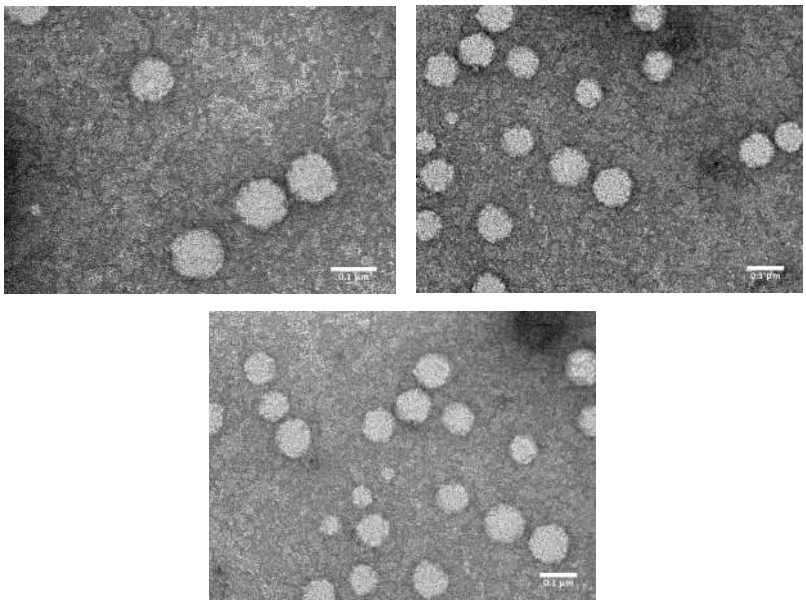

Fig. 2.1.2.2: TEM images of LPD-U11 NPs; scale bars = 100 nm.

Then, the stability of LPD-U11 NPs was evaluated in different medium by DLS analysis and compared with non-targeted NPs (LPD NPs) (Fig. 2.1.2.3): the scattering technique was chosen for its great sensitivity for small amounts of aggregates [22].

As expected LPD-U11 NPs maintained the same distribution properties (in terms of mean diameter and PDI) when dispersed in water and glucose 5 % w/V: the latter medium was previously used for NPs injection [17], while the water was normally employed for the characterization.

On the other hand, in phosphate buffer (PBS, pH 7.4) both the mean diameter and PDI increased. Since this increment was not observed in LPD NPs, this aggregation was due to U11 functionalization. This was not surprising given that the peptide was almost not soluble and tended to agglomerate when suspended in PBS.

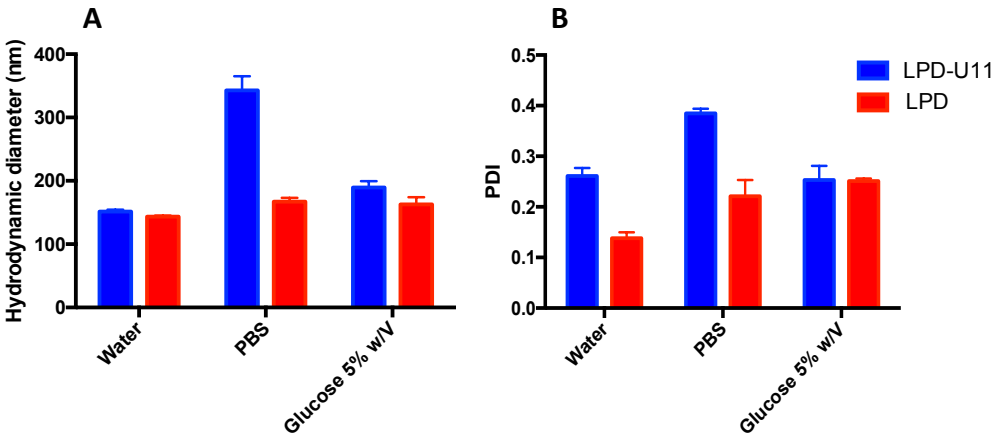

Fig. 2.1.2.3: Evaluation of LPD and LPD-U11 NPs stability in different medium.

A. hydrodynamic diameter B. PDI (mean ± SD n = 3).

Finally, in order to establish the storage condition, the batches stability at 4°C was evaluated. After 1 day (time set in view of the use requirements), no visible aggregation occurred and the preparation was stable as confirmed by the DLS and Z-potential analysis (Fig. 2.1.2.4)

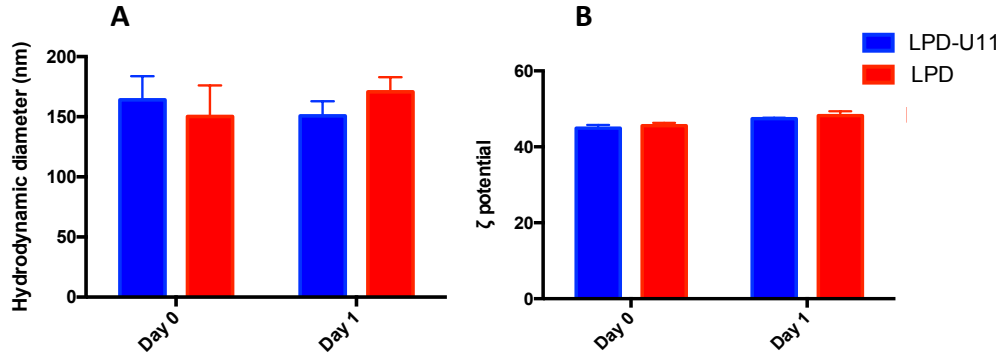

Fig. 2.1.2.4: Evaluation of LPD and LPD-U11 NPs stability at 4°C

A. hydrodynamic diameter B. Z-potential; Mean ± SD (n = 3) are reported.

2.1.3 Fluorescent NPs synthesis and characterization

In order to study their uptake and distribution, detectable NPs were required. Fluorescent NPs are commonly used for this purpose and may be obtained by two different approaches namely surface conjugation or encapsulation.

Due to the generally higher dye stability, the encapsulation strategy was selected and among the possible fluorophores, the intercalating agent 1,1'-dioctadecyl-3,3,3',3'-tetramethyl-indodicarbocyanine, 4-chlorobenzenesulfonate salt (DiD) was chosen [17]. This far-red dye is normally employed for cellular membrane staining since it is weakly fluorescent in water, but highly fluorescent and quite photostable when incorporated into the lipid bilayers [23].

For the purpose to produce fluorescent NPs, the DiD was included during the liposome synthesis.

The DiD liposomes size distribution and surface charge properties were the same of unlabeled liposomes. Moreover, the dye intercalation was complete and stable as demonstrated after the purification by size-exclusion chromatography: the fluorescence recovery was 88.8 % of the starting value and the resin slightly colored probably more for liposomes entrapment rather than DiD intercalation failure [24]. This result was consistent with those reported in literature where dye was demonstrated to be stably retained after lipids intercalation [25].

Afterwards, targeted and non-targeted fluorescent NPs (DiD-LPD-U11 NPs and DiD-LPD NPs respectively) were synthetized and characterized.

The recorded fluorescence spectra, after excitation at 647 nm wavelength, almost overlapped and maximum intensity was similar in both the

formulations (Fig. 2.1.3.1). Comparing the fluorescence intensity values of LPD NPs at 665 nm with that of the liposomes a slight decrease was recorded (-36.4% ± 2.68 mean ± SD n=7): this variation in the brightness was probably related with the PEGylated lipids inclusion and the subsequent change in membrane composition.

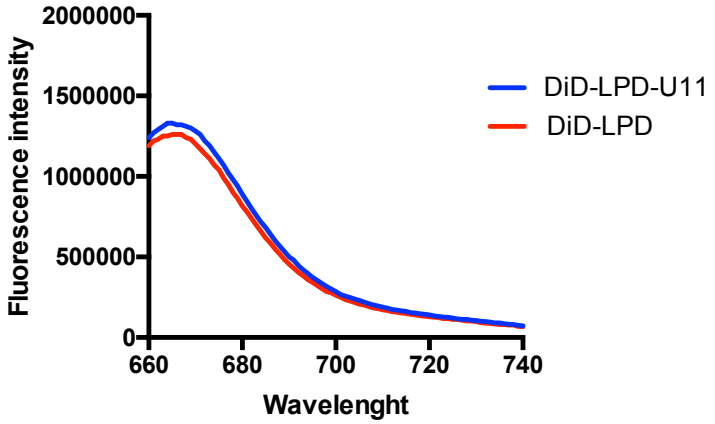

Fig. 2.1.3.1: Fluorescence spectra of fluorescent NPs (excitation wavelength = 647 nm).

After the fluorescence assessment, DLS and Z-potential analysis were conducted. As reported (Tab. 2.1.3.1), compared to non-fluorescent NPs, in both cases, the positive Z-potential was maintained, while the mean hydrodynamic diameter was significantly higher. This variation was caused by technical limitation of DLS analysis: since the wavelength of the instrument light source was 633 nm, the measurement was affected by the sample fluorescence. Indeed, as reported in the correlogram (Fig. 2.1.3.2 A), unlike LPD-U11 NPs (Fig. 2.4.2 B), the intercept value of DiD-LPD-U11 was below the appropriate values (*i.e.* 0.1-1 range) indicating an inadequate signal/background ratio [26].

Table 2.1.3.1: Characterization of fluorescent NPs by DLS and Z-potential analysis (mean ± SD n = 3).

Formulation	Hydrodynamic diameter (nm)	Z-potential (mV)
DiD-LPD-U11 NPs	225.8 ± 19.1	+41.4 ± 4.8
DiD-LPD NPs	201.4 ± 38.4	+50.2 ± 1.7

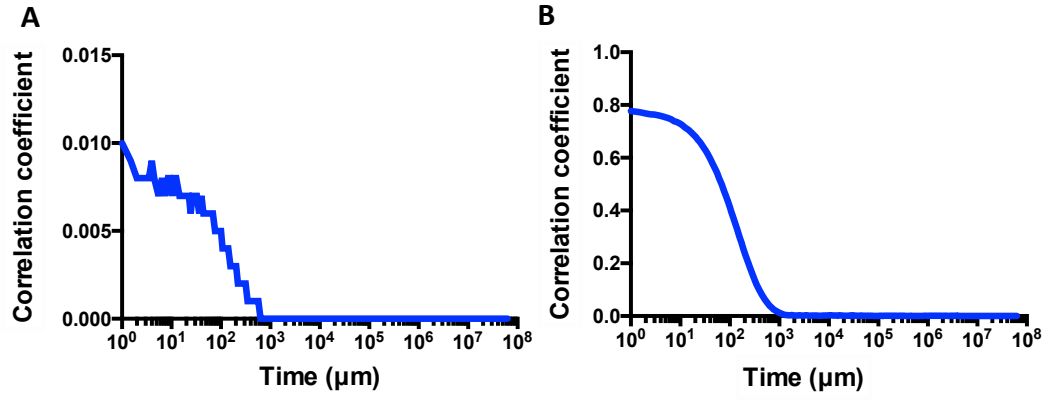

Fig. 2.1.3.2: Correlogram measured by DLS for DiD-LPD-U11 (A) and LPD-U11 (B) NPs.

Hence, for characterizing the size distribution properties, another technique namely nanoparticle tracking (NT) analysis was used.

NT and DLS analysis work with different principles: in NT analysis, the trajectories of individual scattering objects are recorded and their displacement related to each object's size, whereas for DLS analysis the intensity fluctuations in the scattered light are analyzed and related to the diffusion of the scattering objects. Thus, unless the analyzed NPs are monodispersed, the mean hydrodynamic diameter observed with NT is generally lower then DLS one.

When analyzed with the alternative technique (Tab. 2.1.3.2, Fig. 2.1.3.3), DiD-LPD-U11 NPs mean diameter was slightly higher than DiD-LPD NPs and both diameter values were comparable non-fluorescent LPD-U11 NPs and LPD NPs.

This data confirmed that the inclusion of DiD did not lead to significant changes in size distribution.

Table 2.1.3.2: Characterization of fluorescent and non-fluorescent NPs by NT analysis (mean ± SE n = 5).

Formulation	Mean hydrodynamic diameter (nm)	SD (nm)
DiD-LPD-U11 NPs	138.2 ± 1.4	38.9 ± 3.6
DiD-LPD NPs	135.4 ± 2.7	41.7 ± 6
LPD-U11 NPs	138.6 ± 5.9	31.9 ± 1.9
LPD NPs	134.3 ± 6.0	36.8 ± 5.1

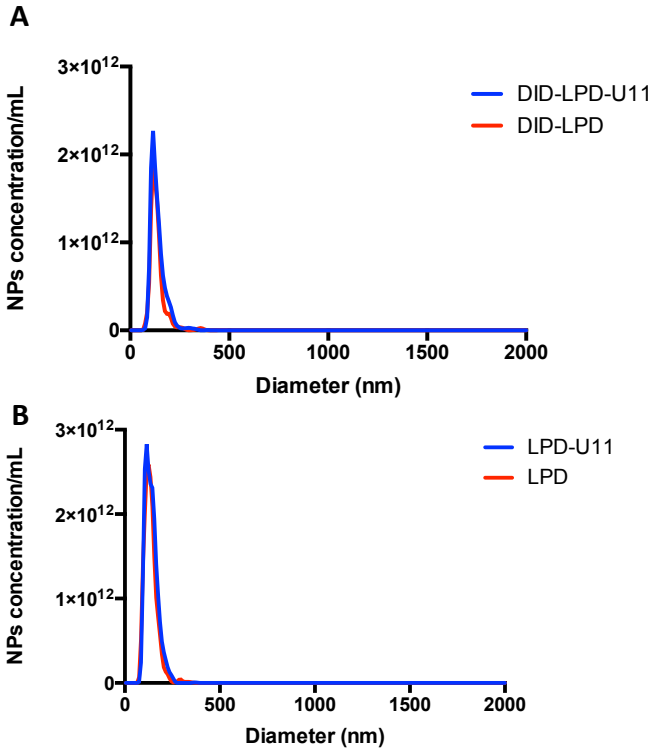

Fig. 2.1.3.3: Size distribution of fluorescent (A) and non-fluorescent (B) NPs evaluated by NT analysis.

Finally, in view of *in vivo* biodistribution experiment, the DiD intercalation stability in plasma was assessed by fluorescence analysis.

The test was conducted on DiD-LPD-U11 after plasma suspension and sample centrifugation 15 min at 1500×g.

The NPs concentration was set according with the blood concentration expected after *in vivo* administration of 30 μg plasmid/mouse, whereas the centrifugation step was performed for mimicking the plasma extraction.

A reduction of fluorescence intensity was recorded (-30% of the starting value) and this result may be related with some aggregation phenomena induced by the interaction with negatively charged plasma proteins [27]. However, this decrease was considered acceptable and the sample fluorescence was stably maintained even after 2 days of incubation at 4°C (Fig. 2.1.3.4).

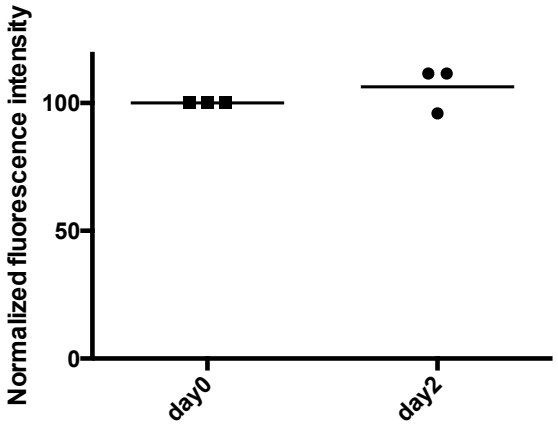

Fig. 2.1.3.4: DiD-LPD-U11 stability after plasma suspension and centrifugation (15 min at 1500×g) was assessed at 4°C. The fluorescence intensity of each preparation was normalized on day 0 intensity. Bars indicate the mean values.

2.2 *In vitro* experiments

Before studying the cell-NPs interaction, the UPAR expression on MDA-MB-231 cells surface was assessed by double-antibody immunostaining. In control samples, the same cell line was used, but the immunodecoration was performed using just the secondary antibody. In the results, the fluorescence intensities of control and treated samples were normalized with the untreated one. As reported (Fig. 2.2.1), the receptor levels of the treated samples were significantly different both from control and untreated ones indicating UPAR expression.

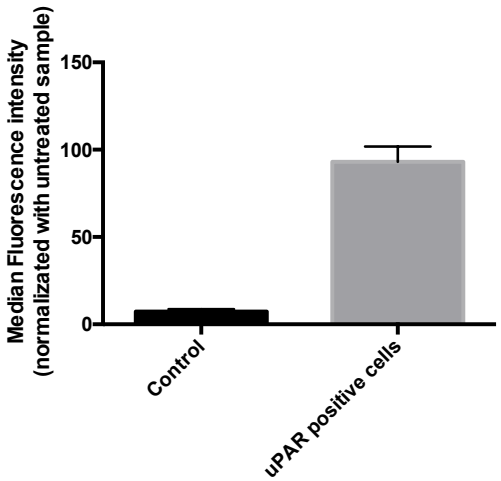

Fig. 2.2.1: UPAR expression evaluated by flow cytometry (double antibody immunostaining). Median intensity values were normalized to the untreated sample (mean ± SD n = 3).

Afterwards, NPs binding efficiency was studied by fluorescence-based flow cytometry (FACS) as a function of their concentration. Cell-associated fluorescence was examined 1 h after incubation of DiD-LPD-U11 NPs and DiD-LPD NPs. The incubation was performed at 4 °C to assess the UPAR-U11 interaction and minimize endocytosis phenomena.

As reported in Fig. 2.2.2, the cell binding was concentration dependent and no significant difference both in fluorescence intensity and percentage of positive cells was observed between targeted and non-targeted NPs, even in non-saturated conditions (0.0012 μg/well plasmid). This was likely due to the strong non-specific association of positively charged NPs with the negatively charged cell membrane [28].

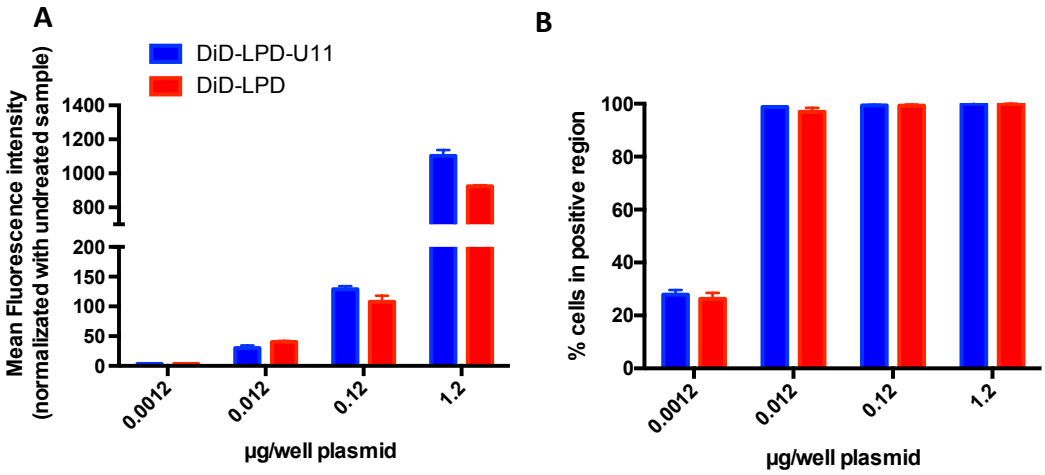

Fig. 2.2.2: Binding assay results: MDA-MB-231 cells were incubated with targeted and non-targeted NPs (LPD-U11 and LPD formulation respectively) for 1 h at 4 °C and then processed with flow cytometry. Reported values are median fluorescence intensity (A) and percentage of positive cells (B) normalized vs. untreated cells (mean ± SD n = 3).

In light of the above considerations, another test was performed to evaluate if there was a different cellular internalization capacity between targeted and non-targeted NPs.

Cells were incubated with DiD-LPD-U11 NPs and DiD-LPD NPs for 30 min, 2 and 6 h at 37°C and analyzed by confocal microscopy to assess the uptake and intracellular trafficking. For this purpose, the cell membrane was stained in order to differentiate the cytosol from the extracellular compartment.

As reported in Fig. 2.2.3 and 2.2.4, both the formulations were quickly internalized, since the NPs signal was recovered inside the cell cytoplasm after only 30 min of incubation, and they continued to accumulate until 6 h.

Along with the intensity increasing over time, the signal appeared as spotted at the early stages, while at 6 h large amount of DiD scattered throughout the cytoplasm. This pattern was consistent with what previously observed by Luo C. et al. with a similar preparation: indeed, this lipidic NPs were expected to enter by endocytosis and release their cargo after endosome destabilization [17] [41] (for further information see 2.3.2.2 of Introduction). In addition, LPD-U11 showed greater cellular internalization than LPD NPs and this result was supported by uptake quantification performed calculating the fluorescence intensity per cell area at 2 (Fig. 2.2.5 panel A) and 6 h (Fig. 2.2.5 panel B).

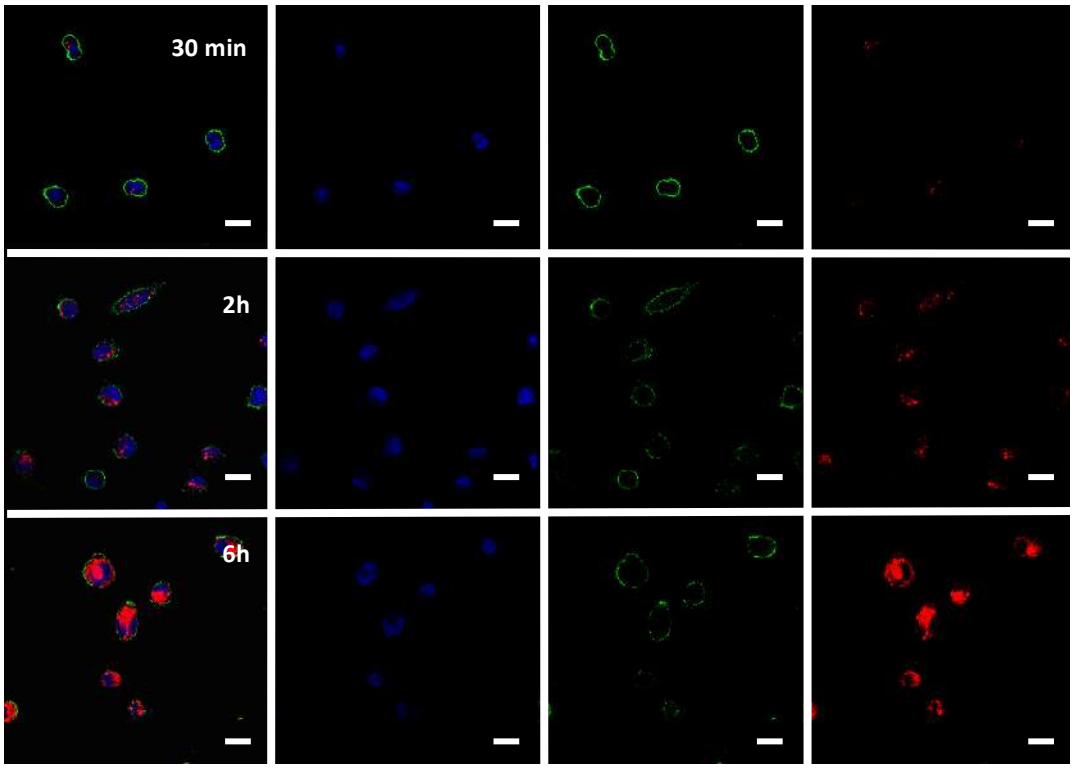

Fig. 2.2.3: *In vitro* time-dependent cellular uptake of DID-LPD-U11 NPs; Red: NPs; Green: Wheat Germ Agglutinin (WGA) membrane staining; Blue: nuclei staining; scale bars = 20 μm.

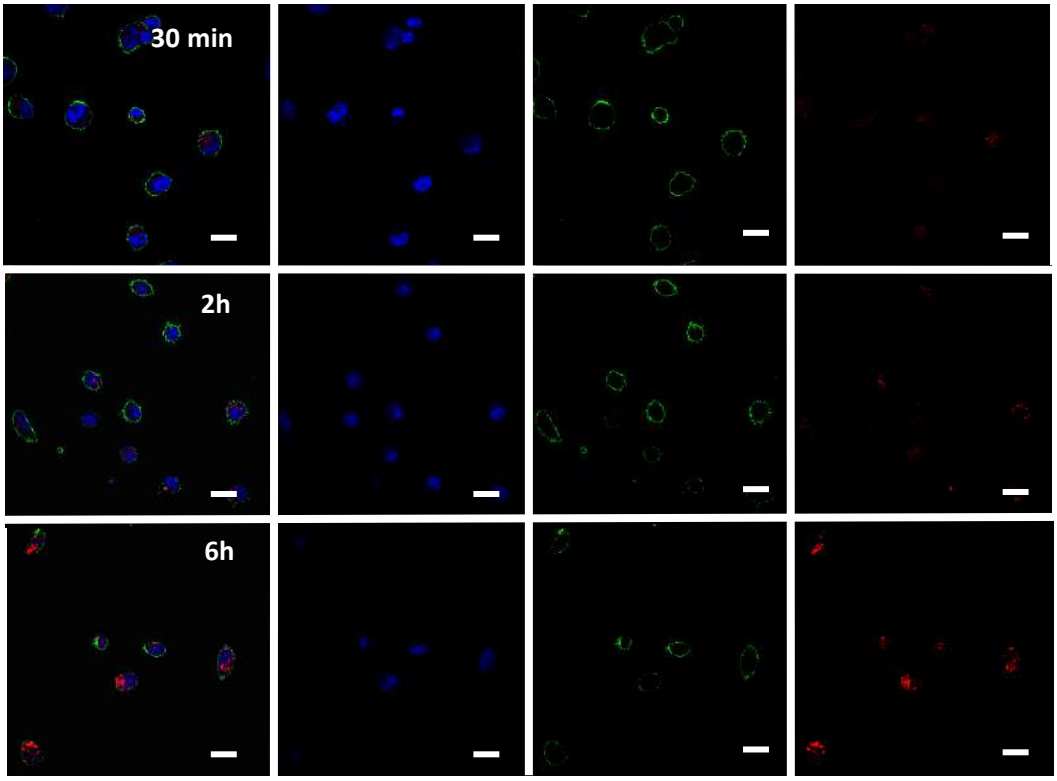

Fig. 2.2.4: *In vitro* time-dependent cellular uptake of DID-LPD NPs; Red: NPs; Green: Wheat Germ Agglutinin (WGA) membrane staining; Blue: nuclei staining; scale bars = 20 μm.

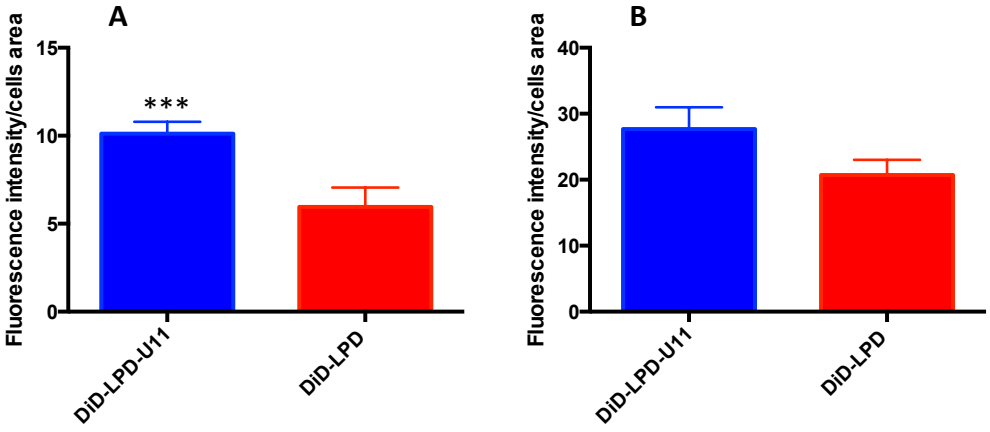

Fig. 2.2.5: Uptake quantification (A) at 2h (n=60) and (B) 6h (n=40) of targeted and non-targeted NPs (DiD-LPD-U11 and LPD formulation respectively) expressed as fluorescence intensity per cell area (mean ± SE). Statistical significance vs. non-targeted NPs ***p<0.005.

Once confirmed the NPs internalization, the activity of LPD-U11 NPs encapsulating SAPO encoding plasmid (LPD@SAPO-U11) was investigated.

Cell viability test (Fig. 2.2.6) was performed comparing the selected formulation with other samples namely non-targeted NPs encapsulating SAPO encoding plasmid (LPD@SAPO) and targeted NPs encapsulating a control non-encoding pDNA (LPD@empty U11). These two formulations were tested to evaluate targeting efficacy and the nanocarrier toxicity respectively. The viability was assessed as function of NPs concentration.

When incubated with the lowest concentration (0.2 μg plasmid/well), all the formulations induced minimally *in vitro* cytotoxicity, while at the highest concentration (1 μg plasmid/well), the cell viability was greatly reduced by all the preparations probably because the well-known non-specific antitumor activity of cationic lipids [29].

At 0.5 μg plasmid/well, a difference among the samples was observed: indeed, the inhibition of cell viability using LPD@SAPO-U11 was significantly higher than that after treatment with LPD@SAPO and LPD@empty-U11 (Table 2.2.1).

It was likely that the enhanced UPAR-mediated uptake of LPD@SAPO-U11 increased the SAPO expression and its anticancer activity. Moreover, the reduction in cell viability observed in samples incubated with LPD@empty-U11 at this concentration was considered not biologically significant as compared with the lowest concentration values.

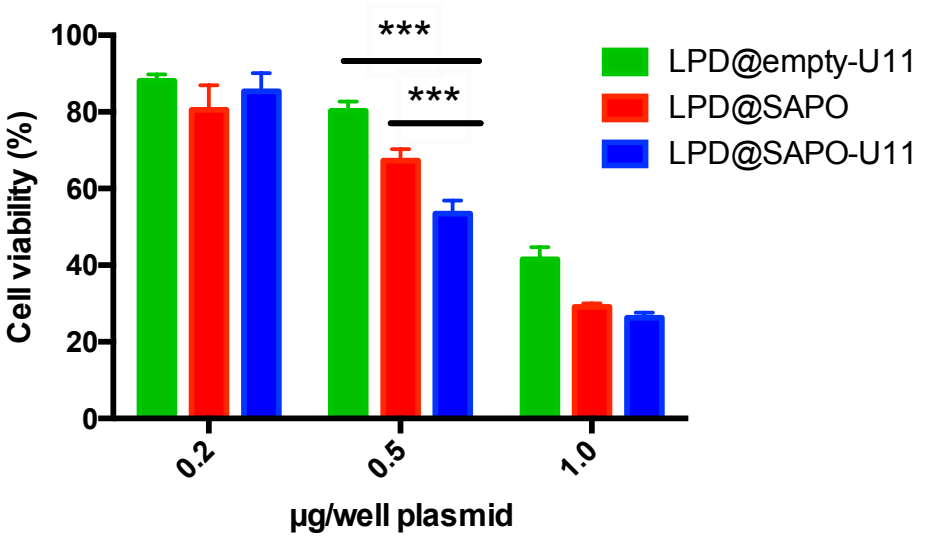

Fig. 2.2.6: Viability of cells treated with targeted NPs encapsulating control DNA (LPD@empty-U11), targeted and non-targeted NPs encapsulating SAPO pDNA (LPD@SAPO-U11 and LPD@SAPO respectively). Reported values are the mean of 5 replicates ± SD, normalized (as percentage) on cell proliferation of untreated cells. Statistical significance *** $p<0.005$.

Table 2.2.1: Cells viability after LPD@SAPO-U11, LPD@SAPO and LPD@empty-U11 NPs treatments. Reported values are the mean of 5 replicates ± SD, normalized (as percentage) on cell proliferation of untreated cells.

Formulation	Cells viability (%)
LPD@SAPO-U11 NPs	53.5 ± 3.38
LPD@SAPO NPs	67.3 ± 2.98
LPD@empty-U11 NPs	80.3 ± 2.37

2.3 *In vivo* experiments

2.3.1 Biodistribution study

In vivo biodistribution of DiD-LPD-U11 NPs were performed in nude mice bearing MDA-MB-231 xenograft tumors. In this study, the NPs were administered via retrobulbar injections with a dose of 30 μg plasmid/mouse and the mice (n=5-6 per group) sacrificed at different time points (10 min, 1, 3, 24 and 72 h) after blood sampling. Retrobulbar injection was chosen as alternative to tail vein injection because it is safer and less technically challenging for large volumes administration (*i.e.* ~150 μL) [30].

First, after the blood collection, the plasma was extracted, the NPs concentration determined using a calibration curve (Fig. 2.3.1.1) and the percentage of the injected dose (ID%) calculated for each mouse (n=5-6 per group). For detailed information about the method refer to materials and method (section 4.9.2).

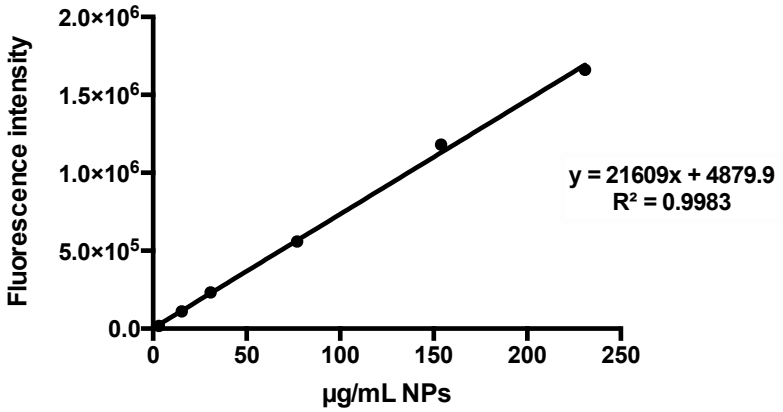

Fig.2.3.1.1: Fluorescence intensity detected at 460 nm wavelength as a function of NPs concentration.

As shown in Fig. 2.3.1.2, the blood concentration had a rapid drop (ID% ~ 40) and the mean value was consistently maintained over the early stages (10 min, 1 and 3 h), while at longer times (24 and 72 h) some injected dose (23.2% and 8.2% respectively) was still available. Given the long-term circulation properties of these NPs, the fluctuations and the response observed in the early timepoints may be attributed to a rapid tissue absorption combined with clearance phenomena.

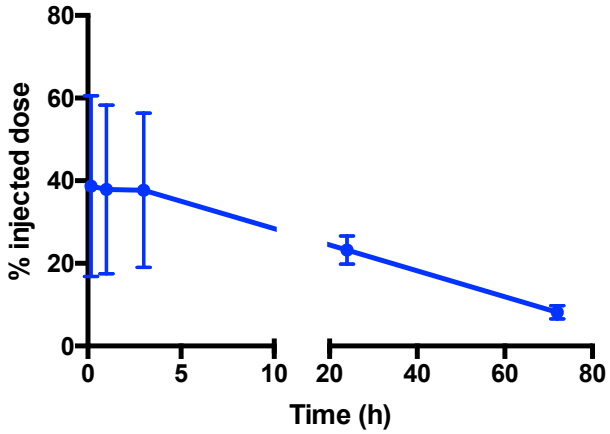

Fig. 2.3.1.2: Percentage of injected dose as a function of time (mean ± SD n=5-6).

In order to further investigate the NPs fate, the biodistribution in the major organs was evaluated in homogenate tissue (Fig. 2.3.1.3).

As reported, the NPs accumulated in the liver and spleen indicating as major clearance mechanism the mononuclear phagocyte system (MPS) uptake: indeed, large and cationic NPs are not expected to be cleared by renal filtration [31].

In addition, pronounced lung accumulation was observed at short times and this result was consistent with those reported in literature where cationic lipid NPs were transiently found in this organ [32]. This phenomenon may be

caused by entrapment of NPs aggregates in lung capillaries or NPs uptake by the resident macrophages [31] [33].

In conclusion, in all the organs, even at 72 h, we didn't observe a total washout of the dye: the lacking drop of the fluorescence intensity was likely due to DiD intercalation in the cellular membrane after NPs uptake or elimination [34].

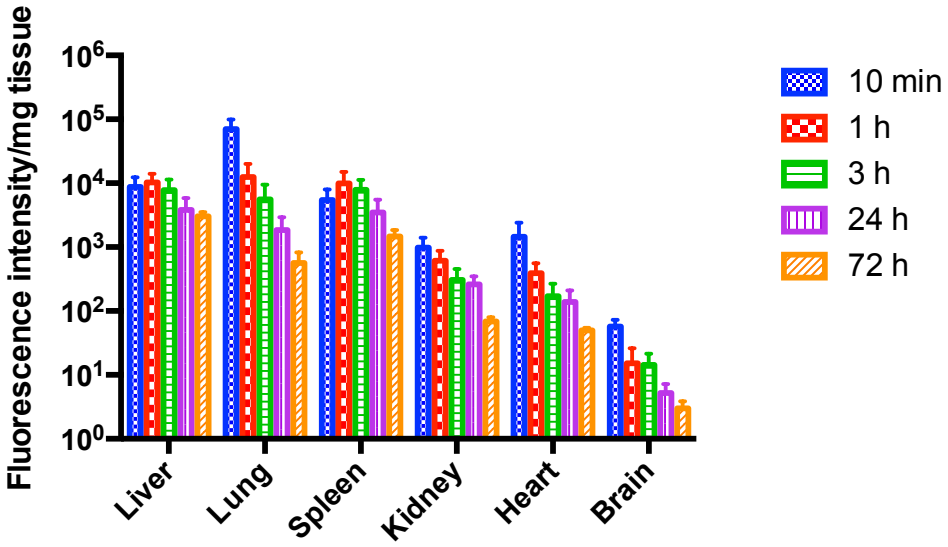

Fig. 2.3.1.3: Fluorescence intensities of organ homogenates obtained after autofluorescence subtraction (mean± SE n=6-2)

Once assessed the NPs biodistribution, the interaction of the nanocarrier with tumor tissue was investigated (Fig. 2.3.1.3).

Ex vivo imaging by IVIS revealed that after 10 min, NPs were already accumulated in the tumor region and the fluorescence signal had a slightly decrease over 72 h. Despite the low tissue homogeneity and the subsequent data variability, the fluorescence detected was in all cases considerably higher than the control, making consistent the previous hypothesis.

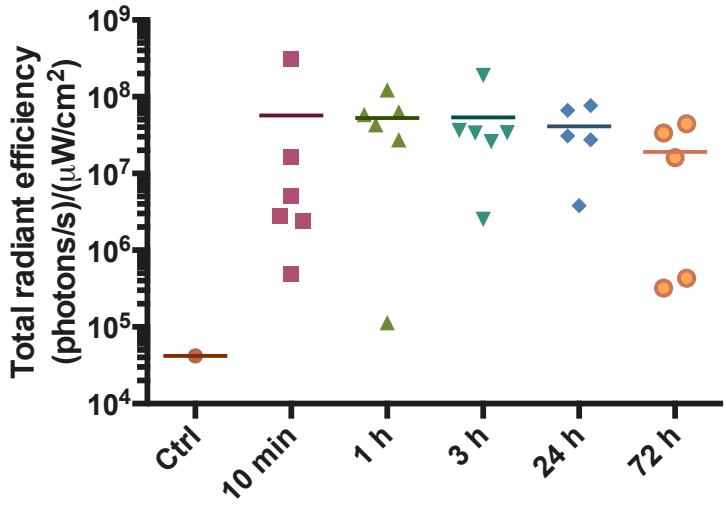

Fig. 2.3.1.4: Time dependent changes of isolated tumors' fluorescent intensity evaluated by IVIS (bars indicate mean values; n=5-6).

However, the quantification of fluorescence intensity in tumor homogenate samples (n=3) suggested that most of the NPs initially gathered at the cancer tissue were not actually deeply penetrated, but they were mainly stationing into the blood vessels around the tumor (Fig. 2.3.1.5).

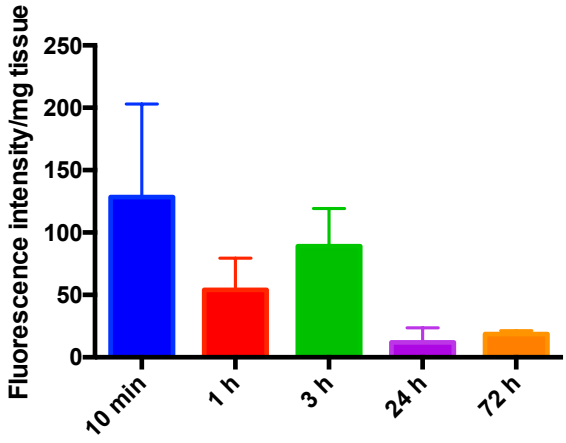

Fig. 2.3.1.5: Fluorescence intensity of tumor homogenates normalized to control autofluorescence (mean± SE n=3-2).

To confirm these results, more detailed investigations were conducted. Confocal microscopy of tumor cryosections (Fig. 2.3.1.6) revealed that at early stages the NPs signal was found focused in certain areas, whereas, at 24 and 72 h, it appeared uniformly distributed within the tissue. From this result, we can assume that the NPs were firstly localized around the vessels (Fig. 2.3.1.6 arrows) then they spread in the tumor stroma.

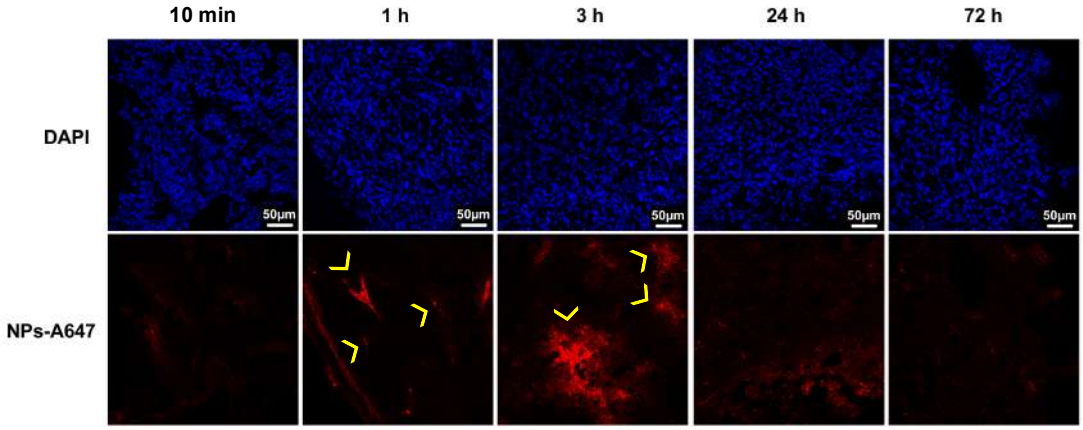

Fig. 2.3.1.6: Tumor slices observed by confocal microscopy. Nuclei stained with DAPI; Arrows indicate possible vascular and perivascular areas; Scale bars = 50 µm.

In order to determine the extent of cells actually labelled with NPs, the tumor tissues were processed with a dissociation kit and the obtained single cell suspension analyzed by FACS. As reported in Fig. 2.3.1.7, the percentage of positive cells and mean fluorescence intensity strongly increased until 24 h indicating a time-dependent accumulation of the NPs.

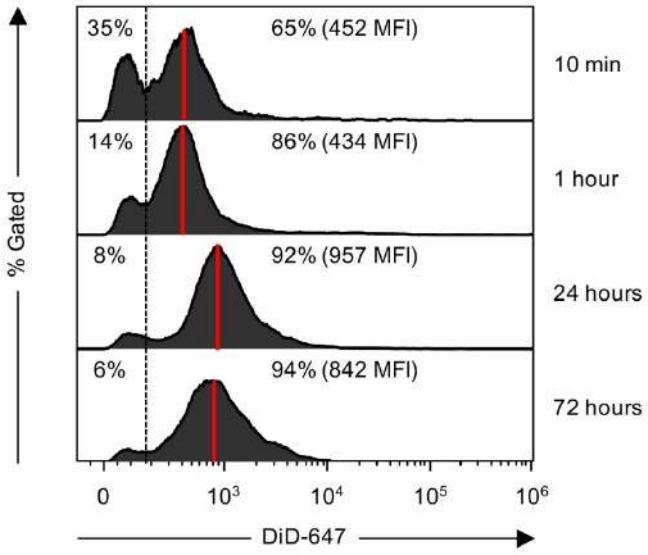

Fig. 2.3.1.7: Representative flow cytometry measurements of NPs labelled cells after tissue dissociation. Mean fluorescence intensity (MFI; red line) and positive and negative cells percentages are reported.

Since the flow cytometry signal may indicate both the surface binding and cellular uptake of NPs, the nanocomplex internalization was evaluated by confocal microscopy staining the cellular membrane.

As shown in Fig. 2.3.1.8, where the signal associated with the NPs was found, it was always located inside the cell cytoplasm confirming the occurred uptake.

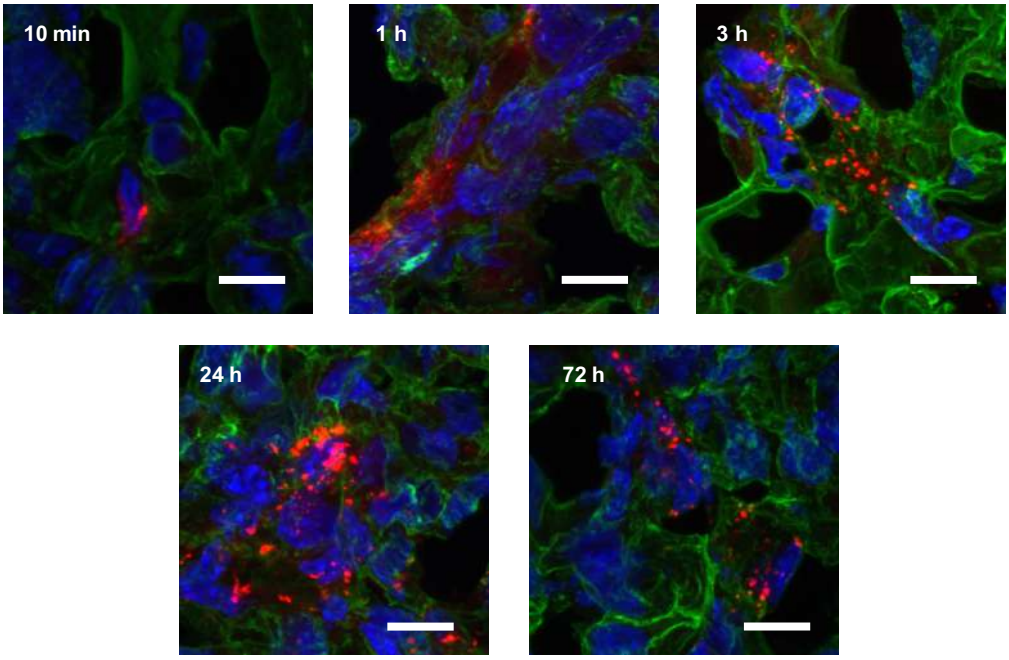

Fig. 2.3.1.8: Cellular uptake of DiD-LPD-U11 in tumor slices observed by confocal microscopy (maximum intensity projection of Z-stack); Red: NPs; Green: Wheat Germ Agglutinin (WGA) membrane staining; Blue: nuclei staining; Scale bars = 10 μm.

2.3.2 Antitumor activity test

The *in vivo* antitumor efficacy of LPD@SAPO-U11 was evaluated in nude mice bearing MDA-MB-231 xenograft tumors. In this study, green fluorescent protein (GFP) pDNA were used as the control DNA (formulation LPD@GFP-U11) and PBS injected animals as negative control. Treatment was administered via retrobulbar injections every other day for a total of 3 injections, with a dose of 30 μg plasmid/mouse per injection (detailed experiment timeline reported in Fig. 2.3.2.1 panel A). Tumor volume and body

weight were measured every 3 days. Mice were sacrificed 3 days after the last injection (day 9).

As shown from the tumor volume measurements (Fig. 2.3.2.1 panel B), at day 9, LPD@SAPO-U11 group exhibited a significant tumor regression compared with PBS and LPD@GFP-U11, confirming the antitumor activity associated with SAPO expression.

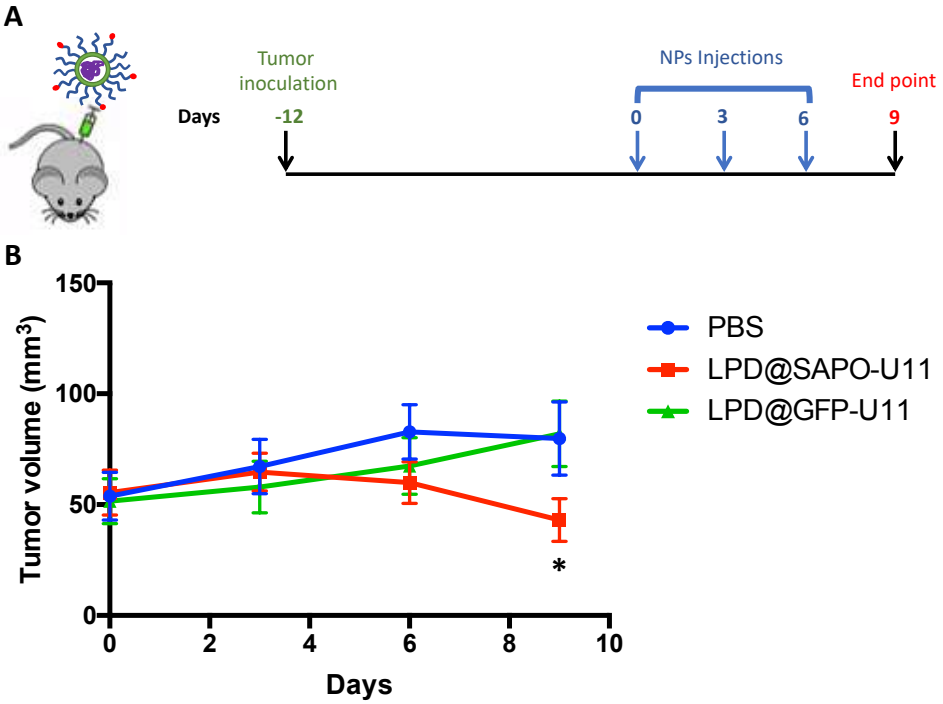

Fig. 2.3.2.1: (A) Schematic experimental timeline; (B) Tumor growth curves (mean± SE n=9-10); statistical significance *vs.* placebo *p < 0.05.

Afterwards, a terminal deoxynucleotidyl transferase dUTP nick end labeling (TUNEL) assay was performed to quantify apoptosis in tumor tissues after treatment. As reported (Fig. 2.3.2.2), LPD@SAPO-U11 treatment showed

significantly higher tumor cell apoptosis than PBS and LPD@GFP-U11, confirming the antitumoral effect of SAPO.

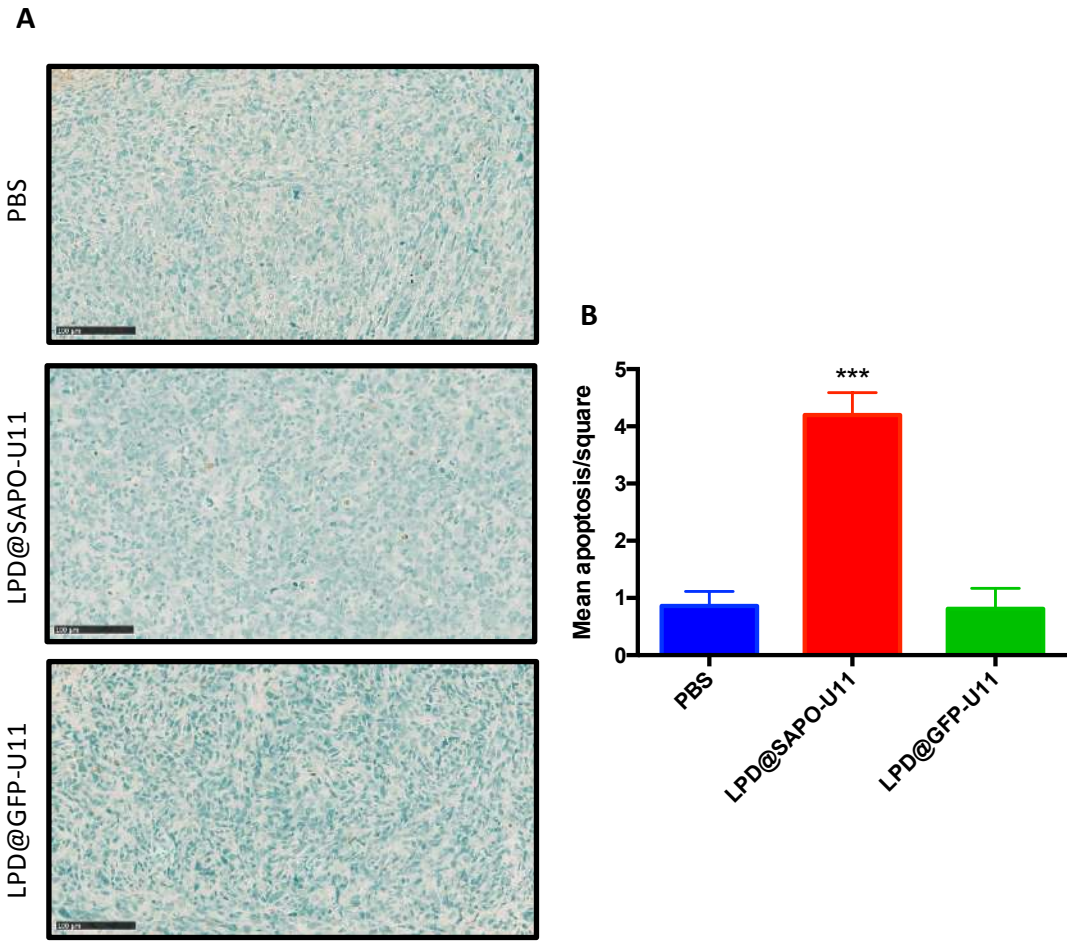

Fig. 2.3.2.2: (A) TUNEL assay representative pictures of tumor sections treating with different formulations; scale bars = 100 μm; (B) TUNEL assay quantitative results of tumor sections treating with different formulations (mean± SE n=5); statistical significance *vs.* placebo ***p<0.005.

Despite the non-specific accumulation of LPD-U11 formulation observed in the biodistribution studies, no noticeable histological changes were observed in

hematoxylin and eosin (H&E)-stained tissue sections of major organs (Fig. 2.3.2.3).

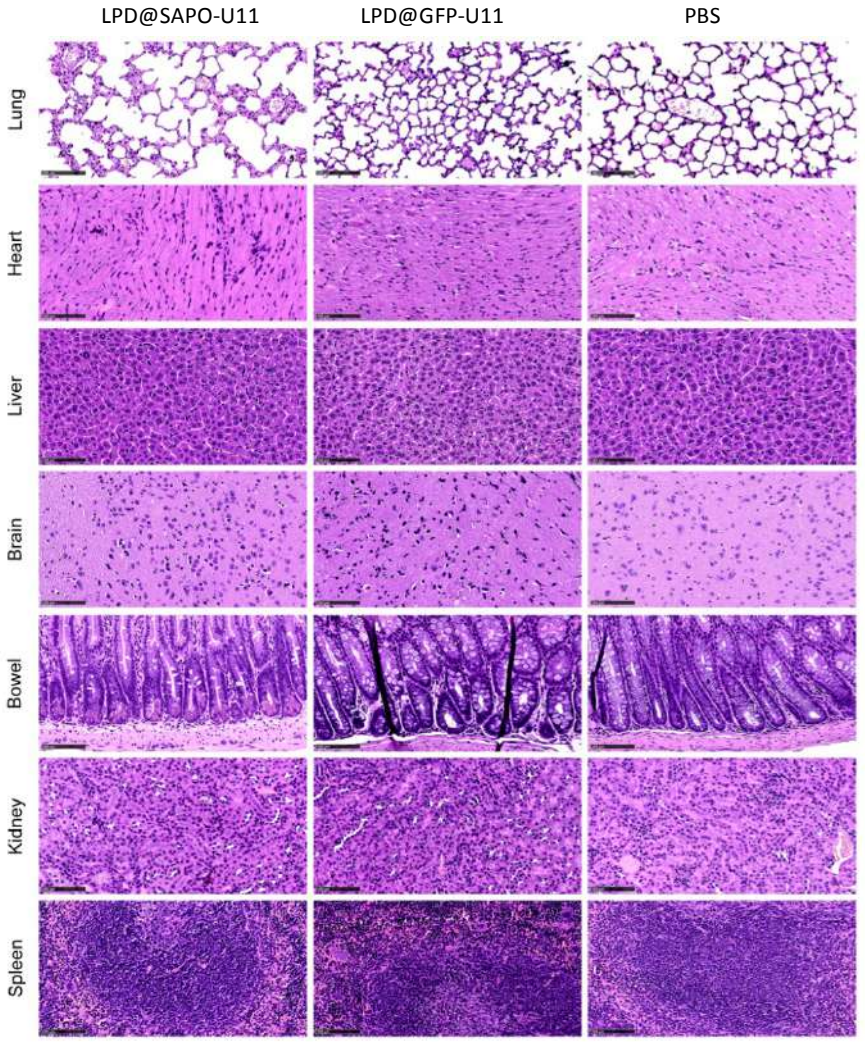

Fig. 2.3.2.3: H&E staining of the major organs; scale bars = 100 μm.

In addition, no significant change in body weight was observed in any of the mice used in this study (Fig. 2.3.2.4) and the hematological parameters didn't indicate a detectable damage (Fig. 2.3.2.5).

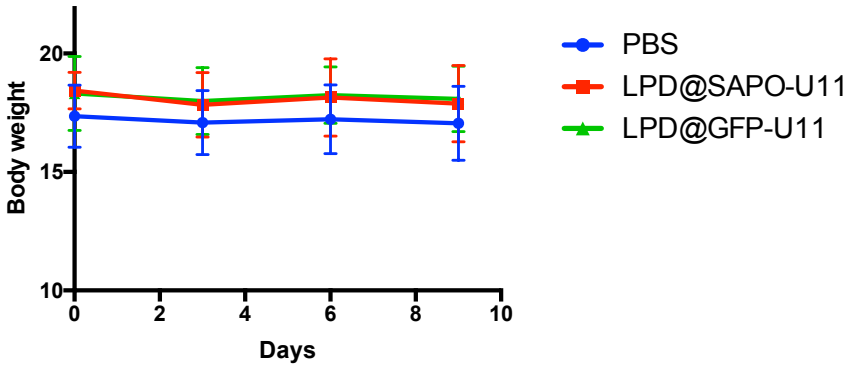

Fig. 2.3.2.4: Body weight changes of mice bearing tumor after treatments (mean ± SD n=9-10).

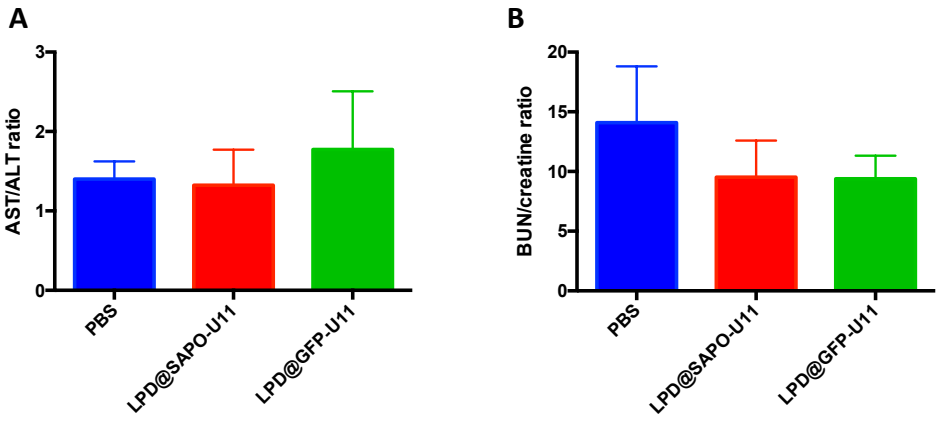

Fig. 2.3.2.5: Hepatic (A) and renal function (B) indicators of mice bearing tumor after treatments (mean ± SE n=6).

Finally, to investigate *in vivo* transfection, western blot assay was performed on GFP transfected mice. This experimental group was selected instead of SAPO treated mice because the toxin was expected to be degraded after triggering the cell death.

As reported in Fig. 2.3.2.6, LPD@GFP-U11 formulation induced an appreciable GFP expression (panel A) and the signal detected was found significantly

different from the background observed both in PBS (panel A and B) and LPD@SAPO-U11 (panel A, unlabeled band) groups.

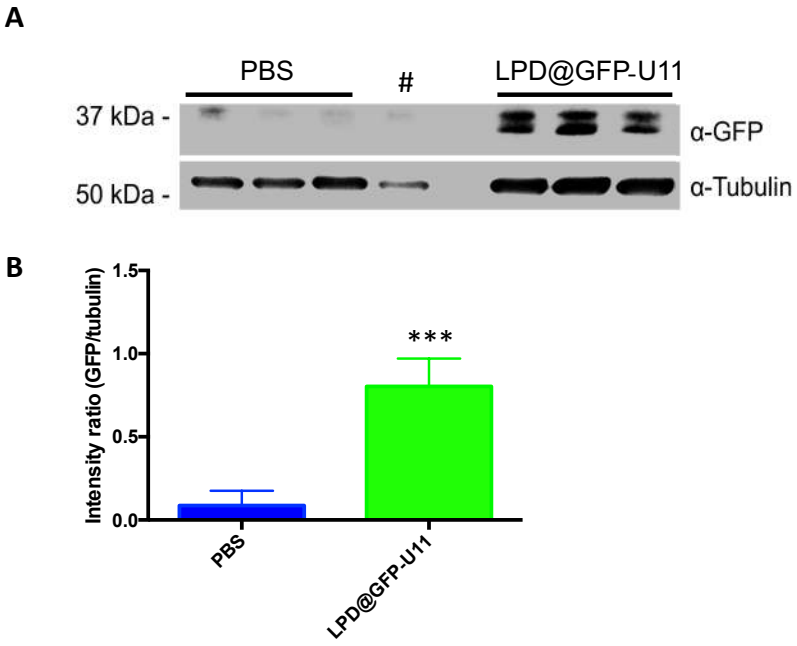

Fig. 2.3.2.6: (A) *In vivo* expression of GFP pDNA at the protein level by Western Blot Assay (the unlabeled band (#) refers to a mouse treated with LPD@SAPO-U11 NPs) and (B) bands quantification by ImageJ software (mean ± SD n=3); statistical significance vs. placebo ***p<0.005.

3. Discussion

Gene therapy involves the intentional modulation of gene expression patterns through the delivery of exogenous genetic material [35]. Ideally, a gene delivery system needs to protect the genic material from degradation, get selectively a targeted cell and release the content in the cytoplasm. Among the gene delivery systems described in literature, we can distinguish viral and non-viral vectors. Viral vectors are more efficient in transferring genes, but their efficacy is limited due to their broad tropism and the possibility of invoking an immune response [35]. Furthermore, attempts to translate viral vectors-based gene therapy into the clinical practice often clash with the huge cost of the treatment and severe adverse effects observed in some trials [42] [43].

Thus, many efforts have been made to develop alternative non-viral vectors composed by biocompatible and biodegradable materials with low/absent immunogenicity and significant target specificity.

In this project, UPAR targeting LPD NPs were developed to transfect TBCN cells with a toxin.

Firstly, the formulation was optimized to obtain NPs suitable for in-vivo application in cancer therapy: in particular, the targeting ligand amount and the PEGylation degree were set to avoid the formation of large particles that are generally rapidly cleared from the blood circulation [31]. Moreover, since the fenestrations in tumor vasculature have a range in size between 380 and 780 nm, smaller NPs generally exhibit improved tumor passive accumulation [36].

The final NPs (LPD-U11) shown a hydrodynamic diameter of 173.3 ± 5.15 nm (mean ± SD) with a polydispersity index of 0.281 ± 0.006 (mean ± SD) measured by DLS analysis.

This preparation was further characterized by NT analysis, where particle-by-particle measurements of size were conducted obtaining a number distribution: the detected hydrodynamic diameter was 138.6 ± 5.9 (mean ± SE) with a standard deviation of 31.9 ± 1.9 (mean ± SE). In addition, a positive Z-potential (+35.0 ± 0.3 mV) was observed and correlated with the large amount of cationic lipids (i.e. DOTAP).

Then, fluorescent NPs were synthetized for tracking their fate *in vitro* and *in vivo.* In order to achieve an acceptable *in vivo* imaging sensitivity, fluorescent contrast agents should emit light in the red or near infrared (near-IR) wavelengths (∼600 - 1000 nm) [37]. Thus, the intercalating agent DiD was selected and incorporated in the formulation. As expected, the dye inclusion didn't cause relevant differences in NPs size distribution and Z-potential.

Afterwards, the effect of the targeting agent functionalization was investigated: indeed, targeted LPD NPs displayed a better cancer cell uptake than non-targeted formulation. This data was confirmed by a cell viability assay conducted after the incubation with NPs encapsulating SAPO pDNA: indeed, LPD-U11 showed enhanced cytotoxicity than LPD NPs.

Subsequently, an *in vivo* biodistribution study of the targeted nanocomplex was conducted.

It is well known that positively charged NPs mainly distributed in three major organs: liver, spleen and lungs [33] [31]. In our experiment, we observed the same behavior which may be caused by the interaction of these NPs with the negatively charged serum proteins that enhance the lung retention and the

uptake of liver and spleen resident macrophages [33]. In addition, regarding the tumor tissue, time-dependent diffusion of the NPs with a progressive accumulation in the cancer cells was observed.

Finally, the *in vivo* antitumoral activity of LPD-U11 NPs encapsulating SAPO pDNA was investigated. Compared with the controls, this formulation was able to induce a significant regression of the tumor which was associated with SAPO expression. Among the cell death pathways induced by SAPO, apoptosis seems to be the main detectable effect reported in literature [8]. Even in this experiment, the induction of apoptosis was found significantly higher in SAPO pDNA-treated tumors compared with the controls. Furthermore, LPD-U11 NPs encapsulating SAPO pDNA showed no significant non-specific toxicity to major organs and tissues under the investigated conditions.

In conclusion, an efficient targeted system for suicide gene therapy purpose was developed, although further research is needed for investigating any possible long-term side effect or the duration of the antitumoral activity. Moreover, as future perspective, in order to further target the tumor tissue increasing the specificity and safety of suicide gene therapy, pDNA with specific promoters may be developed and included in the final formulation [38].

4. Conclusion

Despite most of the clinical trials are conducted with viral vectors, still the use of nanoparticle-based approach represents a valuable alternative to protect nucleic acids in the bloodstream and improve their biodistribution and cellular uptake. Indeed, whereas viral structure and capacity are strictly determined, these “synthetic” vectors can be potentially tailored for precise applications.

Along with the transfection efficiency, the specificity towards the cancer cells represents the other major issue for suicide gene therapy success. In this project, the active targeting approach (*i.e.* U11 surface functionalization) was exploited in order to limit the off-target toxicity associated with the proposed nanovector.

As result, it was found that SAPO gene delivered by suitably designed cationic lipid NPs was able to promote tumor regression in an *in vivo* model of TNBC. Actually, the use of liposome-protamine system was crucial: in contrast to what previously reported using targeted nanoparticles, LPD-U11 did not necessitate co-administration of transfection enhancers to achieve satisfactory transfection efficiency in living animals [44]. In addition, the treatment was safely feasible without affecting normal functionality of healthy tissues suggesting that the proposed system was actually able to target TNBC cells.

5. Materials and Methods

5.1 Materials

Protamine sulfate, cholesterol, triethylamine (Et_3N) and N,N-dimethylformamide (DMF) were purchased from Sigma-Aldrich (MO,USA). 1,2-dioleoyl-3-trimethylammonium-propane chloride salt (DOTAP), 1,2-distearoryl-sn-glycero-3-phosphoethanolamine-N-[methoxy(polyethylene glycol- 2000)] ammonium salt (DSPE-PEG-OCH_3) and 1,2-distearoryl-sn-glycero-3-phosphoethanolamine-N-[maleimide(polyethyleneglycol- 2000)] ammonium salt (DSPE-PEG-mal) were obtained from Avanti Polar Lipids, Inc. (AL, USA) (Fig. 5.1.1).

DOTAP

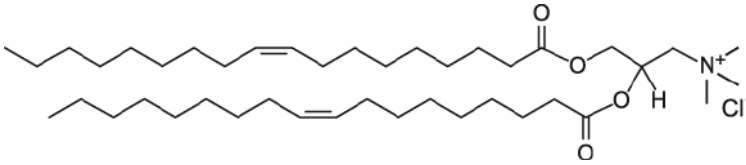

DSPE-PEG-OCH_3

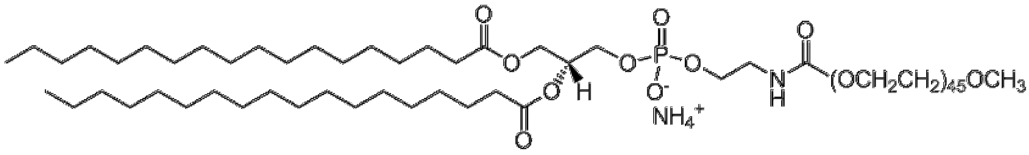

DSPE-PEG-mal

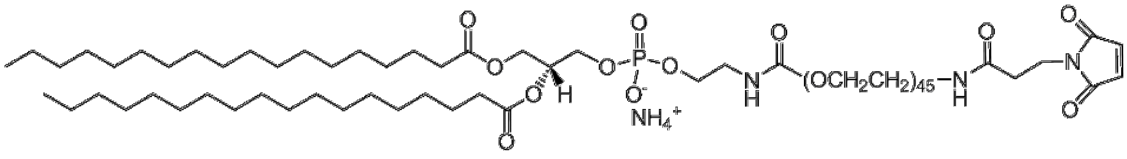

Fig. 5.1.1: Chemical structure of DOTAP, DSPE-PEG-OCH_3 and DSPE-PEG-mal.

1,1'-Dioctadecyl-3,3,3',3'-Tetramethylindodicarbocyanine, 4-Chlorobenzenesulfonate Salt (DiD solid) was purchased by Thermo Fisher Scientific (MA, USA).

Thiolated U11 (C-linker-VSNKYFSNIHW) was synthetized by CNR institution as previously described [39].

Pci-SAPO (Saporin encoding pDNA – SAPO pDNA) was kindly donated from San Raffaele hospital, whereas pcDNA3-EGFP (GFP encoding pDNA – GFP pDNA) was a gift from Doug Golenbock (Addgene plasmid # 13031).

5.2 Statistical analysis

Statistical analyses were conducted using one or two-tailed Student's t-test. Unless otherwise specified, plots show mean ± standard error (SE) and mean ± standard deviation (SD) for *in vivo* and *in vitro* experiments, respectively. The statistical significance is set as follows: $*p < 0.05$, $**p < 0.01$, $***p < 0.005$.

5.3 Cell culture

MDA-MB-231 cell line was cultivated in Eagle's Minimum Essential Medium (EMEM) supplemented with 10% fetal bovine serum (FBS), L-glutamine (2 mM), penicillin (50 UI/mL), and streptomycin (50 mg/mL) at 37 °C in humidified atmosphere containing 5% CO_2. Cell culture medium, supplements and antibiotics were purchased by EuroClone.

5.4 DSPE-PEG-U11 synthesis

First, thiolated U11 and DSPE-PEG-mal were dissolved in DMF with a final concentration of 10 mg/mL. Then, the peptide, the lipid and Et_3N (1:1:10 molar ratio) were mixed and stirred at room temperature for 36 h. After the reaction, the mixture was diluted with milliQ water (Millipore) and peptide excess washed away (x3) with 10 KDa Amicon® Ultra Centrifugal Filter (MerkMillipore, MA, USA).

The product extinction spectrum was recorded by NanoDrop 2000c Spectrophotometer (Thermo Scientific, MA, USA) and the protein quantification made by comparison with a calibration curve at 280 nm wavelenght.

5.5 NPs synthesis

5.5.1 LPD NPs synthesis

DOTAP and cholesterol (1:1, mol/mol) were dissolved in chloroform and the solvent was evaporated under reduced pressure. The lipid film was hydrated overnight with distilled water obtaining a reagents final concentration of 10 mM. The liposomes were sequentially extruded through 800 nm, 200 nm and 100 nm polycarbonate membranes (Whatman, UK).

The polyplex core of the LPD NPs was prepared by mixing 250 µL of 0.26 mg/mL protamine in 5% glucose w/V with equal volume of plasmid solution concentrated 0.5 mg/mL. The mixture was incubated under stirring (400 rpm) at room temperature for 10 min before 150 µL of liposomes were added. After 10 min, PEGylation and targeting modification were achieved by adding in the formulation DSPE-PEG or DSPE PEG and DSPE PEG U11 mixture for non-

targeted and targeted NPs (LPD and LPD-U11), respectively. The mixture was incubated at 65°C for 15 min.

All the formulations investigated with each ingredient relative percentages were reported below. In all these conditions the absolute amounts of Cholesterol and DOTAP were maintained.

U11 functionalization degree optimization:

	Formulations		
Ingredients	0%	1%	2.8%
Cholesterol	47.2	47.2	47.2
DOTAP	47.2	47.2	47.2
DSPE PEG OCH_3	5.6	4.6	2.8
DSPE PEG U11	-	1.0	2.8

PEGylation degree optimization:

	Formulations			
Ingredients	5.6%	10%	12.5%	15%
Cholesterol	47.2	45	43.75	42.5
DOTAP	47.2	45	43.75	42.5
DSPE PEG OCH_3	4.6	9	11.5	14
DSPE PEG U11	1	1	1	1

5.5.2 Fluorescent LPD NPs synthesis

For making fluorescent NPs, DiD (final concentration 1 mM) were included as intercalating agent in the liposome preparation and the targeted and non-

targeted NPs (DiD-LPD-U11 and DiD-LPD respectively) were synthetized as above.

5.6 NPs characterization

A. DLS and Z-potential analysis

The NPs hydrodynamic diameter and Z-potential were analyzed on a Zetasizer Nano ZS ZEN3600 (MALVERN Co., UK) operating at a light source wavelength of 633 nm and a fixed scattering angle of 173°. The results were expressed as mean ± SD of 3 independent measurements.

B. TEM

The morphology of NPs was observed by FEI 120 KV Tecnai G2 spirit Bio TWIN Instrument.

The sample (1:40 NPs suspension dilution) was deposited onto a formvar-coated 200-mesh copper grid (Ted Pella, CA, USA), negatively stained with 2% uranyl acetate and allowed to dry before examination. For the mean diameter determination, images were processed with ImageJ software. The reported value was calculated measuring 60 particles.

C. Nanoparticle tracking analysis (NTA)

NPs size distribution were further characterized employing NanoSight NS300 (Malvern Co., UK) equipped with a 405 nm laser excitation source and high

sensitivity scientific CMOS camera. NTA 3.0 was used for data collection and analysis. Samples were prepared by dilution of NPs in ultrapure sterile water. Samples were manually injected into the sample chamber using 1 mL silicon oil-free plastic syringes. All video capture and analysis settings, including camera shutter, camera gain, and detection threshold, remained identical for all samples. The results were expressed as mean ± SE of 5 independent measurements.

D. Fluorescence spectroscopy

Fluorescence analysis of DiD-LPD and LPD-U11 was performed on a FluoroMax-4 HORIBA Scientific spectrometer using quartz cuvettes. The samples were diluted with milliQ water (1:1000) prior to analysis and the spectra were acquired in the range of 650-750 nm after excitation at 647 nm wavelength. The emission peak at 665 nm was attributed to fluorescent NPs.

E. Stability tests

Stability in PBS, glucose 5% w/V and water

LPD and LPD-U11 samples were incubated in the selected medium (1:100 dilution) and their stability assessed by DLS analysis (method reported above). The results were expressed as mean ± standard deviation (SD) of 3 independent measurements.

Stability at 4°C

LPD and LPD-U11 samples were kept at 4°C for 24 h and their stability assessed by DLS analysis and Z-potential analysis performed as reported above.
The results were expressed as mean ± standard deviation (SD) of 3 independent measurements.

Stability in plasma

DiD-LPD-U11 were incubate in plasma and centrifuge 15 min at 1500×g. The sample dilution (1:10.5) was set according with the expected NPs concentration *in vivo* after intravenous administration.
The stability after treatment were assessed by fluorescence spectroscopy (method reported above) at time 0 and 2 days post incubation (4°C storage). The obtained fluorescence intensity was subtracted to background value and the result expressed as percentage of the untreated sample suspended in water.

5.7 *In vitro* experiments

5.7.1 UPAR expression

3×10^5 cells were immunodecorated in FACS tubes with anti-uPAR antibody (3 µg/tube; ADG3937, Sekisui, MA, USA) in Phosphate buffered saline (PBS), 1% Bovine Serum Albumin (BSA; Sigma) for 30 min at RT. Then, cells were washed thrice with PBS and immunodecorated with Alexa Fluor 647 goat anti-mouse secondary antibody (3 µg/tube; A-21235 Thermo Fisher Scientific, MA, USA) in

PBS, 1% BSA for 30 min at RT. After three washes with PBS, cells were analyzed by flow cytometry. 10,000 events were acquired for each analysis, after gating on viable cells and on singlets. The data (median fluorescence intensity) were normalized against the untreated sample and expressed as mean ± SD of 3 independent replicates. Cells immunodecorated with the secondary antibody only were used as control.

5.7.2 Cellular binding

3×10^5 cells/tube were collected and incubated for 1 h at 4 °C in presence of fluorescent DiD-LPD and DiD-LPD-U11 in complete medium at final concentration of 1.2, 0.12, 0.012 and 0.0012 μg GFP plasmid/well, respectively. After incubation, cells were washed three times with PBS, suspended in 0.3 mL of PBS EDTA 2 mM and analyzed by flow cytometer. 10,000 events were acquired for each analysis and a sample of untreated cells was used to set the gate on viable cells and the region of positivity. The results (median fluorescence intensity) were normalized with the untreated group and expressed as mean ± SD of 3 independent replicates.

5.7.4 Cellular uptake

3×10^5 cells were cultured on cover glass slips pre-coated with gelatin and, after 48 h, incubated with 0.03 μg GFP plasmid/well of fluorescent DiD-LPD and DiD-LPD-U11. At 0.5, 2, and 6 h post incubation, cells were washed PBS, fixed with 4% paraformaldehyde (RT, 10 min) and then subjected to membrane and nucleus staining by incubation with Wheat Germ Agglutinin (WGA), Alexa Fluor™ 488 Conjugate (1 μg/mL) and DAPI (1 μg/mL), respectively. After

washing with PBS, cover slips were mounted with ProLong Antifade reagent (Thermo Fisher Scientific, MA, USA) and examined by Nikon A1 Confocal Microscope (Nikon Instruments Europe BV, Amsterdam, the Netherlands) equipped with laser excitation lines 405 nm, 488 nm and 633 nm.

Images were acquired at 1,024 × 1,024 pixel resolution and with a ×63 magnification oil-immersion lens. In order to confirm the correct setup of DiD channel, an untreated sample was as well analyzed and no signal was found.

The uptake quantifications at 2 h (n=60) and 6 h (n=40) were performed calculating by FIJI the fluorescence intensity per cell area.

5.7.4 Cell viability assay

1×10^4 cells were seeded on a 96-well dish the day before the experiment. Then, the cells were incubated with different amounts of LPD and LPD-U11 at final concentration of 0.2, 0.5, 1 µg of Saporin plasmid/well. In this study, empty plasmid was used as control DNA. Medium was refreshed 5 h after transfection. At 24 h, 20 µL of 3-(4,5-dim ethylthiazol-2-yl)-5-(3-carboxymethoxyphenyl)-2-(4-sulfophenyl)-2H-tetrazolium (MTS) stock solution (CellTiter 96® AQueous One Solution Reagent; Promega, WI, USA) were pipette into each well and the cells incubated at 37°C for 3 hours in a humidified, 5% CO_2 atmosphere. The absorbance was recorded at 490 nm using EnSight™multimodeplate reader (PerkinElmer). The results were normalized on viability of untreated samples (as %) and expressed as means ± SD (n=4-5).

5.8 *In vivo* experiments

5.8.1 Production of orthotopic tumor model

For the *in vivo* experiments, (6-8 weeks old) female nude Balb/C mice purchased by Charles River Laboratories (Calco, IT), were maintained in a fully equipped facility, housed in single cages, fed ad-libitum and observed daily. Mice were used in accordance with an experimental protocol subjected to the direct approval of the Italian Ministry of Health.

1×10^7 MDA-MB-231 cells, grown as described above, were suspended in growth medium, mixed 1:1 with Matrigel high factor (Corning, USA) and injected into mammary fat pad of mice.

Animals were observed, and tumor formation was recorded at least two times per week.

5.8.2 Biodistribution of LPD-U11 NPs

Mice were orthotopically implanted with MDA-MB-231 cells, as described above.

12 days after implant, mice (n=5-6/group) were anesthetized with 2.5% Isoflurane and DiD-LPD-U11 NPs (30 µg plasmid/mouse) were administered via retro-orbital injection (left side). An untreated mouse was used as control.

At 10 min (n=6), 1 (n=6), 3 (n=6), 24 (n=5) and 72 (n=5) h post-injection, retro-orbital (right side) blood samples were collected in EDTA coated hematology tubes (BD Vacutainer®) and centrifuged 15 min at 1500×g leading to plasma recovery. Then, samples fluorescence was analyzed by FluoroMax-4 HORIBA Scientific spectrometer and fitted with a calibration curve. The standard

solutions were prepared by suspending known amounts of fluorescent NPs in plasma and measuring the fluorescence intensity as described above (section 5.7 D). The percentages of the injected dose were calculated by setting the mouse weight 20 g and blood volume/weight as 80 mL/kg [40]. The data were expressed as mean ± SD (n=5-6).

After blood recovery, the mice were sacrificed. Major organs and tumor tissues were collected and analyzed as reported below.

A. Major organs biodistribution

The dissected organs were weighted and homogenized with Potter in water 10% w/v. The fluorescence intensity of homogenates was recorded by a Jasco FP-8300 spectrofluorometer after blank subtraction. Appropriate organ homogenates obtained from an untreated mouse were used as blank. The data were expressed as mean ± SE (n=6 for 10 min, 1h and 3 h groups, n=5 for 24 h group and n=2 for 72 h group).

B. Tumor accumulation

Epifluorescence imaging was performed by placing the dissected tumors (n=5-6) in an IVIS Lumina II imaging system (Perkin Elmer) working at 37 °C. Images were acquired with a 680 nm emission filter while excitation was scanned from 570 to 640 nm. Autofluorescence was removed by spectral unmixing and obtained images were quantified identifying an appropriate ROI.

The fluorescence intensity of tumor homogenates was also measured using the method reported above. The data were expressed as mean ± SE (n=3 for 10 min, 1h and 3 h groups, n=2 for 24 h and 72 h groups).

For the confocal microscopy analysis, tumors were fixed in 4% paraformaldehyde solution, washed in PBS and embedded in frozen tissue matrix (OCT) for freezing in liquid nitrogen.

Afterwards, the organs were sectioned and the 10 µm-thick tumor cryosections were air-dried at room temperature for 1 h. Nuclei were stained with DAPI (0.1 µg/mL) and the slices mounted with ProLong Antifade reagent (Thermo Fisher Scientific, MA, USA). Microscopy analysis were performed with a Leica SP8 confocal microscope (Leica Microsystems, Wetzlar, Germany). Images were acquired at 1,024 × 1,024 pixel resolution and with a 20X magnification.

To evaluate the NPs uptake, the tumor slices were additionally stained with Alexa Fluor 488 labelled WGA and the images acquired with 63x magnification.

In order to quantify the cells actually labelled with NPs, tumor samples (n=3/group) were dissociated using the Mouse Tumor Dissociation kit (Miltenyi Biotech, Bergisch Gladbach, D). Dissociated cells were fixed with 4% paraformaldehyde, stained with DAPI and analyzed by flow cytometer selecting the single cells. The mean fluorescence intensity and % of positive and negative cells were calculated.

5.8.3 Activity of LPD-U11 NPs

Mice were orthotopically implanted with MDA-MB-231 cells, as described above.

12 days after implant, mice were randomly divided into three experimental groups: PBS (n=9), LPD@SAPO-U11 (n=10) and LPD@GFP-U11 (n=10) injected with NPs encapsulating SAPO and GFP encoding pDNA respectively.

GFP encoding pDNA was used as control DNA, whereas PBS injected mice as placebo.

Mice were treated by retro-orbital injections every three day in order to receive 3 injections with a dose of 30 μg plasmid/mouse.

Tumor volume and body weight were measured every 3 days. Mice were sacrificed 3 days after the last injection (day 9) and plasma was collected as reported above for hepatic and renal function analysis.

A. TUNEL assay

Paraffin embedded tumor sections were treated with the Tumor TACS In Situ Apoptosis Detection kit (Trevigen, MD, USA) according to manufacturer's protocols, which labels apoptotic nuclei in paraffin-embedded tissue sections. All samples were observed with NanoZooomer digital slide scanner (magnification 20X, Hamamatsu) and apoptotic nuclei were counted on 10 squares/sample (n=4-5 per group).

B. Histopathological analysis

Liver, kidneys, spleen, heart, brain, gut and lung samples obtained from mice (n = 1/group) were fixed in 10% buffered formalin for at least 48 h and embedded in paraffin. Three micrometer sections were cut, stained with hematoxylin and eosin, and examined in a blinded manner.

C. Assessment of kidney and liver functionality

Kidney and liver functionality were assessed by measuring the amount of urea, creatinine, AST and ALT in plasma (n = 6/group) after the treatment. Quantifications were performed according to the manufacturer's protocols using the following kits: QuantiChromTM Urea Assay Kit, QuantiChromTM Creatinine Assay Kit, EnzyChromTM Aspartate Transaminase Assay Kit and EnzyChromTM Alanine Transaminase Assay Kit (BioAssay Systems).

The results expressed as mean ± SD of AST/ALT and urea/creatinine ratio.

D. *In vivo* transfection

The GFP transfection efficiency was evaluated in the tumors by western blotting.

Briefly, tumors were homogenized in 10% water with Potter and lysed in Triton lysis buffer (20 mM Tris-HCl pH 7.6, 150 mM NaCl, 1 mM EDTA, 10% Glycerol, 1% Triton X-100), containing 4% Protease Inhibitor Cocktail (Roche), 1 mM Phenylmethanesulfonyl fluoride (Sigma-Aldrich), 1 mM Na_3VO_4 (Sigma-Aldrich), 10 mM NaF (Sigma-Aldrich). Total protein in lysate was quantified using the Coomassie Plus Protein Assay Reagent (Thermo Fisher Scientific, MA, USA) with BSA as standard protein.

30 µg of protein from each sample were separated by SDS-PAGE using 12% (v/v) polyacrylamide gels and then transferred onto PVDF membrane. The membrane was blocked in 1% BSA in PBS with 0.1 % Tween 20 for 1 h. The membrane was incubated overnight with mouse-polyclonal antibody against GFP (cat N. A-11122; Thermo Fisher Scientific, MA, USA) at 1:3000 dilution or a mouse monoclonal antibody anti-α-tubulin (Sigma-Aldrich, MO, USA) at 1:1000 dilution in 1% BSA in PBS with 0.1 % Tween 20. The membrane was washed

three times with PBS with 0.1 % Tween 20 and reacted 1 h with the secondary antibody anti-mouse conjugated with horseradish peroxidase (1:5000 dilution; Abcam, Cambridge, UK) for 1 h. The bound antibody was revealed using ECL star reagent (Euroclone, Milan, Italy) and the chemoluminescence signal was detected using the Chemidoc System (Biorad, CA, USA). Tumors of PBS and SAPO transfected groups were used as control. Densitometric analysis of protein bands was performed with ImageJ software on PBS and GFP groups.

Bibliography

[1] L. Hutchinson, “Challenges, controversies, breakthroughs,” Nature Reviews Clinical Oncology, vol. 7, pp. 669-670, 2010.

[2] F. W.D., “Triple-Negative Breast Cancer,” N Engl J Med, vol. 363, pp. 1938-1948, 2010.

[3] G. Bianchini, “Triple-negative breast cancer: challenges and opportunities of a heterogeneous disease,” Nat Rev Clin Oncol, vol. 13, no. 11, pp. 674-690, 2016.

[4] L. Newman, “The 2014 Society of Surgical Oncology Susan G. Komen for the Cure Symposium: triple-negative breast cancer.,” Ann Surg Oncol, vol. 22, no. 3, p. 874, 2015.

[5] H. Amer, “Gene therapy for cancer: present status and future perspective,” Molecular and Cellular Therapies, vol. 2, no. 27, pp. 1-19, 2014.

[6] K. Wang, “Nanoparticles for cancer gene therapy: Recent advances, challenges, and strategies,” Pharmacological Research, vol. 114, pp. 56-66, 2016.

[7] R. Ortiz, “New Gene Therapy Strategies for Cancer Treatment: A Review of Recent Patents,” Recent Patents on Anti-Cancer Drug Discovery, vol. 7, pp. 297-312, 2012.

[8] L. Polito, “Immunotoxins and Other Conjugates Containing Saporin-S6 for Cancer Therapy,” Toxins, vol. 3, no. 6, pp. 697-720, 2011.

[9] K. Nielsen, “Ribosome incativating proteins: a plant perspective,” Annu Rev Plant Physiol Plant Mol Biol, vol. 52, pp. 785-816, 2001.

[10] N. Zarovni, “Saporin as a novel suicide gene in anticancer gene therapy,” Cancer Gene Therapy, vol. 14, p. 165–173, 2007.

[11] L. Barbieri, “Ribosome-inactivating proteins from plants,” Biochim Biophys Acta. , vol. 1154, no. 3, pp. 237-282, 1993.

[12] D. Scherman, Advanced Textbook on Gene Transfer, Gene Therapy and Genetic Pharmacology, London: Imperial college press, 2014.

[13] S. Li, "*In vivo* gene transfer via intravenous administration of cationic lipid–protamine–DNA (LPD) complexes," Gene Therapy, vol. 4, p. 891–900, 1997.

[14] R. Li, "Be Active or Not: the Relative Contribution of Active and Passive Tumor Targeting of Nanomaterials," Nanotheranostics, vol. 1, pp. 346-357, 2017.

[15] M. Huber, "uPAR enhances malignant potential of triple-negative breast cancer by directly interacting with uPA and IGF1R," BMC Cancer, vol. 16, no. 615, pp. 1-12, 2016.

[16] Q. Huai, "Structure of human urokinase plasminogen activator in complex with its receptor," Science, vol. 311, pp. 656-659, 2006.

[17] C. Luo, "A novel cationic lipid with intrinsic antitumor activity to facilitate gene therapy of TRAIL DNA," Biomaterials, vol. 102, pp. 239-248, 2016.

[18] L. S., "Nanoparticles evading the reticuloendothelial system: Role of the supported bilayer," Biochimica et Biophysica Acta - Biomembranes, vol. 1788, no. 10, pp. 2259-2266, 2009.

[19] B. Northrop, "Thiol–maleimide "click" chemistry: evaluating the influence of solvent, initiator, and thiol on the reaction mechanism, kinetics, and selectivity," Polym. Chem., vol. 6, pp. 3415-3430, 2015.

[20] W. Song, "Synergistic and low adverse effect cancer immunotherapy by immunogenic chemotherapy and locally expressed PD-L1 trap," Nature communication, vol. 9, no. 2237, pp. 1-11, 2018.

[21] M. Wang, "Targeting the Urokinase Plasminogen Activator Receptor with Synthetic Self-Assembly Nanoparticles," Bioconjugate Chem. , vol. 20, pp. 32-40, 2009.

[22] "Detection Limits of DLS and UV-Vis Spectroscopy in Characterization of Polydisperse Nanoparticles Colloids," Journal of Nanomaterials, vol. 2013, pp. 1-10, 2013.

[23] Thermofisher, "DiD' solid; DiIC18(5) solid," Thermofisher scientific, [Online]. Available: https://www.thermofisher.com/order/catalog/product/D7757. [Accessed 11 09 2018].

[24] T. Ruysschaert, “Liposome retention in size exclusion chromatography,” BMC Biotechnology20055:11, vol. 5, no. 11, 2005.

[25] S. Snipstad, “Labeling Nanoparticles: Dye Leakage and Altered Cellular Uptake,” Cytometry Part A, vol. 91, p. 760 766, 2017.

[26] M. Instrument, “Technical note: size quality report for Zetasizer Nano,” 2014.

[27] N. Oku, “Effect of serum protein binding on real-time trafficking of liposomes with different charges analyzed by positron emission tomography,” Biochimica et Biophysics Acta, vol. 1280, pp. 149-154, 1996.

[28] E. Fröhlich, “The role of surface charge in cellular uptake and cytotoxicity of medical nanoparticles.,” Int J Nanomedicine, vol. 7, pp. 5577-5591, 2012.

[29] W. Yan, “Mechanism of adjuvant activity of cationic liposome: Phosphorylation of a MAP kinase, ERK and induction of chemokines,” Molecular Immunology, vol. 44, p. 3672–3681, 2007.

[30] T. Yardeni, “Retro-orbital injections in mice,” Lab Anim (NY), vol. 40, no. 5, p. 155–160, 2011.

[31] E. Blanco, “Principles of nanoparticle design for overcoming biological barriers to drug delivery,” Nat. Biotech., vol. 33, pp. 941-951, 2015.

[32] J. Zhang, “Implications of pharmacokinetic behavior of lipoplex for its inflammatory toxicity,” Advanced Drug Delivery Reviews, vol. 57, p. 689–698, 2005.

[33] S. Li, “Pharmacokinetics and Biodistribution of Nanoparticles,” Molecular pharmaceutics, vol. 5, no. 4, p. 496–504, 2008.

[34] J. Mérian, “Synthetic Lipid Nanoparticles Targeting Steroid Organs,” Journal of nuclear medicine, vol. 54, pp. 1996-2003, 2013.

[35] A. Hill, “Overcoming Gene-Delivery Hurdles: Physiological Considerations for Nonviral Vectors,” Trends in Biotech., vol. 34, pp. 91-105, 2016.

[36] S. Hobbs, “Regulation of transport pathways in tumor vessels: role of tumor type and microenvironment,” Proc. Natl. Acad. Sci., vol. 95, pp. 4607-4612, 1998.

[37] L. Arms, “Advantages and Limitations of Current Techniques for Analyzing the Biodistribution of Nanoparticles,” Front. Pharmacol, vol. 9, no. 802, 2018.

[38] S. Navarro, “Cancer suicide gene therapy: a patent review,” Expert Opin Ther Pat, vol. 26, no. 9, pp. 1095-1104, 2016.

[39] S. Avvakumova, “Development of U11-Functionalized Gold Nanoparticles for Selective Targeting of Urokinase Plasminogen Activator Receptor-Positive Breast Cancer Cells,” Bioconjugate Chem., vol. 25, no. 8, pp. 1381-1386, 2014.

[40] Harkness, The biology and medicine of rabbits and rodents, Philadelphia: Lea & Febiger, 1989.

[41] L.I. Selby, “Nanoescapology: progress toward understanding the endosomal escape of polymeric nanoparticles,” Wiley Interdiscip Rev Nanomed Nanobiotechnol., vol. 9, no. 5, 2017.

[42] K. Lundstrom, “Viral Vectors in Gene Therapy,” Diseases, vol. 6, p. 42, 2018.

[43] E. Mastrobattista, “Artificial viruses: a nanotechnological approach to gene delivery,” Nat Rev Drug Discov, vol. 5, p. 115-221, 2006.

[44] S. Sama, “Targeted suicide gene transfections reveal promising results in nu/nu mice with aggressive neuroblastoma,” J Control Release, vol. 10, p. 208-216, 2018.

[45] G. Caracciolo, “Factors Determining the Superior Performance of Lipid/DNA/Protammine Nanoparticles over Lipoplexes,” J Med Chem., vol. 54, p. 4160-4171, 2011.

[46] D. Delgado, “Understanding the mechanism of protamine in solid lipid nanoparticle-based lipofection: the importance of the entry pathway,” Eur J Pharm Biopharm, vol. 79, p. 495-502, 2011.

Appendix

During the fellowship preceding the PhD, I was involved in another project out of my thesis topic, namely cosmetic applications of silver nanoparticles. This project proceeded during the PhD resulting in one publication (Paper 2 in the list of personal publications).

List of personal publications

L. Salvioni, L. Fiandra, M.D. Del Curto, S. Mazzucchelli, R. Allevi, M. Truffi, L. Sorrentino, B. Santini, M. Cerea, L. Palugan, F. Corsi, M. Colombo; Oral delivery of insulin via polyethylene imine-based nanoparticles for colonic release allows glycemic control in diabetic rats. Pharmacol. Res., 2016, 110, 122-130.

DOI: 10.1016/j.phrs.2016.05.016

The online version of this paper is attached in the next pages.

L. Salvioni, E. Galbiati, V. Collico, G. Alessio, S. Avvakumova, F. Corsi, P. Tortora, D. Prosperi, M. Colombo; Negatively charged silver nanoparticles with potent antibacterial activity and reduced toxicity for pharmaceutical preparations. Int. J. Nanomed. 2017, 12, 2517-2530.

DOI: 10.2147/IJN.S127799

Pharmacological Research 110 (2016) 122–130

Contents lists available at ScienceDirect

Pharmacological Research

journal homepage: www.elsevier.com/locate/yphrs

Oral delivery of insulin via polyethylene imine-based nanoparticles for colonic release allows glycemic control in diabetic rats

Lucia Salvioni[a,1], Luisa Fiandra[b,1], Maria Dorly Del Curto[c,1], Serena Mazzucchelli[b], Raffaele Allevi[b], Marta Truffi[b], Luca Sorrentino[b], Benedetta Santini[a], Matteo Cerea[c], Luca Palugan[c,*], Fabio Corsi[b,*], Miriam Colombo[a,*]

[a] Università degli Studi di Milano-Bicocca, NanoBioLab, Dipartimento di Biotecnologie e Bioscienze, piazza della Scienza 2, 20126 Milan, Italy
[b] Università degli Studi di Milano, Dipartimento di Scienze Biomediche e Cliniche "L. Sacco", via G.B. Grassi 74, 20157 Milan, Italy
[c] Università degli Studi di Milano, Dipartimento di Scienze Farmaceutiche, Sezione di Tecnologia e Legislazione Farmaceutiche "Maria Edvige Sangalli", via G. Colombo 71, 20133 Milan, Italy

ARTICLE INFO

Article history:
Received 14 April 2016
Received in revised form 10 May 2016
Accepted 10 May 2016
Available online 12 May 2016

Keywords:
Polymeric nanoparticles
Multiple-unit formulation
Insulin release
Peptide oral delivery
Type 1 diabetes

ABSTRACT

In this study, insulin-containing nanoparticles were loaded into pellet cores and orally administered to diabetic rats. Polyethylene imine-based nanoparticles, either placebo or loaded with insulin, were incorporated by extrusion and spheronization technology into cores that were subsequently coated with three overlapping layers and a gastroresistant film. The starting and coated systems were evaluated *in vitro* for their physico-technololgical characteristics, as well as disintegration and release performance. Nanoparticles-loaded cores showed homogeneous particle size distribution and shape. When a super-disintegrant and a soluble diluent were included in the composition enhanced disintegration and release performance were observed. The selected formulations, coated either with enteric or three-layer films, showed gastroresistant and release delayed behavior *in vitro*, respectively. The most promising formulations were finally tested for their hypoglycemic effect in diabetic rats. Only the nanoformulations loaded into the three-layer pellets were able to induce a significant hypoglycemic activity in diabetic rats. Our results suggest that this efficient activity could be attributed to a retarded release of insulin into the distal intestine, characterized by relatively low proteolytic activity and optimal absorption.

1. Introduction

Current therapy for diabetes mellitus relies on a correct diet, physical exercise, and oral hypoglycemic agents [1]. In case of disease progression or in Type 1 diabetes, insufficient insulin secretion or inadequate activity need to be considered. Therefore, replacement with exogenous insulin becomes mandatory for survival [1,2]. Unfortunately, nowadays the only administration route available for insulin is parenteral which implies one or more daily injections, with a significant reduction in quality of life and, sometimes, poor patient adherence to therapy [3,4]. Moreover, administration of insulin by subcutaneous injection may induce peripheral hyperinsulinaemia and portal hypoinsulinaemia. Under normal conditions, half of insulin produced by the pancreas is used for liver metabolism via the portal circulation, resulting in fine regulation of blood glucose levels and adequate metabolism of carbohydrates and proteins [2]. Thus, several research studies have been focused on the development of novel formulations of the hormone through alternative routes of administration [5]. Particularly, the oral route has been considered as possibly leading to a better glucose regulation exploiting the liver first-pass metabolism of insulin, thus preventing the risks of fluctuating blood glucose levels and possibly the resulting morbidity due to chronic microvascular complications [6]. Therefore, an oral formulation of insulin could revolutionize the management of insulin-dependent diabetic patients due to its potential clinical benefits. However, the oral bioavailability of insulin is very low and several efforts have been attempted to promote insulin bowel absorption, avoiding gastric or intestinal degradation by proteases. Such attempts included formulations with protease inhibitors and/or absorption enhancers or mucoadhesive systems. Still, oral delivery of insulin remains an unmet need [3]. As a result of this, colonic delivery and release of insulin has gained increasing interest by researchers because of the longer transit time, prolonged localization of insulin on the gut mucosa,

* Corresponding authors.
E-mail addresses: luca.palugan@unimi.it (L. Palugan), fabio.corsi@unimi.it (F. Corsi), miriam.colombo@unimib.it (M. Colombo).
[1] Equally contributed.

http://dx.doi.org/10.1016/j.phrs.2016.05.016
1043-6618/

lower levels of proteases in the colon or mucosal P-glycoprotein and greater responsiveness to permeation enhancers compared to the more proximal regions of the gastrointestinal tract. Such features would point to the colon as an interesting target for insulin oral delivery but, so far, an efficient drug delivery system for this propose is still missing [3,6,7–9].

A few attempts to improve the oral delivery of insulin by means of nanoparticle-based vectors have been reported [10–12]. Several nanoparticle (NP) types have been designed to protect biological drugs, including insulin, against chemical and enzymatic degradation and to enhance the intestinal absorption through paracellular and transcellular pathways [10,11]. Structural characteristics of nanoparticles, including size and surface charge, have been shown to influence the insulin absorption by the enterocytes. In general, small particles, provided with a positive charge are absorbed more efficiently through the intestinal epithelium. This is due to the interaction of NPs bearing positive charges with mucin residues that are negatively charged at physiological pH. The consequent prolonged residence time and increased concentration gradient at the surface of the intestinal mucosa might therefore promote protein absorption [3,11]. *Ex-vivo* and *in vivo* studies have also proven the potential of colloidal nanoparticles in increasing insulin absorption throughout the colonic region, but the lack of an appropriate delivery system that ensures their safe transit through the upper gastrointestinal tract strongly limits their usefulness [12,13]. Therefore, a solid dosage form, including pellets and tablets, which could host drug-loaded nanoparticles and possibly undergo a subsequent coating process, might represent a valuable strategy to enhance stability and provide release versatility of these colloidal systems administered via the oral route [6].

The objective of the present study was to prepare, characterize and evaluate both *in vitro* and *in vivo,* a novel nanoformulated, multiple-unit colon release system, *i.e.* coated pellets, as a possible oral nanocarrier for insulin. The novelty of this approach was the evaluation of the synergistic effect of colon release, mucoadhesive nanoparticles and the presence of a permeation enhancer, sodium glycocholate. The proposed multi-approach strategy combines the well-known benefits of this multiple-unit formulation in terms of reproducible transit time through the gastrointestinal tract, the consequent absorption pattern with the advantages of colloidal nanoparticles [14]. For this purpose, a recently proposed three-layer release technology platform was applied, consisting of a flexible film composed of a neutral polymethacrylate Eudragit® NE and a superdisintegrant sodium starch glycolate Explotab®, added as a pore former, applied to a hydroxypropyl methylcellulose (HPMC) coating of reduced thickness in order to improve the efficiency of the erodible layer in delaying the drug liberation [14–16]. An outer gastroresistant layer was also added in order to neutralize the variable residence time in the stomach of the coated dosage form and allow its activation only following the entry into the duodenum. This time-dependent relies on the relative consistency of short intestinal transit time, the subsequent colon targeting and favoring the intestinal absorption of insulin at that level [17].

2. Materials and methods

2.1. Materials

Bovine insulin (MW 5734 Da), polyethylene imine (MW 750 kDa), dextran sulfate (MW > 500 kDa), zinc sulfate, streptozotocin (STZ) and cellulose ester dialysis membrane tubing with a molecular weight cut-off (MWCO) of 1.000.000 Da (Spectra/Por® Biotech CE) were purchased from Sigma-Aldrich (St Louis, MO, US). All chemicals were used as received without further purification. Lactose was obtained from Prodotti Gianni (Milan, Italy). Microcrystalline cellulose co-processed with sodium carboxymethyl cellulose (Avicel® CL611) and hydroxypropyl methyl cellulose acetate succinate (Aqoat® LG, HPMCAS) were gifts from FMC Europe (Brussels, Belgium, distributed by IMCD Italia, Milan, Italy) and from Shin-Etsu (Tokyo, Japan, distributed by Seppic, Milan, Italy), respectively. Hydroxypropyl methylcellulose (Methocel® E50, HPMC) was kindly donated by Colorcon (Milano, Italy). Poly(ethylacrylate, methylmethacrylate) (2:1 monomer molar ratio) as 30% V:w aqueous dispersion (Eudragit® NE 30 D) of Evonik Röhm (Darmstadt, Germany) was a kind gift of Rofarma (Gaggiano, Italy). Polyethylene glycol (PEG 400) and size 4 hard-gelatin capsules were purchased from ACEF (Fiorenzuola D'Arda, Italy). Sodium glycocholate (NaGly) was obtained from and Tokyo Chemical Industry (Tokyo, Japan). Sodium starch glycolate (Explotab® CLV) was a gift from JRS Rettenmaier Italia (Castenedolo, Italy).

2.2. Synthesis of insulin-containing nanoparticles (nanoformulated insulin, NI)

22.1 mL of insulin solution (10 mg/mL in 0.01 M HCl), 10.8 mL of a 10% w/V dextran sulfate (DS) solution and 18.0 mL of 10 mM tris buffer, pH 9, were added under stirring (500 rpm) to 12.6 mL of polyethylene imine (PEI) solution (25% w/V). Afterwards, the mixture was heated at 40 °C and maintained under stirring because of its high viscosity and 7.8 mL zinc sulfate solution (2 M) were added, dropwise. As a result of the addition of the stabilizer, the formation of the nanoparticles took place and the viscosity of the solution decreased. The product was stirred for 15 min at 40 °C. The product was finally dialyzed in Milli-Q® water with cellulose ester dialysis membrane tubing with a molecular weight cut-off (MWCO) of 1.000.000 Da.

2.3. Synthesis of placebo nanoparticles (NPs)

22.1 mL of HCl 0.01 M, 10.8 mL of a 10% w/V DS solution and 18.0 mL of 10 mM tris buffer, pH 9, were added under stirring (500 rpm) to 12.6 mL of polyethylene imine (PEI) solution (25% w/V) and then treated as described above.

2.4. Nanoparticle characterization

2.4.1. Dynamic light scattering (DLS) and zeta potential measurements

The mean diameter and surface charge of the nanoparticles were assessed with a Zetasizer Nano ZS ZEN3600 from Malvern Instruments Ltd (Worcestershire, United Kingdom) operating at a light source wavelength of 633 nm and a fixed scattering angle of 173°. The sample concentration was chosen to keep attenuator values between 7 and 9. The refractive index of material was 1.524. The measurements were performed in triplicate, after dilution of the nanoparticles respectively with MilliQ® water and aqueous solution of sodium chloride (1 mM).

2.4.2. Transmission electron microscopy (TEM) analysis

Nanoparticles were visualized using 120 keV TEM (Jeol 1010, Tokyo, Japan). Two microliters of the sample, along with 2% w:V uranyl acetate solution, were deposited onto a piece of ultrathin 200-mesh copper grid (Ted-pella, Redding, CA, US) and left to dry in air before examination by TEM.

2.4.3. Determination of the entrapment efficiency (EE%) of insulin into the nanoparticles

The amount of insulin encapsulated into the nanoparticles was determined suspending the NI, corresponding to 30 μg/mL theoretical insulin concentration, in 0.05 M HCl and centrifuging at 12000 rpm for 20 min (ScanSpeed 1730R, Labogene, Lynge,

Denmark). After centrifugation, the amount of insulin in supernatant was measured by a reverse-phase, high-performance liquid chromatography (RP-HPLC) analysis with a method reported in Eur. Pharm. 8th Ed. for insulin and its degradation product A21-desamido insulin (A21) quantitation that was previously set-up [18]. Insulin quantitation was performed using a freshly prepared standard having identical insulin concentration and analyzed the same day of nanoparticles. The EE% is expressed as ratio percentage between the insulin amount in the suspension and the theoretical value of the insulin added.

2.4.4. In vitro *insulin release from NI*

In vitro release was assessed following incubation of the nanoparticle suspension containing theoretically 0.35 mg of insulin in 10 mL of 0.095 M phosphate buffer pH 6.8 prepared as indicated in the Eur. Pharm. 8th Ed. at 37 °C under stirring (MIX15eco, 2mag, München, Germany; 600 rpm). Bovine albumin (0.2% w/V) was added to the dissolution medium to avoid non-specific adsorption of insulin to glass surface. At pre-determined time intervals, 1 mL of medium was withdrawn, filtered by 0.2 μm polyethersulfone (PES) membrane (VWR) and acidified with 40 μL of 1 M HCl before the analysis by RP-HPLC as previously described. Dissolution studies were performed in triplicate.

2.5. Preparation and coating of cores

All cores were prepared by extrusion and spheronization (E-S) process.

Powders (9.2 g) were mixed in a mortar for 5 min. Nanoparticle suspensions, either placebo or loaded with insulin, (70 g) were then added in small aliquots to the powder blend under continuous mixing, in the same mortar, over a total period of 8 h; during that time the most of water could evaporate to allow the moisture content suitable to the next step. The room was maintained at 30 °C with 25% relative humidity. The resulting wetted mass was extruded through an 850 μm sieve. Spheronization was performed in a spheronizer (Nica™ S320, GEA, Düsseldorf, Germany) with a cross-hatched plate (400 rpm, 5 min). Pellets cores were finally dried in a static oven at 40 °C for 24 h. As a reference, a pellet formulation containing the non-encapsulated peptide was prepared by mixing insulin powder with Avicel® CL611, NaGly, lactose and Explotab® CLV (9.4 g) and adding deionized water (3.5 g). The E-S was then performed as for nanoparticles loaded formulations.

In order to obtain three-layer colonic systems, pellets were coated in a fluid bed (GCPG 1.1, Glatt®, Binzen, Germany). The following formulations were in turn sprayed: i) a hydro-alcoholic solution (1:9 w/w, water/ethanol) of Methocel® E50 (5% w/w) and PEG 400 (0.5% w/w) (10 g/min spray rate), ii) an aqueous suspension of Eudragit® NE 30D-Explotab® CLV (20% *vs.* solid Eudragit® NE) (1.4 g/min) and iii) a hydro-alcoholic solution (23% w/w, water/ethanol) of Aqoat® (5.8% w/w) (8 g/min). In the case of the coatings with the hydro-alcoholic solutions of both Methocel® E50 and Aqoat® the rotor insert was employed while for Eudragit® NE-based suspension a Wurster process was applied. In the case of gastroresistant formulations, pellets were directly coated with the hydro-alcoholic solution of Aqoat®, as previously described. The operating conditions for all coatings were: inlet air temperature, 40 °C; product temperature, 33–35 °C; airflow rate, 70 m^3/h; nozzle diameter, 1.2 mm; spray pressure, 2.0 bar; final drying time at 40 °C, 5 min. A curing step in a static oven at 40 °C was performed on intermediate systems coated with Eudragit® NE-Explotab® CLV and final enteric formulations for 24 h and 2 h, respectively. In all process steps, placebo mini-tablets (weight 10.5 mg, diameter 2.5 mm, height 2.3 mm) were added in the process chamber to reach the minimum capacity of the fluid bed.

2.6. Pellets characterization

2.6.1. Particle size and shape analyses

Particle size distribution of the pellets was determined by a set of analytical sieves (500, 600, 710, 850, 1000, 1180, 1400, 1700, 2000 μm) piled in a sieve shaker (Endecotts, Octagon 200, London, United Kingdom) operated for 5 min at an amplitude of 4. Mean diameter and aspect ratio were determined using an image analysis system. Digital photomicrographs (n = 30, DinoCapture, Hsinchu, Taiwan) were analyzed by ImageJ software (Version 1.48, 19 April 2014, National Institute of Health, Bethesda, MD, US) that allow calculation of pellets dimensional and shape descriptors. The aspect ratio (AR) was calculated as follows:

$$Aspect\ ratio\,(AR) = \frac{Major\ Axis}{Minor\ Axis}$$

AR indicates the particle's fitted ellipse.

Yield% was calculated as ratio between the mass of obtained cores (500–2000 μm range) and the weighed amount of excipients.

2.6.2. Disintegration test

Disintegration test was performed in a dissolution apparatus 2: 300 mg of pellets in the 850–1000 μm range were poured in a vessel containing 1000 mL of pH 6.8 phosphate buffer (37.0 ± 0.5 °C), and stirred at 100 rpm for 30 min. Then, pellets retained by a 400 μm net were dried (40 °C, 24 h) and weighted; finally, the percentage of mass loss was calculated [19].

2.6.3. Insulin assay and in vitro release

In order to assess insulin content, approximately 10 mg of cores of pellets, exactly weighed, were added to 0.05 M HCl, stirred at 350 rpm for 10 min, sonicated for 10 min and centrifuged (12000 rpm, 20 min). The supernatant was analyzed by RP-HPLC analysis as described in section 2.4.3. *In vitro* release from nanoparticles, uncoated cores and coated pellets was assessed following incubation in 10 mL of phosphate buffer (pH = 6.8) containing 0.2% bovine albumin at 37 °C under stirring. At pre-determined time-points, 1 mL of medium was withdrawn and replaced with fresh buffer solution, centrifuged and analyzed by RP-HPLC as previously described in section 2.4.3. In the case of three-layer and gastroresistant formulations, coated pellets were tested in HCl 0.1 M for 2 h prior to the buffer stage.

2.6.4. Re-dispersion studies

25 mg of cores (PNI02) were incubated in 5 mL of 0.1 M HCl at 37 °C under stirring (600 rpm) for 5 h. After incubation, an aliquot (2 mL) was filtered with 0.45 μm membrane and analyzed by DLS. The choice of the medium is occurred by checking the non-influence of other excipients in analysis result and the stability of the nanoparticles in this solution. The study was conducted in triplicate.

2.7. In vivo *studies*

2.7.1. Diabetic rat model

For the *in vivo* experiments, Sprague Dawley rats, purchased by Charles River Laboratories (Calco, Italy), were maintained in a fully-equipped facility in appropriate cages and provided with a proper environment. Diabetes was induced by two intraperitoneal injections of 50 mg/kg streptozotocin diluted in 0.1 M sodium citrate buffer pH 4.5 (one injection per week for two weeks). Seven days after the first administration, all rats were weighted and glycaemia was measured by puncturing the tail vein with an 18-gauge needle and collecting the blood droplet in the test strip of a blood glucose meter (Contour Link, Bayer, Milan, Italy). After the first injection, around 40% of treated rats developed glycemic values

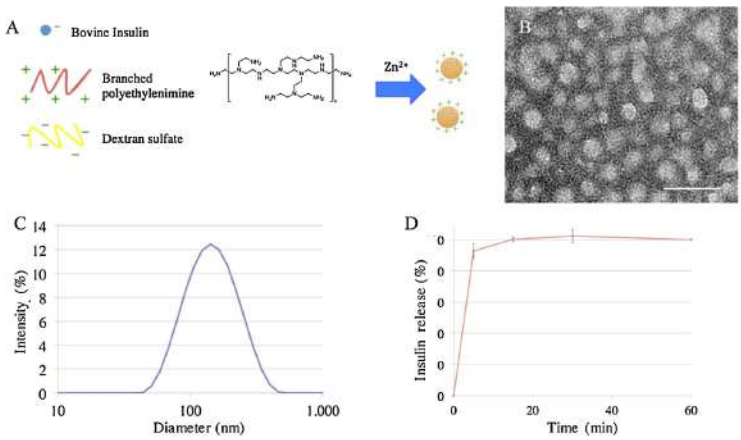

Diameter (nm) - intensity	177.1 ± 12.3 PDI 0.244 ± 0.023
ζ-potential (mV)	28.9 ± 0.45
Entrapment efficiency (%)	62.3 ± 3.5

Fig. 1. Schematic representation of NI synthesis (A). TEM image of NI, scale bar: 100 nm (B). Hydrodynamic size of NI measured by DLS (C). Dissolution profile of NI at 6.8 pH (mean ± SD, n = 3) (D).

Table 1
Compositions of cores under investigation.

Formulation	% (w/w)						
	Insulin	NI[a]	Placebo NPs[a]	Avicel® CL611	Sodium glycocholate (NaGly)	Lactose	Explotab® CLV
PN01	–	–	50.0	50.0	–	–	–
PN02	–	–	50.0	26.4	–	15.7	7.9
PNI01	–	43.2	–	43.2	13.6	–	–
PNI02	–	43.2	–	22.7	13.6	13.8	6.7
PI02	2.3	–	–	39.1	23.4	23.7	11.5

[a] The percentage refers to the solid nanoparticles.

over 350 mg/dL, indicative of diabetes onset [20]. All animals were treated again and, after further seven days, we obtained 75–80% of stably diabetic rats (glucose concentration ranging between 350 and 600 mg/dL).

2.7.2. Administration of insulin formulations to diabetic rats

Three groups of diabetic rats have been in turn injected subcutaneously with a solution of free insulin (n = 3, 0.07 mg/kg in phosphate buffer pH 6.8), and orally by gavage with a peptide solution (n = 5, 1.33 mg/kg in 10^{-3} M HCl) as well as with a nanoparticle formulation (n = 6, NI, 1.33 mg/kg). All other rats have undergone a surgical gastrostomy, upon anesthetization by intraperitoneal injection of 500 mg/kg of Avertin, for the insertion into the stomach of one capsule containing pellets formulations loaded with insulin (1.33 mg/kg): GPNI (n = 5, 53 mg), GPI (n = 3, 55 mg) CPNI (n = 4, 168 mg), CPI (n = 4, 63 mg). After insertion of the capsule, the stomach was sutured with 4-0 resorbable running suture, and the abdomen closed by 2-0 silk interrupted stitches. The gastrostomy procedure was chosen due to the impossibility to obtain a suitable oral administration of the free pellets in aqueous solution: low stability and high electrostatic interaction with the gavage tube were observed. One group of 5 rats was left untreated. The blood glucose levels were monitored by collecting blood droplets as described above at 1, 2, 3, 4, 5, 6, 7, 8, and 48 h post-treatment. Rats were used in accordance with an experimental protocol subjected to the direct approval of the Italian Ministry of Health.

3. Results

3.1. Nanoparticle synthesis and characterization

Insulin-loaded polymeric nanoparticles were synthesized according to previously published protocols with some modifications with the aim of scaling up the amount of synthesized nanoparticles and reduce the amount of excipients to include in the final pellet formulation [21,22]. Briefly, insulin and dextran sulfate solutions were added to a PEI solution under heating at 40 °C. The driving force for the formation of the nanoparticles was the opposite charges of PEI and dextran sulfate resulting in the insulin entrapment into the polymeric matrix. The weight ratio between the two polymers was optimized in order to control the particle size and zinc sulfate solution was added dropwise to stabilize the nanoparticles (Fig. 1A). The resulting insulin-containing nanoparticles (NI) were washed by dialysis against deionized water that was chosen as the dialysis medium instead of recommended 5% (w/v) mannitol solution [21]. The amount of NI in the final dialyzed product was 72% of the starting amount. Compared to previously reported preparation, bulky stabilizer exclusion, along with the 5-fold increase of insulin loading, resulted in a 35-fold reduction of the material amount required to form the pellets [21,22]. Furthermore, added solutions were at the minimum volumes needed to ensure the reagents solubility. With this adjustment, concentrated colloidal suspension was obtained, more suitable for following pellets inclusion.

Table 2
Physico-chemical properties and process yield of cores prepared by extrusion and spheronization.

Batch	d_{geo} (μm)	σ_{geo} (μm)	AR	Yield (%)	Insulin recovery%	A21%
PN01	913	1.18	1.36 ± 0.18	59.9	–	–
PN02	804	1.21	1.38 ± 0.20	40.1	–	–
PNI01	809	1.21	1.21 ± 0.18	41.3	102.1 ± 1.6	1.8 ± 0.2
PNI02	1137	1.28	1.16 ± 0.10	61.9	88.8 ± 3.7	0.9 ± 0.3
PI02	1066	1.16	1.29 ± 0.15	74.4	91.8 ± 1.1	2.2 ± 0.3

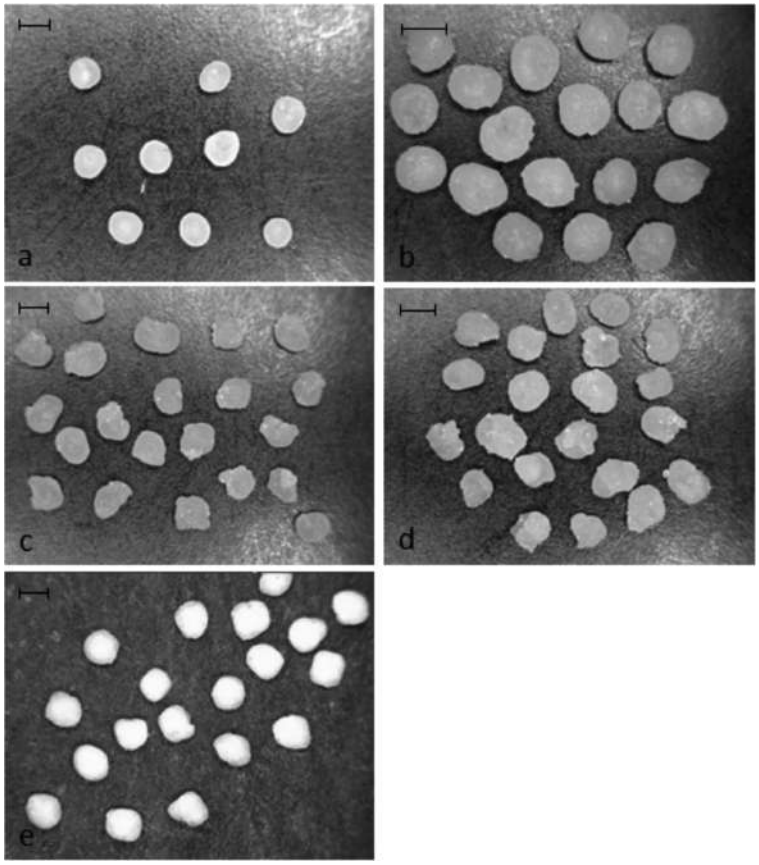

Fig. 2. Digital photographs of core formulation under investigation: a) PN01, b) PN02, c) PNI01, d) PNI02 and e) PI02. Scale bar: 1 mm.

Transmission electron microscopy (TEM) images of the negatively stained NI (Fig. 1B) showed spherical and nearly monodisperse 30 nm nanoparticles. However, the mean hydrodynamic size of NI as determined by DLS was 177.1 ± 12.3 nm, probably due to the high solvation efficiency of the polymeric matrix, and the zeta potential was +28.9 ± 0.5 mV. The entrapment efficiency (EE%) determined after extraction in acidic solution and measured by RP-HPLC was 62.3 ± 3.5%, while the % of the degradation product A21-desamido insulin was 1.2 ± 0.1%. Although slightly lower than previous reports, EE% was in the range of interest to conduct the subsequent loading steps. In addition, the A21% levels below the limits reported in the bovine insulin monograph of the Pharm. Eur. 8th Ed. confirmed that no major hydrolytic degradation had occurred during the preparation of colloidal nanoparticles.

Insulin nanoparticles subjected to release test showed a fast peptide dissolution at pH 6.8 (over 90% within 5 min). This behavior is consistent with that of similar nanoparticles reported in the literature [21].

3.2. Core preparation and characterization

In order to achieve a prompt release of the nanoparticles at the desired site, an appropriate core formulation was designed. A cellulose derivative, Avicel® CL611, a co-processed microcrystalline cellulose and sodium carboxymethyl cellulose, was identified as suitable spheronization agent due to the well-known advantages in terms of improved disintegration and dissolution performance over the traditional formulations based on microcrystalline cellulose [19,23]. Moreover, a superdisintegrant agent (Explotab® CLV) and a soluble diluent (lactose) were added in an alternative formulation in order to further improve the pursued fast-disintegration properties (Table 1). Only in the case of pellets loaded with NI, sodium

Table 3
Physico-technological characteristics of gastroresistant and three-layer colonic pellets.

Formulations	d_m (μm)	SD (μm)	AR	Methocel® E50 mg/cm²	Eudragit® NE-Explotab® CLV 20% mg/cm²	Aqoat® mg/cm²
GPNI	1355	114	1.14	–	–	13.1
CPNI	1865	102	1.07	89.9	4.0	13.0
GPI	1392	121	1.25	–	–	11.9
CPI	2070	149	1.24	85.1	3.1	12.5

glycocholate (NaGly), an absorption enhancer with protease inhibition properties, was considered [24,25]. The latter functional agent was indeed demonstrated to promote the oral absorption of a pancreatic hormone in rats administered with a minitablet formulation at 1:10 protein/adjuvant ratio [26]. In addition, NaGly, due to its high solubility in aqueous media, could help to prevent the undesired matrix formation when pellets interact with water, thus possibly aiding their disintegration. Based on preliminary extrusion and spheronization trials, a 1:1 Avicel® CL611/placebo nanoparticles binary mixture was acknowledged as starting formulation suitable to lead to a dough with appropriate plasticity and pellets with adequate morphological characteristics (Table 1). When insulin-containing formulations or all other systems containing Explotab® CLV and lactose were used, the process appeared facilitated probably due to the concomitant decrease of nanoparticle amount and increase in the total solid mass attributable to the presence of the NaGly powder. In all cases, the possible issue associated with the large amount of colloidal suspension needed to obtain the required insulin dose for the *in vivo* studies, *i.e.* 4:1 w/w water *vs.* total solid mass, was overcome by adding the liquid in small aliquots and allowing the subsequent evaporation that limited the moisture content of the extrudable mass.

All the process yields were > 40% and, taking into account the low amounts of processed material, were considered satisfying. All batches showed a mean particle size comprised within the desired 710–1400 μm range and a nearly spherical shape (Table 2, Fig. 2). Only in the case of formulation batches PNI02 and PI02 a slightly higher mean diameter was observed. No differences in size or shape were observed between placebo and insulin-loaded pellets, which was not surprising considering that the final core product structure was not significantly affected by the low amount of protein payload within the colloidal suspension.

The protein content in the pellets was ≥ 90% of the theoretical amount and, despite the long wetting and evaporation phases, the % of A21 remained below the limits indicated in the monograph of bovine insulin reported of Pharm. Eur. 8th Ed., *i.e.* 3%. The overall results suggested that extrusion and spheronization might be a promising technology for loading a nanoparticle suspension into pellets.

3.2.1. In vitro *studies on cores*

Pellets containing the insulin-loaded nanoparticles were subjected to *in vitro* studies aiming to assess the disintegration and insulin release performances from the two different formulations.

PNI02 formulation showed enhanced disintegration compared to PNI01, *i.e.* 26.4 *vs.* 10.8%. This behavior could be ascribed to the presence of the superdisintegrant Explotab® and that of lactose acting as pore former compared to the formulation where the excipients were only Avicel® CL611. However, comparing such performance with that of a reference formulation containing paracetamol as analytical tracer instead of insulin nanoparticles and Avicel® CL611/lactose/Explotab® CLV in the same ratios as PNI02 formulation, a ≥ 75% disintegration was obtained. It can be thus inferred that the presence of nanoparticles considerably contributed to the formation of a slow-eroding matrix.

To confirm this result, re-dispersion studies were performed on batch PNI02, which appeared the most promising system from *in vitro* disintegration and dissolution tests. These studies were set up in order to evaluate the presence of NI after exposure of the solid dosage form to aqueous fluids. Samples of this medium were collected and analyzed by DLS.

Nanoparticles with a mean diameter of 146.1 ± 1.0 nm (n = 3) were detected. Comparing the size of NI, before and after E-S process, it was noticed that the mean diameter was slightly lower than the initial value (177.1 ± 12.3 nm), although the size distribution appeared to be maintained as evaluated by DLS polydispersity index (0.296 ± 0.005). To figure out the cause of this reduction, the same test was performed on 25 mg of a dried dough obtained by using the same components and operating conditions of the cores of PNI02 batch avoiding extrusion and spheronization steps. Also in this case, a decrease of mean diameter occurred, suggesting that it may depend on the mechanical stress during the dough formation. It can be thus inferred that cores under investigation might convey and liberate the colloidal system upon exposure to aqueous media.

3.2.2. *Preparation and characterization of coated pellets*

Pellets batches PNI02 and PI02 were selected as core formulations for preliminary *in vivo* testing on the basis of the *in vitro* results in terms of enhanced disintegration and dissolution properties. The cores were therefore coated either with a hydroalcoholic solution of Aqoat® or in turn with a Methocel® E50-, Eudragit® NE/Explotab® CLV- and Aqoat®- based formulations in order to prepare gastroresistant (G) and three-layer colonic (C) systems, respectively (Table 3). In the three-layer system, the hydrophilic layer based on Methocel® E50 was demonstrated to delay the drug release by a swelling/erosion mechanism, while the Eudragit® NE/Explotab® CLV film was aimed at prolonging the duration of the lag phase as imparted by the underlying HPMC coat. Finally, an outer gastroresistant film was added to the system to overcome the unpredictable gastric residence time of the system thus allowing its activation only at the duodenum and the consequent colonic release based on a time-dependent approach [17,26].

The adopted process operative conditions and the coating levels needed to achieve gastroresistance or a delayed release after a lag-phase suitable for colonic delivery were previously set up with an analogous formulation containing paracetamol as analytical tracer (data not shown). In particular, gastroresistance criteria were accomplished with an Aqoat® coating level of 12–13 mg/cm². When using colonic systems, an *in vitro* lag time of approximately 60 min corresponded to 85–90 mg/cm² of Methocel® E50, 3.0-4.0 mg/cm² of Eudragit® NE-Explotab® CLV 20% and 12–13 mg/cm² of Aqoat® [26]. Particularly, a similar multiple-unit system with an *in vitro* lag phase of the latter duration showed an insulin peak in rats and a corresponding drop in blood glucose levels 6 h post-dose following oral administration. Based on typical gastrointestinal transit times reported in the literature for rats, the delivery system, after this lag time, was expected to be able to arrive, mostly intact, to the ileo-colonic region [27].

All coated batches showed a mean particle size in the 1.3-2.1 mm range and coating levels in line with what expected based on pre-

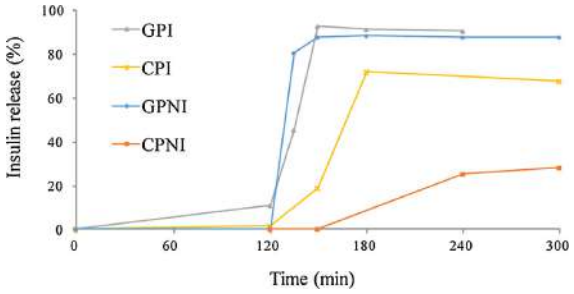

Fig. 3. *In vitro* insulin release of coated pellets.

liminary set up results. The shape was closer to roundness than the starting cores, as a result of the subsequent coating steps.

When subjected to *in vitro* release tests all formulation met gastroresistance criteria (< 10% release after 2 h in 0.1 M HCl), albeit the release test was conducted under more vigorous stirring, performed by magnetic stirrer, compared to the compendial method (Fig. 3).

When exposed to a pH 6.8 buffer, all enteric systems showed a prompt release due to core disintegration following dissolution of the enteric coat. The three-layer colonic systems containing the NI showed a lag-phase preceding the onset of release. The time corresponding to 10% release, $t_{10\%}$, was 65 min. Moreover, the CPI pellet formulation used as reference showed a shorter lag time that was demonstrated to be caused by the adopted release testing conditions (data not show).

3.3. In vivo *hypoglycemic effect*

The NI loaded into the pellets were tested *in vivo* in diabetic rats. The rat model was chosen since the gastrointestinal transit time is comparable to that of humans [28]. The animals that reached stable glucose values in blood of at least 350 mg/dL following streptozotocin administration were subjected to one of the following treatments: 1) oral administration of 1.33 mg/kg insulin (OI) or as NI, 2) subcutaneous injection of 0.07 mg/kg insulin (SCI), 3) insertion through gastrostomy of different amounts of pellets in capsules (GPI, GPNI, CPI, CPNI) to allow administration of 1.33 mg/kg. A group of non-treated rats was used as control (NT). Fig. 4 shows the % variation of glycaemia from 1 to 48 h post-treatment. The baseline for each experimental group was the mean value of blood glucose measured before the treatment, considered as 100%. In the first 8 h post-treatment, physiological oscillation of glucose blood levels was observed in NT rats, which however did not exceed 30% of the initial value. Orally administered insulin, either free or in NI, had no significant effect on blood glucose levels, while the subcutaneous injection of insulin caused a rapid and marked reduction of the glycemia to 25% of the initial values at 1 h post-treatment. However, blood glucose levels returned to the initial level when measured after 8 h. The treatment with GPI or GPNI did not show any significant effect on the glucose blood levels as compared to NT during the first 8 h. In contrast, the rat treatment with CPNI was able to induce an immediate, significant decrease in blood sugar levels as compared to the NT, with a significant fall in glycaemia, as much as 50% of the initial value, at 6 h post-treatment, and a subsequent further decrease of up to 30% at 8 h. On the other hand, the treatment with CPI did not exert any significant hypoglycemic effect. At longer times (48 h), NT and SCI-, OI-, NI-, and GPI-administered rats had blood glucose equal the initial values, while in rats administered with CPNI the glucose concentration remained at 45% of the starting level and significantly different from those of all other

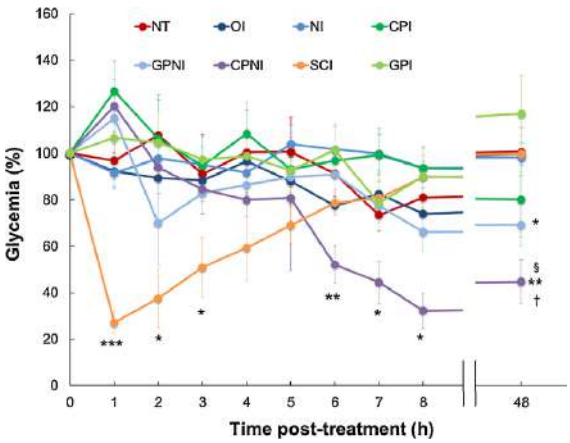

Fig. 4. Time course of the *in vivo* activity of different insulin formulations, expressed as percentage variation of rat blood glucose levels after treatment. Diabetic rats were exposed to oral (OI) or subcutaneous (SCI) administration of insulin, oral administration of insulin nanoparticles (NI), or insertion through gastrostomy of capsules containing gastroresistant pellet-formulated insulin (GPI) or insulin-nanoparticles (GPNI), colon-release pellet-formulated insulin (CPI) or insulin-nanoparticles (CPNI); NT: untreated rats. Mean ± SE of 3–6 animals for group. ***$p < 0.0005$; **$p < 0.01$; *$p < 0.05$ vs NT; §$p < 0.0005$ vs OI, NI, GPI and SCI; †$p < 0.05$ vs GPNI and CPI (one-tailed Student *t*-test).

experimental groups. At 48 h post-treatment, a slight decrease of glycaemia was observed upon administration of CPI, while in GPNI-treated rats glucose values became about 70% of initial values and significantly lower than those of controls.

4. Discussion

Preparation method of nanoparticles allows a considerable amount of insulin loaded and to a high concentration of nanosuspension: these factors are both favorable for the preparation of NI loaded pellets. Extrusion/spheronization of a formulation containing Avicel® CL611, lactose and Explotab® CLV wetted by nano-suspension leads to cores with technological and biopharmaceutical characteristics suitable for the following coating steps and for allowing a rapid NI release. Finally, in vitro performances of three layers coated pellets pledged a delayed release to promote colon targeting.

Orally administered insulin, either “free” or formulated in nanoparticles (NI) were not effective in reducing blood glucose levels in diabetic rats at 8 h after treatment. That was expected since insulin is rapidly degraded in the stomach. On the other hand, the subcutaneous injection of insulin, as used in clinical practice, caused a rapid and significant hypoglycemic effect with a subsequent gradual return to the initial blood glucose levels at 8 h. Curiously, at 1 h post-treatment all rats treated with the different capsules (GPI, GPNI, CPNI, or CPI) showed a temporary increase in blood glucose concentrations, possibly due to the effect of surgery and anesthesia, which is known to cause stress-related acute hyperglycaemia in fed rats [29]. The treatments with GPI or GPNI, enteric coated pellets which were supposed to release the nanoformulated insulin in small intestine, in the duodenum and the jejunum, did not significantly reduce the blood glucose levels as compared to NT in the first 8 h ($p > 0.05$). This may be due to the degradation of insulin by the high proteolytic activity of pancreatic peptidases but also to the effect of the insulin-degrading enzymes inside the cytosol of the small intestine enterocytes which can internalize the peptide by specific insulin receptors [30,31]. In contrast, the rat treatment

with CPNI induced a significant decrease in blood glucose levels as compared to the NT group. The reduction was significant at 6 h post-treatment with as much as 50% of the initial values, with a subsequent further decrease of up to 30% at 8 h. This result suggested that, unlike the gastroresistant pellet (GP) which releases the insulin into active small intestine, the three-layer colon-release pellet (CP) passed this tract without being degraded and released the NI in the distal part of the small intestine or in the colon. There are several reasons which make the colon as a desirable tract for insulin delivery and release: 1) the enzymatic activity, such as pancreatic endopeptidases, is remarkably lower and most of proteins, including insulin, would be available to intestinal absorption; 2) the microvilli are less developed in this tract as compared to the small intestine and their membrane-associated peptidases are limited making such microvilli more susceptible to permeation; 3) the P-glycoprotein is less expressed in colonic mucosa, and colon enterocytes and M-cells easily internalize nanoparticles; 4) there is a prolonged localization of insulin on the colonic mucosa due to slow transit time, thinner unstirred water layer (UWL) adjacent to mucosa, and slow turnover of colon mucosal film [5]. The lack of significant decrease in glycaemia of the rats treated with CPI indicates that the delivery of insulin as such to the colon by pellets is not sufficient to exert the hypoglycemic effect. A drug delivery system is required to properly address and release insulin to the colonic mucosa. Therefore, insulin nanoformulation plays a key role in reaching this goal. It has been demonstrated that polyethylenimine, as other cationic polymers (e.g. chitosans-CS), is able to loosen tight junctions (TJ) resulting in increased permeability of intestinal epithelium cells, which leads to paracellular permeation of molecules [32]. Many studies have already demonstrated the ability of different kinds of CS nanoparticles to increase the intestinal permeation of conjugated insulin through TJ opening [33]. In particular, Lin and colleagues suggested a mechanism for the paracellular transport of insulin to the blood circulation based on CS nanoparticles, whose stability and release of loaded insulin greatly depended on the environmental pH. In this model, the neutral pH, typical of the jejunum and the ileum, favors the degradation of the nanocomplex resulting in the complete release of CS and insulin. CS interaction with the TJ proteins enhances the paracellular pathway, promoting the absorption of greater amounts of insulin [34]. An equivalent mechanism could be suggested also for the NI released from pellets into the colon. Indeed, the pH values of this tract, from 6.5 in the ascending colon to 7 in the descending colon, could promote nanoparticle instability and cause the release of insulin (Fig. 1). Considering that the entire nanocomplex was not allowed to permeate across the TJ, even under the effect of paracellular enhancers, a few conclusions can be drown: 1) the released NI undergoes degradation in the colon lumen; 2) the released insulin that is not subjected to significant proteolytic activity in this tract of the gut and the PEI fragments both reach the mucosal surface; 3) PEI is supposed to interact with the TJ and opens the paracellular pathway, thus promoting a significant insulin absorption [35]. In addition, the presence of sodium glycocholate, that is known to promote insulin passage through the colonic mucosa by different mechanisms, including the rearrangement of the phospholipid bilayer and increase of the relevant fluidity, could have a synergistic effect on the overall protein absorption.

At 48 h, NT and SCI-, OI-, NI-, and GPI-administered rats had the blood glucose values return to initial levels while in rats administered with CPNI the blood glucose levels remained persistently and significantly reduced, as compared to the initial values. Such a long-lasting effect could be ascribed to the mucoadhesive properties of the nanocomplex, involving ionic interactions between the positively charged PEI and the negative charges of the mucosal surface. It may be hypothesized that, even if most of the nanoparticles were degraded in the colon lumen, part of them still interacted with the membrane-bound mucins on the intestinal epithelium, releasing the insulin beyond UWL, in the proximity of the absorptive cells. The UWL, forming a diffusion barrier between the luminal contents and the epithelium, probably maintained an adequate concentration of insulin in proximity of the enterocytes, allowing a prolonged insulin absorption over the whole period. On the contrary, most of the other administered formulations were eliminated previously. These results suggest a two-phase mechanism in rats administered with CPNI. During the first phase, a massive absorption of insulin takes place within the initial hours from the treatment (*i.e.* 6–8 h) as an effect of the rapid release of the drug from the nanoparticles into the colon lumen followed by the PEI-mediated opening of the paracellular route. During the second phase, a long-lasting absorption of the insulin released in proximity of the colon epithelium by the nanoparticles is triggered by active interaction with the negatively charged mucus layer.

At 48 h post-treatment, a slight decrease of blood glucose levels, not significantly different from that observed in NT and orally treated rats, was observed upon administration of CPI, while in GPNI-treated rats, glucose values were still about 70% of the initial values and significantly lower than those of controls. It is likely that the hypoglycemic effect could be attributed to the release of insulin by those nanoparticles which escaped luminal degradation and reached the mucosal surface. In this case, a certain amount of the protein, protected from the proteolytic activity due to the presence of the secretory mucin barrier [36], is still available for the intestinal absorption. This likely occurs through the PEI-activated paracellular pathway.

The colonic delivery of nanoformulated insulin holds a significant potential in clinical practice. This study provides the proof of the concept that the oral delivery of insulin targeted at colonic release and absorption may survive the hostile environments of gastric acidity or the peptidase rich small bowel. Moreover, blood glucose remained nearly half of the initial levels at 48 h post-administration of CPNI, thanks to slow and continuous release of insulin in the colon. This fact is particularly significant, since it may indicate that a prolonged control of glycaemia may be reached with a possible reduction in the overall insulin requirements of the patient resulting in a possible reduction in the number of daily injections. This would result in improved quality of life and potential reduction in long-term complications related to unstable glycemic control. Another goal reached by this novel insulin nanoformulation is the restoration of a physiological delivery of insulin into the portal vein, with a proper liver metabolism. This avoids fluctuating blood glucose levels and allows a more precise control of glycaemia. No fluctuation was observed in blood glucose levels of CPNI-treated rats, in favor of a progressive regular fall of the glycaemia [2,6]. In addition, a low between-subjects variability in blood glucose levels was observed in rates treated with CPNI, suggesting a reproducible response of glycaemia to this novel insulin nanoformulation. The clinical impact of this phenomenon could be important considering that, currently, a major limitation encountered in clinical and preclinical trials with oral insulin delivery so far was the highly variable response of glycemic control [37]. Furthermore, mimicking the physiological insulin circulation in the portal vein and the extraction by the liver, this formulation might obviate the drawbacks of insulin administered subcutaneously: systemic hyperinsulinemia with subsequent possible hypoglycaemia, local lipoatrophy with consequent day-to-day variability of subcutaneous absorption, weight gain, atherogenesis and enhanced lipogenesis. The peripheral administration of insulin is also implicated in the worsening of insulin resistance which makes the adjustment of insulin dosing difficult in, for instance, diabetes Type 2 patients.

Finally, hepatic insulin extraction after colon absorption as opposed to that after peripheral administration might improve

the liver inflammation and the oxidant production involved in the pathogenesis of hepatic steatosis. Therefore, the multitasking nanodevice described in this study for oral delivery of insulin is promising, although further research is needed to better clarify, for example, the efficacy in glycemic control immediately after a meal and the variations caused by oral insulin on various others metabolic and diabetes indicators, such as glucagon, insulin-like growth factor 1 (IGF-1), fructosamine and glycated hemoglobin.

5. Conclusion

Oral insulin delivery remains a clinical challenge, and despite a growing body of publications on this topic, there is still no oral formulation for insulin. In this study, a new approach for the oral administration of insulin is proposed targeting the colon as the release and absorption site. The synergistic effect due to the nanoformulation of insulin and the encapsulation in a triple-layer pellet system for colon-release delivery resulted in a significant and long-lasting hypoglycemic effect. The impact of our multi-tasking delivery system for oral insulin in controlling diabetes is clinically appealing, since it represents an oral route for insulin administration, with a prolonged hypoglycemic activity and a more physiological insulin metabolism. However, further research is needed to promote this novel nanoformulation into clinical trials.

Acknowledgments

This work was supported by Fondazione Regionale per la Ricerca Biomedica (FRRB).

We thank Maurizio Bevilacqua, MD, head of Endocrinology Unit Hospital L.Sacco Milan for methodological support.

References

[1] T. Bailey, Options for combination therapy in type 2 diabetes: comparison of the ADA/EASD position statement and AACE/ACE algorithm, Am. J. Med. 126 (2013) S10–20.
[2] S. Dal, N. Jeandidier, A. Schaschkow, A.H. Spizzo, E. Seyfritz, C. Sookhareea, W. Bietiger, C. Péronet, F. Moreau, M. Pinget, E. Maillard, S. Sigrist, Portal or subcutaneous insulin infusion: efficacy and impact on liver inflammation, Fundam. Clin. Pharmacol. 29 (2015) 488–498.
[3] A. Maroni, L. Zema, M.D. Del Curto, A. Foppoli, A. Gazzaniga, Oral colon delivery of insulin with the aid of functional adjuvants, Adv. Drug. Deliv. Rev. 64 (2012) 540–556.
[4] M.R. Rekha, C.P. Sharma, Oral delivery of therapeutic protein/peptide for diabetes-Future perspectives, Int. J. Pharm. 440 (2013) 48–62.
[5] F. Sousa, P. Castro, P. Fonte, B. Sarmento, How to overcome the limitations of current insulin administration with new non-invasive delivery systems, Ther. Deliv. 6 (2015) 83–94.
[6] M.M. Patel, Colon targeting: an emerging frontier for oral insulin delivery, Exp. Opin. Drug Deliv. 10 (2013) 731–739.
[7] A. Gazzaniga, A. Maroni, M.E. Sangalli, L. Zema, Time-controlled oral delivery systems for colon targeting, Exp. Opin. Drug Deliv. 3 (2006) 583–597.
[8] S. Haupt, A. Rubinstein, The colon as a possible target for orally administered peptide and protein drugs, Crit. Rev. Ther. Drug Carr. Syst. 19 (2002) 499–551.
[9] S. Bourgeois, R. Harvey, E. Fattal, Polymer colon drug delivery systems and their application to peptides proteins, and nucleic acids, Am. J. Drug Deliv. 3 (2005) 171–204.
[10] C. Damge, C.P. Reis, P. Maincent, Nanoparticle strategies for the oral delivery of insulin, Exp. Opin. Drug Deliv. 5 (2008) 45–68.
[11] L.M. Ensign, R. Cone, J. Hanes, Oral drug delivery with polymeric nanoparticles: the gastrointestinal mucus barriers, Adv. Drug Deliv. Rev. 64 (2012) 557–570.
[12] A. Bayat, F.A. Dorkoosh, A.R. Dehpour, L. Moezi, B. Larijani, H.E. Junginger, M. Rafiee-Tehrani, Nanoparticles of quaternized chitosan derivatives as a carrier for colon delivery of insulin: ex vivo and in vivo studies, Int. J. Pharm. 356 (2008) 259–266.
[13] K. Cheng, L.Y. Lim, Insulin-loaded calcium pectinate nanoparticles: effects of pectin molecular weight and formulation pH, Drug. Dev. Ind. Pharm. 30 (2004) 359–367.
[14] L. Palugan, M. Cerea, L. Zema, A. Gazzaniga, A. Maroni, Coated pellets for oral colon delivery, J. Drug Deliv. Sci. Technol. 25 (2015) 1–15.
[15] A. Maroni, M.D. Del Curto, M. Cerea, L. Zema, A. Foppoli, A. Gazzaniga, Polymeric coatings for a multiple-unit pulsatile delivery system: preliminary study on free and applied films, Int. J. Pharm. 440 (2013) 256–263.
[16] M.D. Del Curto, L. Palugan, A. Foppoli, L. Zema, A. Gazzaniga, A. Maroni, Erodible time-dependent colon delivery systems with improved efficiency in delaying the onset of drug release, J. Pharm. Sci. 103 (2014) 3585–3593.
[17] S.S. Davis, The design and evaluation of controlled release systems for the gastrointestinal tract, J. Control Release 2 (1985) 27–38.
[18] A. Maroni, M.D. Del Curto, M. Serratoni, L. Zema, A. Foppoli, A. Gazzaniga, M.E. Sangalli Feasibility, stability and release performance of a time-dependent insulin delivery system intended for oral colon release, Eur. J. Pharm. Biopharm. 72 (2009) 246–251.
[19] F. Casati, L. Palugan, G. Loreti, M.D. Del Curto, L. Zema, A. Gazzaniga, Co-processed microcrystalline cellulose and sodium carboxymethyl cellulose as spheronization aid for disintegrating pellets, in: 54° Simposio AFI, Rimini, 11–13 Giugno, 2014.
[20] J.J. Lee, H.-Y. Yi, J.-W. Yang, J.-S. Shin, J.-H. Kwon, C.-W. Kim, Characterization of Streptozotocin-induced diabetic rats and pharmacodynamics of Insulin formulations, Biosci. Biotechnol. Biochem. 67 (2003) 2396–2401.
[21] W. Tiyaboonchai, J. Woiszwillo, R.C. Sims, C.R. Middaugha, Insulin containing polyethylenimine-dextran sulfate nanoparticles, Int. J. Pharm. 255 (2003) 139–151.
[22] W. Tiyaboonchai, J. Woiszwillo, C.R. Middaugh, Formulation and characterization of amphotericin B-polyrthylenimine-dextran sulfate nanoparticles, J. Pharm. Sci. 90 (2001) 902–914.
[23] G. Di Pretoro, L. Zema, A. Gazzaniga, S.L. Rough, D. Wilson, Extrusion-spheronisation of highly loaded 5-ASA multiparticulate dosage forms, Int. J. Pharm. 402 (2010) 153–164.
[24] A. Yamamoto, T. Taniguchi, K. Rikyuu, T. Tsuji, T. Fujita, M. Murakami, S. Muranishi, Effects of various protease inhibitors on the intestinal absorption and degradation of insulin in rats, Pharm. Res. 11 (1994) 1496–1500.
[25] H. Tozaki, J. Komoike, C. Tada, T. Maruyama, A. Terabe, T. Suzuki, A. Yamamoto, S. Muranishi, Chitosan capsule for colon-specific drug delivery: improvement of insulin absorption from the rat colon, J. Pharm. Sci. 86 (1997) 1016–1021.
[26] A. Maroni, S. Salmaso, M.D. Del Curto, G. Loreti, P. Caliceti, A. Gazzaniga, Preliminary in vivo evaluation of an oral multiple-unit formulation for colonic delivery of insulin, in: 41st Annual Meeting & Exposition of the Controlled Release Society, Chicago, IL, USA, July 13–16, 2014.
[27] C. Tuleu, C. Andrieux, P. Boy, J.C. Chaumeil, Gastrointestinal transit of pellets in rats: effect of size and density, Int. J. Pharm. 180 (1999) 123–131.
[28] J.M. De Sesso, C.F. Jacobson, Anatomical and physiological parameters affecting gastrointestinal absorption in humans and rats, Food Chem. Toxicol. 39 (2001) 209–228.
[29] J.K. Saha, J. Xia, J.M. Grondin, S.K. Engle, J.A. Jakubowski, Acute hyperglycemia induced by ketamine/xylazine anesthesia in rats: mechanisms and implications for preclinical models, Exp. Biol. Med. 230 (2005) 777–784.
[30] J.P.F. Bai, L.L. Chang, Transepithelial transport of Insulin: i. Insulin degradation by insulin-degrading enzyme in small intestinal epithelium, Pharm. Res. 12 (1995) 1171–1175.
[31] L.L. Chang, L.E. Stout, W.D. Wong, J.G. Buls, D.A. Rothenberger, W.T. Shier, R.L. Sorenson, J.P. Bai, Immunohistochemical localization of insulin-degrading enzyme along the rat intestine in the human colon adenocarcinoma cell line (Caco-2), and in human ileum, J. Pharm. Sci. 86 (1997) 116–119.
[32] G. Ranaldi, I. Marigliano, I. Vespignani, G. Perozzi, Y.J. Sambuy, The effect of chitosan and other polycations on tight junction permeability in the human intestinal Caco-2 cell line, Nutr. Biochem. 13 (2002) 157–167.
[33] G. Sharma, A.R. Sharma, J.-S. Nam, G. Priya, C. Doss, S.-S. Lee, C. Chakraborty, Nanoparticle based insulin delivery system: the next generation efficient therapy for Type 1 diabetes, J. Nanobiotechnol. 13 (2015) 74–87.
[34] Y.H. Lin, C.T. Chen, H.F. Liang, A.R. Kulkarni, P.W. Lee, C.H. Chen, H.W. Sung, Novel nanoparticles for oral insulin delivery via the paracellular pathway, Nanotechnology 18 (2007) 105102.
[35] A. Adson, P.S. Burton, T.J. Raub, C.L. Barsuhn, K.L. Audus, N.F. Ho, Passive diffusion of weak organic electrolytes across Caco-2 cell monolayers: uncoupling the contributions of hydrodynamic, transcellular, and paracellular barriers, J. Pharm. Sci. 84 (1995) 1197–1204.
[36] G.J. Strous, J. Dekker, Mucin-type glycoproteins, Crit. Rev. Biochem. Mol. Biol. 27 (1992) 57–92.
[37] E. Zijlstra, L. Heinemann, L. Plum-Mörschel, Oral insulin reloaded: a structured approach, J. Diabet. Sci. Technol. 8 (2014) 458–465.

Acknowledgements

I wanted to thank for their precious support my supervisor Dr. Miriam Colombo along with Prof. Davide Prosperi and Dr. Luca Palugan.
A special thank goes to Prof. Leaf Huang, which kindly host me in his lab always encouraging to get better.
How can I forget all my lab mates from all over the word? In particular, I wanted to thank Michi, Bibi, Sveta, Sbada, Maya, Sai, Tayler, Manisit, Wantong, Serena, Francesco e Luisa for their invaluable help.
Finally, I'd like to thank my family and friends for their patience and my husband for his discreet, but crucial presence.